This project has received funding from the European Union's Horizon 2020 research and innovation programme under grant agreement No 101016608.

BEYOND 5G – OPTICAL NETWORK CONTINUUM
(H2020 – Grant Agreement Nº 101016663)

Deliverable D3.1

First year results on data plane infrastructure

Editor P. Layec (Nokia)

Contributors TID, TIM, BT, ADVA, NOKIA, CNIT, CTTC, INF-P, INF-D, HHI, OLC-E, TUE, PLF

Version 1.2

Date November 30, 2022

Distribution PUBLIC (PU)

DISCLAIMER

REVISION HISTORY

Revision	*Date*	*Responsible*	*Comment*
1.0	*July, 28, 2022*	*P. Layec*	*First draft*
1.1	*November, 8, 2022*	*P. Layec*	*Final draft*
1.2	*November, 21, 2022*	*P. Layec*	*Final version*

LIST OF AUTHORS

Partner ACRONYM	Partner FULL NAME	Name & Surname
Nokia	*Nokia Network France*	*Patricia Layec, Petros Ramantanis, Alix May, Fabien Boitier*
TID	*Telefonica Investigacion y Desarrollo SA*	*Oscar González de Dios, Jose Manuel Rivas Moscoso, Edward James Echeverry Zuleta*
TIM	*Telecom Italia SPA*	*Emilio Riccardi, Anna. Chiadò Piat*
BT	*British Telecommunications Public Limited Company*	*Albert Rafel,* Md Asif Iqbal
INF-G	*Coriant R&D GmbH*	*Antonio Napoli, Carlos Castro*
INF-P	*Infinera Unipessoal, Lda*	*Antonio Eira, Catia Pinho, João Pedro, Nelson Costa*
ADVA	*ADVA SE*	*Lutz Rapp*
CNIT	*Consorzio Nazionale Interuniversitario Per Le Telecomunicazioni*	*Filippo Cugini, Davide Scano*
CTTC	*Centre Tecnològic de Telecomunicacions de Catalunya*	*Laia Nadal*
HHI	*Fraunhofer Gesellschaft*	*Caio Santos, Behanm Shariati, Johannes Fischer*
OLC-E	*OpenLightComm Eu*	*Alexandros Stavdas, Dimitris Uzunidis*
TUE	*Technische Universiteit Eindhoven*	*Nicola Calabretta*
PLF	*pureLiFi Limited*	*Rui Bian*

GLOSSARY

Acronym	Expansion
5G	Fifth Generation
5GPPP	5G Infrastructure Public Private Partnership
AAU	Active Antenna Unit
ADM	Add/Drop Multiplexer
AI	Artificial Intelligence
AP	Access Point
API	Application Programming Interface
AR	Augmented Reality
ASE	Amplifier Spontaneous Emission
B5G	Beyond 5G
BER	Bit Error Ratio
BM	Burst-Mode
BNG	Broadband Network Gateway
BSS	Business Support System
BVT	Bandwidth/bit rate Variable Transceivers
Capex	Capital Expenditure
CAGR	Compound Annual Growth Rate
CBR	Constant Bit-Rate
CDC	Colorless/Directionless/Contentionless
CDC-F	Colorless/Directionless/Contentionless Flexgrid
CDN	Content Delivery Network
CN	Core Node
CNF	Cloud-native Network Function
CO	Central Office
CP	Control Plane
CPRI	Common Public Radio Interface
C-RAN	Centralized-Radio Access Network
CSG	Cell Site Gateway
CU	Central Unit
DC	Data Center
DCI	Data Center Interconnection

DCO	Digital Coherent Optics
DMT	Discrete MultiTone
DSC	Digital Subcarrier
DSCM	Digital Subcarrier Multiplexing
DSLAM	Digital Subscriber Line Access Multiplexer
DSP	Digital Signal Processing
DSR	Digital Signal Rate
DT	Digital Twin
DTC	DT City
DU	Distributed Unit
DWDM	Dense Wavelength Division Multiplexing
E/O	Electrical to Optical
E2E	End-To-End
EC	European Comission
ECOC	European Conference on Optical Communications
eCPRI	Enhanced CPRI
EDFA	Erbium Doped Fiber Amplifier
ENP	E-Lighthouse Network Planner
EPA	Enhanced Platform Awareness
Eth.	Ethernet
ETSI	European Telecommunication Standards Institute
ETSI MANO	ETSI NFV Management and. Orchestration
FCAPS	Fault, Configuration, Accounting, Performance, Security
FTTA	Fiber-To-The-Antenna
FTTH	Fiber-To-The-Home
FWM	Four-Wave Mixing
GN	Gaussian Noise
GGN	Gneneralized GN
gNB	gNodeB
gNMI	gPRC Network Management Interface
gPRC	gPRC Remote Call Procedure
GSNR	Generalized Signal-to-Noise Ratio
GTW	Gateway
HD	High Definition

HLS	High Layer Split
HSI	High Speed Internet
HTC	Holographic-Type Communications
IBN	Intent-Based Networking
IETF	Internet Engineering Task Force
IIoT	Industrial IoT with cloudification
INT	In-band Network Telemetry
ION	Intelligence Operation Network
IoT	Internet-of-Things
IP	Internet Protocol
IPR	Intellectual Property Rights
ISRS	Inter-channel Stimulated Raman Scattering
IT	Information Technology
ITU	International Telecommunication Union
KPI	Key Performance Indicator
KVI	Key Value Indicator
LiFi	Light Fidelity
LLS	Low Layer Split
MAC	Media Access Control
MAN	Metropolitan Area Network
MAS	Multi-Agent System
MB	Multi-Band
MBH	Mobile Back-Haul
MBN	Multi-Band Network
MB-OXC	Multiband - Optical Cross-Connect
MCF	Multi-Core Fiber
MCS	Multicast Switch
MDA	Monitoring and Data Analytics
MFH	Mobile Front-Haul
MIMO	Multiple-Input Multiple-Output
ML	Machine Learning
MMH	Mobile Mid-Haul
mMIMO	Massive MIMO
MPLS	Multiprotocol Label Switching

MSA	Multi Source Agreement
NBI	North Bound Interface
NCC	Network and Computing Convergence
NE	Network Element
NF	Noise Figure
NFV	Network Function Virtualization
NG	Next Generation
NGC	Next Generation Core
NLI	Nonlinear Interference
NMS	Network Management System
NOS	Node Operating System
NR	New Radio
O/E/O	Optical to Electrical to Optical
OADM	Optical Add/Drop Multiplexer
OD	Origin-Destination
ODN	Optical Distribution Network
OFC	Optical Networking and Communication Conference & Exhibition
OFDM	Orthogonal Frequency Division Multiplexing
OIF-ENMI	OIF External Network to Network Interface
OLA	Optical Line Amplifier
OLS	Open Line system
OLT	Optical Line Terminal
ONF	Open Networking Foundation
ONT	Optical Network Termination
ONU	Optical Network Unit
Opex	Operational Expenditure
OSNIR	Optical Signal-To-Noise plus Interference Ratio
OSNR	Optical Signal-To-Noise Ratio
OSS	Operation Support Systems
OTN	Optical Transport Network
OTT	Over-The-Top
OXC	Optical Cross-Connect
P2MP	Point-To-MultiPoint
PCE	Path Computational Engine

PCEP	Path Computation Element Communication Protocol
PE	P-Edge
PM	Project Manager
PMD	Physical Medium Dependent
PO	Project Officer
PoC	Proof of Concept
PON	Passive Optical Network
POP	Point Of Presence
PPP	Point-to-Point Protocol
PtoMP	Point-to-Multi-Point
PtoP	Point-to-Point
QMR	Quarterly Management Reports
QoE	Quality of Experience
QoS	Quality of Service
QoT	Quality of Transmission
R&D	Research and Development
RAN	Radio Access Network
RAT	Radio Access Technology
RL	Reinforcement Learning
RMSA	Routing, Modulation and Spectrum Assignment
ROADM	Reconfigurable Optical Add/Drop Multiplexer
RoF	Radio Over Fiber
RRH	Remote Radio Head
RRU	Remote Radio Unit
RTT	Round-Trip Time
RU	Radio Unit
S-BVT	Sliceable Bandwidth/bitrate Variable Transceiver
SC	Steering Committee
SDM	Space Division Multiplexing
SDN	Software Defined Networking
SDO	Standards Developing Organization
SD-WAN	Software Defined WAN
SL	Supervised Learning
SLA	Service Level Agreement

SME	Small and Medium-sized Enterprises
SoA	State of the Art
SOA	Semiconductor optical Amplifier
SONiC	Software for Open Networking in the Cloud
SRS	Stimulated Raman Scattering
STIN	Space-Terrestrial Integrated Network
TC	Technical Committee
TCO	Total Cost of Ownership
TDM	Time Division Multiplexing
TIP	Telecom Infra Project
TIRO	Tactile Internet and Remote Operations
TM	Technical Manager
TRL	Technology Readiness Levels
UE	User Equipment
UNI	User Network Interface
UP	User Plane
uRLLC	Ultra-Reliable Low Latency Communication
VLAN	Virtual Local Area Network
VM	Virtual Machine
VNF	Virtualized Network Function
VoD	Video on Demand
vOLT	virtual OLT
vPON	virtual PON
VR	Virtual Reality
VV	Volumetric Video
WAN	Wide Area Network
WB	White-Box
WDM	Wavelength Division Multiplexing
WiFi	Wireless Fidelity
WIM	WAN Infrastructure Manager
WP	Work Package
WP-TL	WP Technical Leaders
WSS	Wavelength Selective Switch
XCI	Cross Channel Interference

XR Optics	Infinera Technology for point to muti-point optics
YANG	Yet Another Next Generation
ZTN	Zero Touch Networking

EXECUTIVE SUMMARY

This deliverable reports on the activities of WP3 during the first year of the project. The work was split into different activities with the following objectives:

- Design of an innovative optical transport infrastructure supporting MB connectivity and transparent network continuum potentially from User Equipment to Data Centers.
- Modelling transmission and traffic performance of the identified MB data plane solutions.
- Design, prototyping and experimental assessment of the novel optical network devices for switching, amplification and transmission.
- Exploring and testing optical innovative solutions for MB PON, Point to Multi-point (PtoMP) with low cost and power consumption for next-generation optical access & 5G X-haul.
- Design and testing the effective integration of fiber with LiFi systems supporting multi-cell simultaneous transmission for bandwidth maximization and effective hand-over.
- Design, prototyping and testing advanced monitoring solutions to enable efficient and flexible use of the infrastructure.

To achieve the first objective, this document leverages the reference architecture provided by WP2. It recalls the definition of the terminology of different domains from access to the cloud and highlights the heterogeneity of the high-level data plane requirements in terms of technological options (topology, hardware, capabilities, etc.) and size (traffic, cost, power consumption, etc.).

From this high-level summary requirements, the document then reports for each specific network domain further details and gives options from the transport platform to be considered. The requirements specify capacity, the envisioned operated bands beyond current commercial systems, and the usage of multiple parallel fibers or special multi-core fibers. To efficiently manage (when needed) multi-band and multi-fiber systems, novel node architecture has to be developed including new coherent interface.

Optical transport design is usually based on physical layer models as it provides fast performance prediction notably important for (online) path computation. It approximates performance data that could be determined with higher accuracy with the standard split step Fourier method but at the expense of larger complexity and computing time. With the advent of coherent technologies, nonlinear noise can now be well-approximated by a Gaussian noise. However, when the transmission bandwidth increases beyond approximately 5 THz, an additional effect needs to be accounted for: the inter-channel stimulated Raman scattering. There are different alternatives for NLI and power evolution estimation leading to different trade-offs of accuracy and complexity. A detailed review of GN-like models is carried out with underlying assumptions, pros and cons.

The accuracy of the QoT estimation depends not only on the assumptions but also on the optical fiber characterization. For different bands, D3.1 presents typical reference values and comments on the frequency dependence of several parameters such as chromatic dispersion, attenuation and amplifier technologies. A contribution of B5G-OPEN on physical layer modelling in multi-band systems is then detailed and used to assess performance in different use cases.

B5G-OPEN targets the definition of vendor-neutral YANG data models for SDN-based impairment-aware path computations. Besides C-band, full support to multi-band operations is envisioned leading to a need to extend design parameters compatible with well-recognized initiatives such as IETF and GNPy. D3.1 split the design parameters into two parts: the transmission parameters targeting transponders and the line system parameters dealing with span, fiber, amplifier and ROADM node.

B5G-OPEN targets the definition of vendor-neutral YANG data models for SDN-based impairment-aware path computations. Besides C-band, full support to multi-band operations is envisioned leading to a need to extend design parameters compatible with well-recognized initiatives such as IETF and GNPy. D3.1 split the design parameters into two parts: the transmission parameters targeting transponders and the line system parameters dealing with span, fiber, amplifier and ROADM node.

In metro-aggregation, domain bridging access and core, both direct detection and coherent technologies met. Using coherent it is possible to generate virtual channel at the transmitter, which can be aggregated with passive optical components, thus enabling filterless network by broadcasting signals. This is the so-called point-to-multipoint solution which is compared in this deliverable to point-to-point coherent solutions in two network topologies. Recent results are also further reported in terms of cost savings and several advantages in multilayer redesign.

MB transmission investigates sliceable BVT as it facilitates the coexistence of both PtoP and PtoMP. As a first step, MB transmission is analyzed over different fiber lengths without considering any amplification and filtering stages, in order to evaluate the performance of the different investigated bands, which include S-, L- and C- bands, in similar conditions. D3.1 also reports the review of state-of-the-art commercial pluggable transceivers as cost effective solutions.

MB optical switch relies on two MB optical cross-connect for adding/dropping and bypass the traffic from/to the Metro Aggregation and the traffic to/from Metro-Core. A first MB-OADM prototype operating in the O- and C-bands is assessed. Moreover, the cascadability is also experimentally investigated over the typical distances for three cascaded nodes and 8 WDM channels at 25 Gb/s.

MB amplifiers by enabling additional bands requires the development of new amplification technologies. A bandwidth extension upgrade involves performance degradation due to increased fiber attenuation at some added wavelengths, degradation of the noise figure, and nonlinear fiber effects. For C+L bands, EDFAs is a mature technology. The single device solution is compared with the split–band approach using two amplifier devices in parallel. The increase of the bandwidth requires an OSNR margin presented in D3.1 for various span length and bandwidth increase. Finally, the challenges for introducing MB operation in an existing C-band network is presented.

An emerging wireline and wireless Access & Aggregation network architecture is depicted where all existing connectivity (i.e., PtoP, PtoMP and TDM-PON) can be supported. D3.1 summarizes the changes in the architecture. B5G-OPEN further extends this framework to propose a converged wireline and wireless next-generation architecture in the Access& Aggregation. In this framework, different use cases are presented for the optical technologies.

This integration leads to a need of a novel access planning tool. Currently, it can support one-stage and two-stage splitting design between a designated CO and the ONUs (end-users). Illustrative examples of PON deployment are then described.

The wireline and wireless convergence in B5G-OPEN relies on LiFi technology. LiFi is enabled by an ecosystem of multiuser techniques, resource allocation algorithms and security strategies and this deliverable reports an example of such a network.

Advanced monitoring solutions are presented for both packet and optical network elements to efficiently use the network resources. By proposing a novel monitoring architecture based on P4 processing, the packet-optical node allows peer to peer telemetry reports of commonly use optical monitoring information. Additionally, D3.1 reported evolution of the optical monitoring capabilities by presenting results on power profile monitoring based on coherent receiver. This requires no additional hardware to be deployed and may expose in the medium term more optical parameters to the control and management plane.

TABLE OF CONTENTS

1 INTRODUCTION

This deliverable D3.1 "First year results on data plane infrastructure" describes the activity related to work package 3 in the B5G-OPEN project. It identifies the context for the design and operation of multiband (MB) optical network across multiple segments, by enabling transmission within S, E and O bands in addition to current C + L bands. To meet this challenge, advanced technologies are required, and this deliverable reports the packet-optical node architectures options investigated in the project. A companion document investigating control and management architecture options is the deliverable D4.1.

It covers the design and development of the optical continuum multiband data plane infrastructure incorporating heterogeneous nodes and transmission technologies. It encompasses multiple domains with different characteristics in terms of reach, capacity, cost, scalability, flexibility, etc. The objectives of this work package are:

- Design of an innovative optical transport infrastructure supporting MB connectivity and transparent network continuum potentially from User Equipment to Data Centers.
- Modelling transmission and traffic performance of the identified MB data plane solutions.
- Design, prototyping and experimental assessment of the novel optical network devices for switching, amplification and transmission.
- Exploring and testing optical innovative solutions for MB PON, Point to Multi-point (PtoMP) with low cost and power consumption for next-generation optical access & 5G X-haul.
- Design and testing the effective integration of fiber with LiFi systems supporting multi-cell simultaneous transmission for bandwidth maximization and effective hand-over.
- Design, prototyping and testing advanced monitoring solutions to enable efficient and flexible use of the infrastructure.

The D3.1 document gives the progress of work package 3 during the first year of activity of B5G-OPEN toward the above-mentioned objectives and is structured as follows:

Section 2 reports on the reference architecture provided by work package 2. It encompasses several domains (network segments), ranging from access to the cloud, which makes it very heterogeneous in terms of technological options (topology, hardware, capabilities, etc.) and size (traffic, cost, power consumption, etc.). This reference architecture allows to summarize high-level data plane requirements.

Section 3 reports the detailed requirements for the transport platform and nodes for each domain. To design the physical layer, different assumptions can be accounted for and result in different methods to predict performance. The accuracy of the prediction also depends on the physical layer characterization. A detailed modelling method is then presented across C, L, S, and E bands. B5G-OPEN targets the definition of vendor-neutral YANG data models beyond C-band, and this deliverable compares existing definition for C-band systems. Preliminary design solutions are presented for metro-aggregation.

Section 4 describes the B5G-OPEN optical data plane framework. In particular, transmission subsystems include multiband sliceable transceivers with direct-detection and commercial pluggables. The latter can leverage different form factors with different complexity and power consumption for point-to-point (PtoP) or even point-to-multipoint interconnections. Innovative solutions to enhance optical switch and amplifier is also included. Future-proof solutions are presented.

Section 5 reports on access network architecture which is a converged wireline and wireless segments. It is inherently multiband as TDM-PONs exploit O- and L-bands while WDM technologies with PtoP and PtoMP operate in C and L bands. To carefully design the access with a multitude of technologies, a planning tool is presented to elaborate planning strategies. Finally, the LiFi architecture is presented.

Section 6 describes innovative solution for packet and optical monitoring. On one hand, B5G-OPEN targets integration between the packet and optical layer to save cost. A novel architecture is taking advantage of P4 in-network processing. On the other hand, optical monitoring is continuously evolving to add additional metrics and physical parameters. B5G-OPEN is particularly interested in receiver-based techniques, which requires no extra hardware, such as longitudinal power profile monitoring.

Section 7 concludes the document.

2 B5G-OPEN REFERENCE ARCHITECTURE

In WP2 (Deliverable D2.1 B5G-OPEN "Definition of use cases, requirements, and reference network architecture"), the general structure of a national-wide network including all its domains has been identified and considered as a reference for the project. This is illustrated below in Figure 2-1.

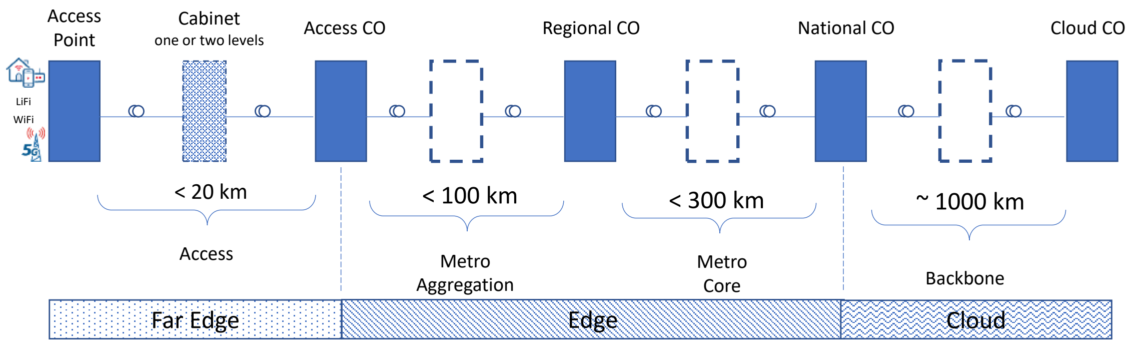

Figure 2-1: High-Level Network Diagram (From WP2).

As it is clear from what is schematically shown in Figure 2-1, the network is encompassing several domains (segments) with very different characteristics in terms of: i) number, size and role of Central Offices (COs), from several thousand in Access to tens in Metro-Core and Backbone with possibly different degree of distribution of data centres for NFV and/or for hosting third-party value-added services; ii) topologies, from simple horse-shoes or ring in Metro Aggregation to meshed in Metro-Core and Backbone; iii) requirements in term of traffic, scalability and flexibility to be supported, approximately increasing from periphery to the centre of the network, but actually greatly dependent on future – difficult to predict – geographical distribution of innovative services and their connectivity requirements; iv) cost and power consumption requirements, which become more and more stringent moving from the centre towards the periphery.

This heterogeneity makes it clearly complex – although highly desirable – to imagine a single technology or a single optical transmissive physical level approach that can fit well in all domains. This could be realized only in case several conditions could be fulfilled, among them: low-cost and low-power consumption, adaptability & scalability, sufficient optical performance over a vast range of network segments, etc. Consequently, heterogeneity in optical networks is determined by the realistic scenarios of operation.

It must also be considered that the large number of nodes of the reference network diagram naturally involves an administrative segmentation, generally associated with the network domains (segments) themselves and often inherited from the current legacy architecture. Furthermore, the number of links (fibers) and nodes are not expected to change significantly in the near future.

This implies that commonly it is not possible to optically and transparently interconnect directly two geographical separated but adjacent metro aggregation or metro core domains; on the contrary, the interconnection between separate domains of the same level must necessarily involve the crossing of segments and nodes of the higher level. For example, the interconnection between two access CO nodes in distinct aggregation networks requires the involvement of at least one core network metro segment and the related nodes. The same is true between two distinct metro core areas that require the involvement of nodes and segments of the backbone network. This results in adding up significant constraints to the optical systems involved, making transparent interconnection a challenge.

Consequently, the general goal of this document is to identify optical solutions well optimized for their specific network domain, but at the same time allowing a sufficient and technically feasible degree of transparent optical interconnection to adjacent domains.

To cope with strong estimates of large traffic growth and the consequent impact on capacity, the flexibility and scalability of the transport network are fundamental, although these estimates are highly dependent on the distribution and growth of value-added services and their clients, and on the delocalization choices of the network functions of each operator. The transport network flexible optical solution is foreseen to allow the use of several optical bands to better exploit the potential capacity of optical fibers. This degree of freedom is used as domain-dependent, nonetheless, the transparency among domains in general is not guaranteed for each band and with full flexibility as different optical systems are generally used in different network domains.

Furthermore, new services and the expected increased spread of points of presence of network and third-party services toward the access, is potentially requiring a new and more dynamic optical way to manage traffic. In B5G-OPEN this is fulfilled by a mix of optical coherent flexible high capacity and reach modules together with innovative upcoming DSCM PtoMP coherent solutions based on digital sub-carrier multiplexing and their independent steering. Thanks to the high optical performance, these interfaces could effectively enable transparent by-pass capability in the optical transport systems to dynamically interconnect nodes located in different optical domains, including access in a way that comes from traditional PtoP to the new DSCM PtoMP optical approach. Such an approach will also allow the reduction of electrical aggregation stages and replace them with simple passive optical components.

Transparency interconnection at the optical layer (media channels) among different domains carries quite naturally as a corollary of the optical partial disaggregation paradigm. In fact, it is reasonable to think that the optical network as a whole cannot be realized by a single vendor, and that different domains can be assigned to different suppliers. At the same time, the coherent transponders must be able to cross the different domains and be able to evolve in a completely independent way from the underlying optical transport systems to allow the full use of the new features that are gradually being made available. This leads precisely to the paradigm of partial disaggregation, as total disaggregation could be possible, but it is considered difficult to apply on so many levels of scale.

Integration of packet and optical domain is something that is becoming a reality thanks to pluggable DCO optical DWDM modules equipped directly on board of L2/3 switch/routers. B5G-OPEN is strongly pushing this approach together with optical partial disaggregation as long as the performance is not too degraded, to the detriment of the general network efficiency.

In summary, the general high-level requirements can be summarised as:

- Partial optical disaggregation with multi-vendor Open Line Systems (OLS) mostly independently optimized for each network segment. Systems should employ the best performance components or subsystems (e.g., an amplifier of good noise figure (NF)) under cost and power consumption constraints of each segment, to enable a reasonable degree of performance for interconnected channels;

- All OLSs should support “alien coherent lambda” and a common demarcation interface to all network segments should be specified;
- Support a fully flexible and scalable network, assuming the pay-as-you-grow paradigm in terms of deployment and also for what concerns multi-band in all network segments to allow reasonable scalability as traffics grows;
- Multi-band should not impose unacceptable performance degradation when compared to C-band parallel systems and should facilitate a smooth upgrade;
- Multi-band should not necessarily be applied to all links on a specific network segment, i.e., local multi-band is allowed for example on a link-by-link basis to support slicing of different services;
- Transparent interfaces between adjacent hierarchical network segments with maximum possible flexibility. In general, different technological solutions in different segments impose severe constrains to interconnection, but common spectral windows that are managed by both systems must always exist;
- Analogical interfaces between adjacent hierarchical network segments should be specified in terms of a range of acceptable powers, frequency, etc.;
- At least one band (or spectral regions) should exist in common to all systems to potentially guarantee end-to-end transparency;
- Nodes in Access and Regional segments are required to meet at least the drop & continue functionality to allow DSCM PtoMP;
- Pluggable transceivers on board of L2/3 switch/routers are the preferred option for “alien lambda”. If performance degradation is unacceptable transponders/muxponders/switchponders are considered as well.

3 TRANSPORT PLATFORM OPTIONS

3.1 REQUIREMENTS FOR TRANSPORT PLATFORM AND OPTICAL NODES

In the following a list of requirements are presented in some detail considering the specific optical network segments and the related COs equipment as identified in Figure 2-1. These requirements have been already identified in the two milestones: MS3.1 “Preliminary specifications and role of key data plane technologies”, and MS3.2 “Preliminary access and LiFi architecture specifications”. What is reported here is heavily based on these two internal documents.

3.1.1 Optical Access Segment and Access Central Office

Legacy operator network access CO is the closest CO to the customer. It includes Telco equipment (packet and optical) of the aggregation part of the Metro-Regional network and several equipment of the Access network including physical OLTs. Access equipment is typically physically separated from transport-packed equipment.

Legacy access CO hosts optical equipment for the metro-aggregation segment. They typically are low-cost ROADM with a low nodal degree (2 to 4); fixed grid is common and transmission client and line rates are typically 10G.

For the purpose of B5G-OPEN, one can observe that different connectivity modes co-exist in this network segment; them being PtoP or PtoMP (e.g., TDM-PON). Moreover, in the B5G era, the landscape in the Access/Aggregation segment will become even more diverse:

- WDM is readily introduced in the Access network to allow the implementation of different mobile network functional splits while saving fiber in the Aggregation segment [ITU-T G.Sup66-201907];
- For a significant period of time, the introduction of TDM PONs meant to make a large number of Access COs redundant, concentrating all (expensive) electronic processing terminals deeper in the network (Metro/Core). Nowadays, various trends related to performance (primarily latency) question this assumption. In fact, the role of Access COs becomes important to migrate processing to the network periphery and node virtualization in the context of NFV.

An Access CO for the B5G era should take into account these, and also facilitate the sharing of resources between mobile and wireline networks, that currently remain relatively decoupled from each other. Specifically, an Access CO should offer the following:

- Wireline and Wireless end-user terminals sharing the same Optical Distribution Network (ODN). This rationalizes the utilization of the fiber plant in Access. Moreover, having both PtoP and PtoMP technologies through the same ODN branch limits the need for separate fibers in the transportation network;
- The need to place cloud resources close to the end-user, at the Far-Edge Nodes, points out the necessity for computing resources (e.g., micro data centre – µDC) at the Access CO;
- It is pointed out that only a fraction of connectivity resources is terminated at the Access CO. As shown in Fig. 3.1, certain ODNs terminate to the Regional CO instead;
- There is an optical packet switch that forwards traffic flows towards the µDC facility and/or aggregate and forward flows towards the Regional CO;
- The µDC facility is used not only to support NFV applications but also it may allow the implementation of distribution unit functionality at the Far-Edge Node as well as AI/ML applications for both fixed and mobile services.

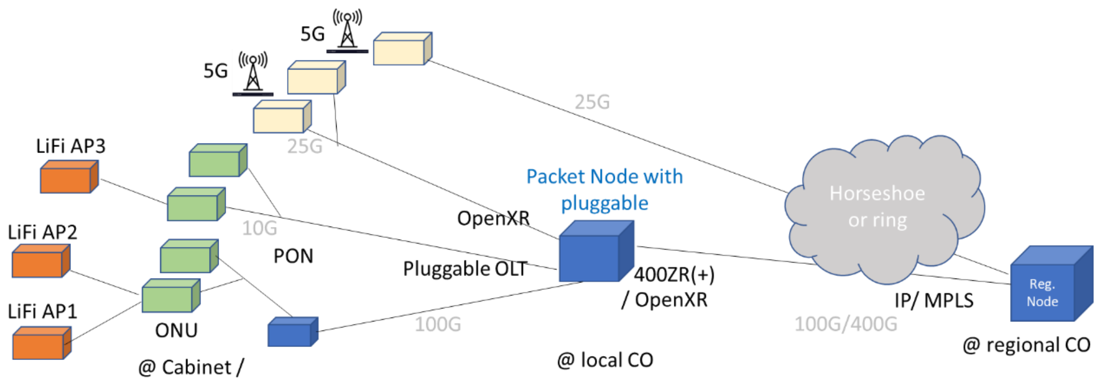

Figure 3-1: Packet Node with coherent pluggable at the central office.

3.1.2 Optical Metro Aggregation Segment

In current design, Photonic Aggregation Networks are typically ROADM-based horse-shoe structures, interconnecting several Access COs to the Metro Core network at two end nodes (Regional COs). Nodal degree is low (2 to 4) for Access nodes and add/drop capability could be quite limited due to the relatively small traffic gathered from peripheral nodes. Both flex grid and fixed grid on C-band are common. Transmission client and line rates are typically 10G or 100G. The number of Aggregation Networks in a National network ranges from one hundred to a few hundred. The maximum physical distance from an Access CO to the furthest Regional CO is of the order of 100 km.

To provide flexible capacity scaling within the metro aggregation segment, it is proposed innovative multi-band and high capacity coherent PtoP transceiversas well as adaptive DSCM PtoMP transmission. They will allow high-capacity connections while dynamically slice/allocate different data flows serving multiple destination nodes. This will enable sliceability and rate/distance adaptability for optimal spectrum usage providing increased network flexibility and availability. On the other hand, MB technology will enable the exploitation of multiple bands beyond C-band, within the transceiver, providing per band slicing towards further enhancing capacity and flexibility of the deployed optical network. Cost-effectiveness and scalability are also key transceiver design requirements to be considered particularly for the metro aggregation segment.

Concerning optical equipment, they should comply at least with these requirements:

- Optical nodes should minimize cost while maintaining sufficient flexibility;
- For Access COs, nodes with a nodal degree 2 is mandatory, while smooth upgradability to 4 degree is an interesting option. In Regional COs even a simple flexible line terminal could be sufficient being the traffic almost completely hubbed toward Regional COs;
- Fixed and flexible grid are both acceptable options;
- C, extended C, or C+L band should be sufficient for the traffic in the metro aggregation network. O-band could be employed for local traffic (single link connecting adjacent COs);
- Optical nodes must have the capability to manage both PtoP and DSCM PtoMP channels: in particular, the capabilities of drop and continue is required, and that of equalizing carriers is appreciated;
- Node in Regional COs should guarantee a sufficient degree of transparent interconnection with optical nodes of the Metro-Core segment;
- Node in Access COs should guarantee a minimum degree of direct transparent interconnection with NEs in the access network to allow local CO bypass;
- System should support a mix of coherent "alien lambdas" with a large spectrum of acceptable options in terms of symbol rate, modulation format, capacity, and capability like PtoP and DSCM PtoMP.

3.1.3 Regional Central Office

Regional COs are the interconnection points of Metro Aggregation and Metro Core networks. In the service architecture of some Operators where IP-edge and other functionalities are delocalized, a Regional CO may not only host packet and photonic equipment but also dedicated appliances for IP-edge or data-centres for services.

Concerning the photonic layer, a Regional CO hosts optical equipment from both Metro Aggregation and Metro Core network. The two systems are actually independent of each other, with different types of nodes, flexibility, grid, and generally of different vendors. No direct transparent optical interconnection between the two is feasible: on both sides, all client signals are typically received and transmitted by legacy transponders/muxponder or switchponder (of the same Vendor as the corresponding transport system) and terminated on L2/3 devices. The number of Regional COs in a National network ranges from one hundred to a few hundred.

As the Regional CO nodes interconnect the Metro Aggregation and Metro Core networks, the regional CO should be capable to process the heterogeneous traffic (at lower data rates) coming from the Metro Aggregation as well as the traffic coming from the Metro Core (at higher data rates). Moreover, the nodes include computing capability for the network and application services. Most of the Metro Aggregation traffics, carried by the multi-band channels, are dropped and processed at the Regional CO. However, there is traffic that can (have to) be directly forwarded to the Metro Core networks, and the other way around. Given the distance, such traffic is mostly transported in the C- band and eventually, as the traffic increases, in the L- and S-band.

Therefore, the Regional CO architecture should have a flexible and dynamic interconnected network that allows the seamless add/drop of the Aggregation and Core traffics to/from the packet switch and local computing network as well as the transparent bypass and direct connectivity between the Aggregation and Core networks. The Regional CO architecture should not only provide such high degree of flexibility but also the granularity and scalability in terms of capacity and number of MB channels to be processed. The node architecture requires different types of optical transmitter/receiver interfaces operating at different data rates according to the source (Aggregation/Core) and destination (Aggregation/Core) of the traffic, and supports PtoP as well as DSCM PtoMP operation. From and to the Aggregation network traffic, the type of optical interfaces are the ones discussed in Section 4. For the Metro Core interfaces, efficient transport tunable pluggable coherent modules on packed switch will be required and investigated in the project according to the capacity and distance to be covered.

3.1.4 Optical Metro Core segment

Current Metro-Core Photonic Networks are typically meshed, and their nodes typically are integrated mono-vendor flex-grid CDC ROADMs, operating in the C-band. In architectures like that of TIM with IP-edge functionalities mainly concentrated to the National COs, the role of Metro-Core network is to interconnect all the aggregation networks of a geographical area to the National Backbone Network; in other words, it gathers already aggregated traffic at packet layers from Regional COs and transport it to National COs. In more distributed architectures some of the Regional COs themselves host IP-edge and higher layer network functions or third-party services. Nodal degree ranges typically from 2 to 7, but it can be higher for National hub nodes (nodes interconnecting the backbone network). Optical channels are typically coherent at 100G or 400G; client rates are 10G and 100G. In a medium-big size European country, the number of Metro-Regional networks can be of the order of ten to twenty, each one covering an administrative region, a part of it, or even more regions. Population covered by each Regional CO can be of the order of one or a few million people. The maximum physical distance between a Regional CO to the furthest National CO is of the order of 300 km.

Requirements for Metro-Core segment should be similar to those for the backbone network (see below). Anyway, total capacity and support to spatial division multiplexing of a fiber bundle could be a bit more relaxed.

The main differences are: i) the reach is here limited to few hundred km; and ii) the need to support both PtoP and PtoMP.

Metro-Core is in a way the hinge between aggregation and core networks and thus shares requirements from both of them.

The following requirements are therefore applicable:

- Optical nodes must have the capability to manage both PtoP and DSCM PtoMP channels: in particular the capabilities of drop and continue, and of equalizing carriers are required;
- System should allow a mix of coherent "alien lambdas" with a large spectrum of acceptable options in terms of symbol rate, modulation format, capacity and capability, like PtoP and DSCM PtoMP;
- Multi-band extending to at least C-, L- and S- bands in all links of the network with low, or no degradation in comparison to parallel C-band systems on different fibers. The expected capacity increase per link should range from factors of 3 to 4 with essentially no, or very low reduction in average reach. O band could be employed for local traffic (single link connecting adjacent COs);
- Smooth upgradability from few channels in C-band to a full system load;
- New coherent interfaces allowing an average increase of spectral efficiency from 5 to 6 bit/s/Hz or more, covering transparently the same traffic paths as the legacy solution;
- Total average required capacity per link could reach a value of 270 Tbit/s (14 times the reference figure of 19.2 Tbit/s) like in the backbone, to be also achieved using parallel fiber links;
- Transparent interconnection with both metro-aggregation and backbone should be guaranteed with the maximum feasible flexibility, by employing suitable common subsets of C-, L-, or S-band.

3.1.5 National Central Office

The National CO is a big structure that hosts Telco and, possibly, IT applications. It includes hundreds to a few thousand servers for Telco virtualized Network Functions and IT applications. Being also the interconnection point among Backbone national network and several Metro Core networks, it includes packet and optical equipment of both the Metro Core and the National Backbone. The two systems are actually independent of each other, with different type of node, flexibility, grid, and generally of different vendors. No direct transparent optical interconnection between the two is feasible: on both sides, all client signals typically are received and transmitted by legacy transponders/muxponder or switchponder (of the same Vendor as the corresponding transport system) and terminated on L2/3 devices. The number of National COs within an operators' network can be between ten and one hundred.

The internal architecture of a National CO including all appliance and capability it hosts at network and service layers is very complex and strongly dependent on the Operator. As many services are delivered from here it is expected that most of the traffic from the locally connected metro core networks is here terminated. However, part of it is crossing the node to reach more central cloud CO or to reach the big internet or other regional networks. This traffic could potentially optically bypass the node transparently when feasible interconnecting the two network segments.

In general, the following requirements are applicable:

- The CO must host optical nodes (ROADMs) of both the metro-core and backbone network segments. In general, they are from different vendors and could adopt different technologies;
- For metro-core facing optical NEs, full add/drop capability should be provided;
- For backbone facing optical NEs, an add/drop capability of 30/40 % should be sufficient;
- As the capacity necessary in both network (metro- core and backbone) segments could be of the same order, both ROADM nodes should allow efficient managing of MB and multi fibers per link in a pay-as-you-grow fashion. For both equipment total node capacity should reach the order of 2 Pbit/s;
- Transparent interconnection between the two domains is mandatory employing a suitable common subset of C-, L-, and S-band;
- Systems should support both proprietary and “alien coherent lambda”. Pluggable on a router is the preferred option. If performance degradation is unacceptable, then transponders/muxponders/switchponders are to be considered as well.

3.1.6 Optical National Backbone

Current National Photonic Backbone networks are typically meshed, and their nodes are integrated mono-vendor Colorless/Directionless/Contentionless Flexgrid (CDC-F) ROADMs, operating in the C-band, with a nodal degree ranging from 2 to 8, and add-drop modules based on a multicast switch (MCS) architecture. They interconnect National nodes at the client level. Optical channel line rates range from 100G to 400G or even more, and occupy spectral slots ranging from 50 GHz to 87.5 GHz. Maximum client rates are 400G or 100G. Due to the long-reach interconnection among nodes transmission performance is the primary requirement in designing such a network. National Packet Backbone networks are based on IP/MPLS routers, and can have a hierarchical structure, with a full mesh higher tier, and lower tiers connected to the higher in dual homing. In a medium-big size European country, the number of National COs could be between ten and a few dozen. The population covered by each National CO can be of the order of one to a few million people. The maximum physical distance from an Access Point to the nearest National CO is of the order of 400 km or more.

To provide a requirement that could be used as a guideline in B5G-OPEN for the backbone network segment, we consider a time frame of 10 years and a CAGR of 30% of traffic increase on a reference network similar to Italian national backbone [ICOP2022]. Traffic is extrapolated from the known reference matrix and incremented maintaining the same distribution. In the considered time frame traffic will increase by a factor of 14. An existing reference high-capacity legacy optical transport system is considered for comparison. A typical transport system in this network segment is based CDC-F ROADM on C-band with an internal architecture placed on a switch and select employing 1x20 WSS (two for each line degree) and typically allowing up to 8 line ports and 16 add/drop flexgrid ports. Such a node scale smoothly up to 8 nodal degrees with a maximum of 13 add/drop modules allowing up to 208 add/drop channels.

Considering state-of-the-art commercially available coherent interfaces and the distribution of distance ranges in connections in the reference network, a weighted average spectral efficiency of order of 4 bit/s/Hz should be achievable with average media channels of 75 GHZ width with 300 Gbit/s average net transported capacity on each media channel. Thus, a typical fiber link connecting two nodes brings in C-band (4.8 THz) an average of 64 media channels for a total aggregated net capacity of 19.2 Tbit/s. Using the same reference numbers, a CDC-F ROADM node could manage up to 150 Tbit/s of total capacity (8 degrees; 64 media channels per fiber/degree; 300 Gbit/s average channel net capacity).

We can now provide some requirements that should allow optical systems to be able to handle the estimated traffic needs in the 10 years frame considered, bringing it to a state equivalent to the current one in terms of use and occupation of the network.

Requirements:

- Total average required capacity per link of at least 270 Tbit/s (14 times the reference figure of 19.2 Tbit/s) to be also achieved using parallel fiber links;
- Multi-band extending to at least C-, L- and S-band (possibly including E- and O-bands) in all links of the network with low or no degradation in comparison to parallel C-band systems on different fibers. The expected capacity increase per link should range from 3 to 4 with essentially no or very low reduction in average reach;
- Smooth upgradability from few channels in C-band to a full system load;
- New coherent interfaces allowing an average increase of spectral efficiency from 4 to 5 bit/s/Hz or more covering transparently the same traffic paths as the legacy solution;
- Spatial Division Multiplexing is unavoidable in the long-term perspective. Thus, nodes should be able to manage at least a few parallel fibers nodal degree. No “special fibers” are in the scope of B5G-OPEN;
- New node architecture should allow efficient managing of MB and multi-fibers per link in a pay-as-you-grow fashion. Total node capacity should reach the order of 2 Pbit/s;
- Systems should support both proprietary and “alien coherent lambda”;
- Concerning “Alien lambda” the common demarcation interface should be implemented by the employed systems.

3.2 Design methodologies

B5G-OPEN investigates the performance and design of multi-band optical systems. A disaggregated abstraction of the physical layer may be considered when evaluating the quality of transmission (QoT) of coherent-transmission systems i.e., we may assume that each network element introduces a power gain or loss and possibly some amount of Gaussian disturbance. In these systems, the impact of nonlinear fiber transmission is well approximated as additive Gaussian noise in lightpaths with sufficient accumulated chromatic dispersion [POG17, Can18], therefore, validating the GN approximation for NLI. Consequently, the QoT of a LP can be estimated using the generalized signal-to-noise ratio (GSNR), which includes the effect of the additive Gaussian disturbances introduced by the optical amplifiers (amplified spontaneous emission) and the nonlinear interference due to the self- and cross-channel nonlinear crosstalk resulting from optical fiber propagation. In this case, the GSNR of channel *i* after transmission along one fiber span is given by:

$$GSNR_i = \frac{P_i}{P_i^{ASE} + P_i^{NLI}}$$

where P_i is the output power, P_i^{ASE} is the accumulated ASE noise and P_i^{NLI} is the power of accumulated nonlinear effects of channel *i*. The same approach is followed in GNPy [GNPY], where it was shown that this is a suitable metric for the QoT estimation in modern coherent multilevel-modulated uncompensated wavelength division multiplexed (WDM) optical transmission systems.

Such optical systems cannot be quickly simulated with standard split step Fourier methods, and therefore approximations are needed. In B5G-OPEN, we are investigating different level of approximations of the Manakov equation – which is the foundation of propagation over fiber with dual polarization – such as the one reported in [GNPY, SEM18, Uzu19].

3.2.1 Quality of Transmission Estimation

The introduction of optical MB transmission systems in the existing Backbone and Metro networks is a challenging task where multi-facet questions need to be concurrently addressed: each optical band under consideration, namely O, E, S, C and L, has its own frequency-dependent propagation characteristics (α, D, γ, a_{eff} , etc.), while the most of the critical components/sub-systems are not mature yet so there are performance-wise questions compared to their C-band only counterparts.

B5G-OPEN is poised to understand what impact the interplay between the performance of components/sub-system and the fiber propagation effects may have on the attainable “*capacity* x *length”* in each band. Moreover, the deduction of a comprehensive method to analyse the physical layer performance of links and paths in Backbone and Metro networks is pivotal to B5G-OPEN’s goal to support network automation that is based in open interfaces under an SDN-enabled control/management framework. To complete this task, the project needs a path computational engine (PCE) that takes into account the physical layer performance of the different bands.

Table 3-1: Physical Modelling (Transmission) Assumptions and Benefits (summary).

Method	**Approach**	**Assumptions**						
		Gaussian Noise	Modulation format effects	Impact of ISRS on NLI	Raman Gain profile	Accumulation of SPM	Accumulation of XPM	Uniform launch power
FWM (OLC-E method)	Closed-form	YES	YES	YES	Triangular	Coherent	Coherent in link, incoherent between links	NO
GGN	Integral	YES	NO (not relevant)	YES	Real	Incoherent	Incoherent	NO
	Closed-form	YES	NO (not relevant)	YES	Triangular		Incoherent	YES
GN-ISRS	Integral	YES	YES	YES	Real	Coherent	Incoherent	NO
	Closed-form	YES	YES	YES	Linear	Coherent	Incoherent	YES
	Closed-form and Exponencial decay	YES	YES	YES	Linear	Coherent	Incoherent	YES
Stanford GN-ISRS	Integral	YES		NO	---			
Enhanced GN-ISRS		YES	YES	NO	---			YES

Table 3-2: Physical Modelling Assumptions and Benefits (detailed discussion).

Method	Approach	Assumptions	Pros	Cons
OLC-E method	**Closed Form**	❖GN-model assumptions are used: the Gaussian Noise assumption is performed due to which NLI is statistically independent from ASE noise while considering it as an additive Gaussian noise source. Each WDM channel can be treated as Gaussian noise source • The impact of modulation format is also accounted for ❖$P_{NLI,SCI}$ is assumed to accumulate coherently between the different spans of the path, considering an average span length. $P_{NLI,XCI}$ is assumed to accumulate coherently between the different spans of the link, considering an average span length and incoherently between the different links ❖Assumes a linear (triangular) Raman gain spectrum of up to 15 THz and includes the impact of spectrum between 15 and 35 THz using a log-like function ❖Assumes a sliding window according to which a specific channel gives energy to higher ones up to 35 THz and gains energy from the lower ones from up to 35 THz ❖Single span assumption: the impact of SRS is equal in each span even when the SRS tilt in power is compensated after a number of spans (e.g. at the node via WSS) ❖Includes the impact of SRS-NLI using the effective channel power attenuation where (the signal power profile) is relatively small. ❖Applies also in cases when the SRS tilt is not compensated after each span	❖Very good balance between accuracy and complexity ❖The only available closed-form expression for SRS's impact beyond 15 THz ❖Has been validated numerically for optical bandwidths of up to 25 THz (E, S, C and L-bands) ❖The maximum error is less than 0.8 dB over an entire path (benchmarked in numerous scenarios against numerical results) ❖Accounts for different power between channels (network case) ❖Very accurate in links with span length <30 km (i.e. Metro networks or short links)	❖Inaccurate when the accumulated dispersion per span is less than about 150 ps/nm (<5-7 km of SSMF) ❖For large ISRS power transfers (e.g. > +21 dBm total power), the signal power profile is not accurately modelled
GGN model	**Default Model**	❖All approximations of Integral-form GN-model hold	❖The gain/loss of each interfering channel is included leading to more accurate estimations	❖Overestimates the variance of nonlinear interference, most notably in the first spans of the link, where this error may amount to several dB's, depending on system parameters and modulation format ❖Requires numerical integration of a triple integral so not suitable in the context of PLI-RMSA algorithms

	Closed Form	❖The presence of an SRS-induced loss is assumed to be a small perturbation vs. the bulk of loss, which is due to fiber loss ❖The triangular approximation for SRS is performed ❖Equal power (uniform power) for all WDM channels is considered	❖Good balance between accuracy and complexity	❖Overestimates the variance of nonlinear interference, most notably in the first spans of the link, where this error may amount to several dB’s, depending on system parameters and modulation format ❖Does not account for different power between the channels ❖Erroneous when dispersion is smaller than about 2 ps/(nm km) ❖The fiber loss should be larger than 8-10 dB (e.g. > 40 km)
GN-ISRS approach	**Integral Form**	❖GN-model assumptions are used: the Gaussian Noise assumption is performed due to which NLI is statistically independent from ASE noise while considering it as an additive Gaussian noise source; also the impact of modulation format is also accounted for; each WDM channel can be treated as Gaussian noise source ❖In the context of perturbation based models, the impact of ISRS on the Kerr effect is modeled by changing the effective attenuation (the signal power profile) across the transmitted spectrum to resemble the average effect of ISRS, neglecting temporal fluctuations. ❖Assumes a linear (triangular) Raman gain spectrum of up to 15 THz ❖only the SPM contribution is assumed to accumulate coherently while the XPM contribution is assumed to accumulate incoherently	❖Has been validated numerically for optical bandwidths of up to 10 THz for specific conditions ❖Has been validated experimentally for 9 THz range	❖Cannot be used to attain results in real-time ❖The formula can be extended beyond 15 THz by reinterpreting α, α^{-} and Cr as channel dependent quantities. The parameters are then chosen to match the actual power profile of each channel and the proposed modulation format correction formula can be applied. The cost is the larger complexity as the Raman equations must be solved numerically and additional regression operations are necessary in order to obtain the channel dependent α, α^{-} and Cr.
	Closed Form	❖All approximations of Integral-form GN-ISRS hold ❖For the XPM, the frequency separation between the channel of interest and the interfering channel is much greater than half of the channel bandwidth ❖The impact of ISRS on the effective channel power attenuation (the signal power profile) is small, which means that it can be approximated by a first-order Taylor series (0.23 · Δρ (L) [dB] << 6) ❖The effective channel power attenuation is only a function of the total launch power and	❖Has been validated numerically for optical bandwidths of up to 10 THz for specific conditions ❖Very good compromise between accuracy and simplicity (average error of 0.45 dB in the examined cases) ❖Accounts for different power between the channels (network case)	❖Increasing discrepancy with increasing launch power is due to the weak ISRS assumption. This assumption has more impact on the outer channels as the net ISRS gain is larger. ❖The assumption $e^{-\alpha L}$ <<1 is erroneous in short spans (e.g. 10, 20 km)

		independent of its spectral distribution. This assumption has no impact on a uniform launch power distribution. ❖ The assumption $e^{-\alpha L} << 1$ is made		
	Closed Form a_{eff}	❖ Approximates ρ (z; f) with exponential decays, that have modified attenuation coefficients or effective lengths. This assumption leads to a modified attenuation coefficient a_{eff} instead of a. ❖ The effective attenuation approach is valid for lumped amplification in the weak ISRS regime	❖ minor additional complexity with respect to the conventional GN model	❖ For higher accuracy one needs to solve the Raman equations and then perform regression operations to obtain the coefficients $a_{eff,l}$ ❖ For large ISRS power transfers, the signal power profile is not accurately modelled by exponential decays ❖ Yields significant errors in the outer channels ❖ The assumption $e^{-\alpha L} << 1$ is erroneous in short spans (e.g. 10, 20 km)
GN-ISRS (Stanford)	**Integral Form**	❖ GN-model assumptions are used: the Gaussian Noise assumption is performed due to which NLI is statistically independent from ASE noise while considering it as an additive Gaussian noise source; also the impact of modulation format is accounted for; each WDM channel can be treated as Gaussian noise source ❖ Assumes that the impact of Raman gain on the strength of the Kerr nonlinearity is negligible	❖ Good approximation in long uncompensated links where the accumulated dispersion is large ❖ Accurate in systems employing pre-dispersion	❖ Overestimates the variance of nonlinear interference, most notably in the first spans of the link, where this error may amount to several dB's, depending on system parameters and modulation format ❖ Requires numerical integration of a triple integral so not suitable in the context of PLI-RMSA algorithms
Enhanced GN-ISRS		❖ The power is uniformly distributed across the WDM bandwidth and SRS is weak ❖ Includes the impact of SRS on ASE noise ❖ Applies in cases when the SRS tilt is not compensated after each span	❖ Significantly lower complexity compared with full integral form of EGN model ❖ Has been validated numerically for optical bandwidths of up to 10 THz for specific conditions	❖ Complex expressions which despite their approximations cannot be used to attain results in real-time

Table 3-3: Quality of transmission (QoT) methods references.

QoT method	**References**

OLC-E Tool	D. Uzunidis, K. Nikolaou, C.Matrakidis, A. Stavdas and A. Lord, “Closed-form Expressions for the Impact of Stimulated Raman Scattering Beyond 15 THz”, ECOC 2022 D. Uzunidis, C. Matrakidis, E. Kosmatos, A. Stavdas and A. Lord, “On the Benefits of Power Optimization in the S, C and L-Band Optical Transmission Systems,” Computer Networks, vol. 211, pp. 108958, Jul. 2022. D. Uzunidis, E. Kosmatos, C. Matrakidis, A. Stavdas and A. Lord, "Strategies for Upgrading an Operator's Backbone Network Beyond the C-Band: Towards Multi-Band Optical Networks," in IEEE Photonics Journal, vol. 13, no. 2, pp. 1-18, April 2021. D. Uzunidis, C. Matrakidis, E. Kosmatos, A. Stavdas, P. Petropoulos, A. Lord, “Connectivity Challenges in E, S, C and L Optical Multi-Band Systems”, in European Conference of Optical Communications, ECOC’ 21, 2021.
GGN Model	A Real-Time Closed-Form Model for Nonlinearity Modeling in Ultra-Wide-Band Optical Fiber Links Accounting for Inter-channel Stimulated Raman Scattering and Co-Propagating Raman Amplification M. Cantono, D. Pilori, A. Ferrari, and V. Curri, “Introducing the Generalized GN-model for Nonlinear Interference Generation including space/frequency variations of loss/gain,” 2017, arXiv:1710.02225. M. Cantono et al., “On the interplay of nonlinear interference generation with stimulated raman scattering for qot estimation,” J. Lightw. Technol., vol. 36, no. 15, pp. 3131–3141, Aug. 2018. M. Cantono, J. L. Auge, and V. Curri, “Modelling the impact of SRS on NLI generation in commercial equipment: An experimental investigation,” in Proc. Opt. Fiber Commun. Conf., 2018, Paper M1D.2.
GN ISRS approach	D. Semrau et al.: Achievable rate degradation of ultra-wideband coherent fiber communication systems due to stimulated Raman scattering, Optics Express, 25, (12), pp. 13024–13034, May 2017 D. Semrau, R. I. Killey, and P. Bayvel, “The gaussian noise model in the presence of inter-channel stimulated raman scattering,” J. Lightw. Technol., vol. 36, no. 14, pp. 3046–3055, Jul. 2018. G. Saavedra et al., “Inter-channel stimulated raman scattering and its impact in wideband transmission systems,” in Proc. IEEE Opt. Fiber Commun. Conf. Expo., 2018. D. Semrau et al.: A closed-form approximation of the Gaussian noise model in the presence of inter-channel stimulated Raman scattering, J. Lightw. Technol., 37, (9), pp. 1924–1936, January 2019 D. Semrau, E. Sillekens, R. I. Killey and P. Bayvel, "A Modulation Format Correction Formula for the Gaussian Noise Model in the Presence of Inter-Channel Stimulated Raman Scattering," in Journal of Lightwave Technology, vol. 37, no. 19, pp. 5122-5131, 1 Oct.1, 2019. D. Semrau, R. I. Killey and P. Bayvel, "Overview and Comparison of Nonlinear Interference Modelling Approaches in Ultra-Wideband Optical Transmission Systems," 2019 21st International Conference on Transparent Optical Networks (ICTON), 2019.
GN ISRS (Stanford approach)	I. Roberts, J. M. Kahn, J. Harley, and D. W. Boertjes, “Channel power optimization of WDM systems following Gaussian noise nonlinearity model in presence of stimulated raman scattering,” J. Lightw. Technol., vol. 35, no. 23, pp. 5237–5249, Dec. 2017.
Enhanced GN ISRS	P. Serena, C. Lasagni, S. Musetti, and A. Bononi, “On numerical simulations of ultra-wideband long-haul optical communication systems,” J. Lightw. Technol., vol. 38, no. 5, pp. 1019–1031, Mar. 2020. C. Lasagni, P. Serena and A. Bononi, "A Raman-aware enhanced GN-model to estimate the modulation format dependence of the SNR tilt in C+L band," 45th European Conference on Optical Communication (ECOC 2019), 2019. C. Lasagni, P. Serena and A. Bononi, "Modeling Nonlinear Interference With Sparse Raman-Tilt Equalization," in Journal of Lightwave Technology, vol. 39, no. 15, pp. 4980-4989, Aug.1, 2021.

Table 3-1 gives an overview of the current state-of-the-art which allows the reader to understand the advantages and disadvantages of the main performance evaluation methods available in the literature. A list of the main references associated with each of the QoT estimation method can be found in Table 3-3.

To give further context to Table 3-1, three key effects must be (accurately) modelled by the QoT estimator: the power evolution of channels along the optical fiber, the NLI and the ASE power. There are different alternatives for NLI and power evolution estimation leading to different trade-offs of accuracy and complexity. An exhaustive discussion on the computational complexity and accuracy of each different approach can be found in [Sou21] where it is shown that the impact of ISRS may be neglected, as done in the GN model, for total transmission bandwidths of up to approximately 5 THz. On the other hand, the effect of ISRS should be taken into account when considering wider transmission bandwidths. For transmission bandwidths of up to approximately 10 THz, such as C+L-band transmission, the triangular approximation of the ISRS gain profile, as used in the ISRS-GN model, is an efficient approach to estimate the NLI and the power evolution of the channels enabling to achieve high accuracy while requiring only very small computational time. For even wider transmission bandwidths of up to 15 THz, the triangular approximation may still be used for the NLI estimation, therefore validating the use of the ISRS-GN model, but the power evolution of the channels should be calculated using the numerical solution of the Raman equations. For even wider transmission bandwidths, the GGN model is an alternative that potentially provides an accurate estimation of the QoT.

As an example in Table 3-2, the method proposed by OLC-E was adopted to model the physical effects that degrade transmission performance via closed-formed expressions. The proposed method offers good accuracy in practical transmission scenarios while it returns results with a computation time that is in pair with the requirements of PCE/planning tools. As such the proposed approach can be used to support higher-layer networking functions.

Within the Telecom Infra Project (TIP), the QoT using the open-source GNPy [GNPY] library was extensively validated numerically and experimentally in C-band, but also in [Dam22] in multi-band transmission systems.

3.2.2 Physical Layer Characterization

The accuracy of the QoT estimation depends not only on the assumptions that are done when developing each method but also on the accuracy of the modelling of the physical layer. As such, a list of the main parameters required for the comprehensive characterization of each element of the optical system is provided in Table 3-4 to Table 3-6.

Table 3-4: Optical Fiber Characterization (SSMF – G.652D used as reference).

Parameter	Example of reference values		
	C-band	L-band	S-band
Input/Output connector attenuation [dB]	0.25	0.25	0.25
Attenuation coefficient [dB]	0.187	0.186	0.203
Chromatic dispersion [ps/nm/km]	17	19.4	14
Effective Area [μm^2]	80	83	76
Nonlinear refractive index	2.2e-20	2.2e-20	2.2e-20
Nonlinear Coefficient[$W^{-1}km^{-1}$]	1.3	1.2	1.4
Raman gain coefficient [m W^{-1}]	0.4	0.4	0.4

PMD [$pskm^{-1/2}$]	0.01	0.01	0.01

Please note that some of the optical fiber parameters shown in Table 3-4 are frequency dependent and only the value at the central frequency of each band is indicated for reference. As an example, the optical fiber attenuation and chromatic dispersion show a frequency dependence as illustrated in Figure 3-2.

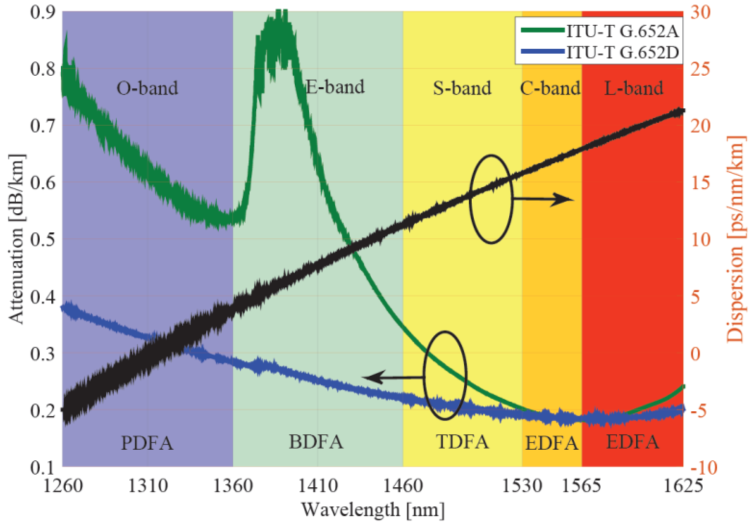

Figure 3-2: Fiber parameters (attenuation and chromatic dispersion) for ITU-T G.652A and G.652D fibers [FER20].

Additionally, the use of several potentially different optical amplifiers is envisioned for each transmission band. The use of several amplifiers may be required due to several reasons: amplifiers have a limited transmission bandwidth and optical output power; the best doping materials for each band may be different, e.g., Erbium for C- and L-band and Bismuth or Thulium for S-band. Additionally, Raman amplification may also be explored to further improve the optical performance of links. A more exhaustive illustration of possible amplification approaches to enable multi-band transmission is depicted in Figure 3-3.

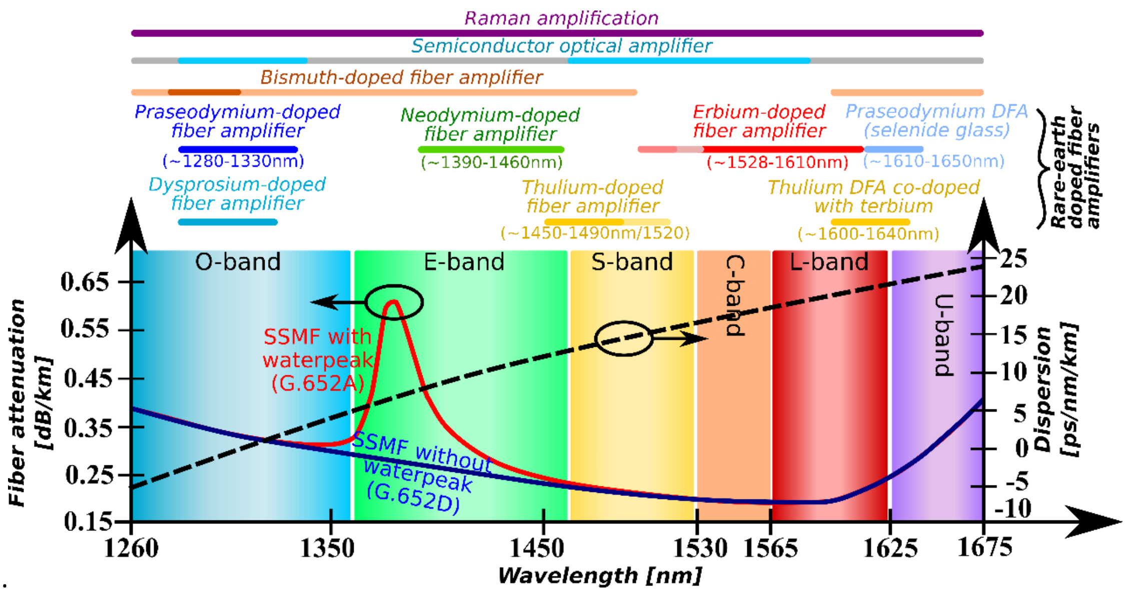

.

Figure 3-3: Possible optical amplification alternatives to enable multi-band transmission [Rap22].

Just as a reference, a possible characterization of optical amplifiers is provided in Table 3-5.

Table 3-5: Optical Amplifiers Characterization.

Parameter	Example of reference values		
	C-band	L-band	S-band
Min Gain [dB]	5	5	5
Max Gain [dB]	30	30	30
Min. Target Output Power [dBm]	-10	-10	-10
Max. Target Output Power [dBm]	20	20	20
Min. Input Power [dBm]	-30	-30	-30
Max. Input Power [dBm]	10	10	10
Noise figure [dB]	5.0	5.5	6
Noise figure ripple[dB/THz]	0	0	0
PDL [dB]	0.2	0.2	0.2

Additionally, the optical transponders' comprehensive characterization is also fundamental for the accurate assessment of the QoT. The main parameters required to characterize an optical transponder can be found in Table 3-6. These parameters are a shortlist of the ones provided in Open ROADM MSA and the most relevant ones for optical performance evaluation analysis.

Table 3-6: Optical Transponders Characterization.

Parameter	200-400G (Open ROADM MSA)
Symbol rate [Gbaud]	63.1
Line rate [Gbps]	200G (QPSK): 252.6 300G(8QAM): 378.8 400G(16QAM): 505.1
ROSNR@0.1nm [dB]	200G: 17 300G: 21 400G: 24
TX power [dBm]	[-5 - 0]
TX OSNR [dB]	36
Laser linewidth [kHz]	300
Roll off factor	0.05-0.2
PDL penalty[dB]	0.5: <1dB accumulated PDL 1: <2dB accumulated PDL 2.5: <4dB accumulated PDL

RX input power (OSNR) penalty [dB]	400G: 1.0 dB at -16dBm input power 400G: 2.0 dB at -18dBm input power 300G: 1.0 at -18dBm input power 300G: 2.0 dB at -20dBm input power 200G: 1.0 at -20dBm input power

3.2.3 Physical layer modelling of optical multi-band systems

In an optical multi-band system, the dominant physical layer impairments that degrade the system performance are ASE noise, Non-Linear Interference (NLI) (intra-band effects) and Stimulated Raman Scattering (SRS) (inter-band effect). In order to assess their impact on the transmitted signal in an MB link, we employ the merit function Optical Signal to Noise plus Interference Ratio (OSNIR) which is given by [UZU21-1], [UZU21-2], [CAS21], [UZU22].

$$OSNIR_j = \frac{P_{ch,j} \cdot \prod_{i=1}^{N_s} G_{SRS,i,j}}{P_{ASE,j} + P_{NLI,j}} \qquad (3.1)$$

where j and i denote the channel and fiber span under examination, respectively. Ns equals to the number of fiber spans a channel is traversing; $P_{ch,j}$ denotes the power at link ingress for the channel under observation, $G_{SRS,i,j}$ calculates the SRS Gain/Loss effect for the i^{th} fiber span and j^{th} channel, $P_{NLI,j}$ is the power of NLI generated in the link and $P_{ASE,j}$ the power of ASE noise accumulated in the link. The closed-form expressions that estimate $P_{NLI,j}$ and $P_{ASE,j}$ are analyzed in Appendix A.

As optical amplification technology, we consider the use of xDFAs placed in parallel (Figure 3-4). This allows to directly extend the ducts deployed for C-band EDFAs while allows a pay-as-you-grow strategy for the activation of new bands [UZU21-1]. Based on the details of commercially available or close to commercialization amplifiers, their main characteristics can be summarized in Table 3-7. As it is evident, the S-band is split into S_1 and S_2 sub-bands since a single TDFA may not provide sufficient power per channel at its output (e.g. larger than -2 dBm) as the S-band is extended to ~ 55 nm, so a disproportionally larger number of channels, compared to those in the C-band, need to be amplified.

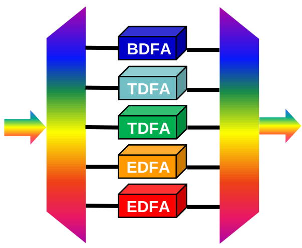

Figure 3-4: Amplifier connectivity scheme.

Table 3-7: Details of xDFA amplifiers used in our study.

	Used Range (nm)	Noise Figure (dB)	Amplifier Type	Pout,max (dBm)
E band	1400-1440	6.0	BDFA	17
S_1 band	1455-1480	5.5	TDFA	20

S_2 band	1485-1510	5.5	TDFA	22
C band	1530-1565	5.5	EDFA	22
L band	1570-1615	6.0	EDFA	22

3.2.3.1 Use Case A – systems extended beyond 15 THz

For the estimation of the SRS-induced gain/loss, the formula of [CHR96] is mainly exploited in the literature as it is accurate and in closed-form which is a very important feature in the context of Physical Layer Aware-Routing Modulation and Spectral Assignment (PLA-RMSA) algorithms. This expression makes the assumption of the *triangular approximation* according to which the power exchange between channels due to SRS can be calculated using a triangular shaped spectrum up to a 15 THz extent [CHR84]. However, although this approximation accurately estimates the power exchange between the channels spaced up to 15 THz, the interference of channels beyond 15 THz is neglected. This can lead to erroneous estimation of SRS impact as the 1260 nm to 1625 nm spectrum corresponds to a spectral window of more than 15 THz. To address this challenge, the straightforward way is to employ coupled differential equations as in [SEM17]. These expressions estimate the impact of SRS across an arbitrarily wide spectrum; however, their computational complexity constrains them for use in network planning tools which need to perform multiple calculations in real-time.

To the best of our knowledge, there is no closed-form expression for the estimation of SRS impact when the channels are spaced more than 15 THz. To tackle this problem, we introduce a novel expression which extends the triangular approximation (~15 THz) to wider spectral parts (up to 35 THz) as shown in Figure 3-5 (red curve).

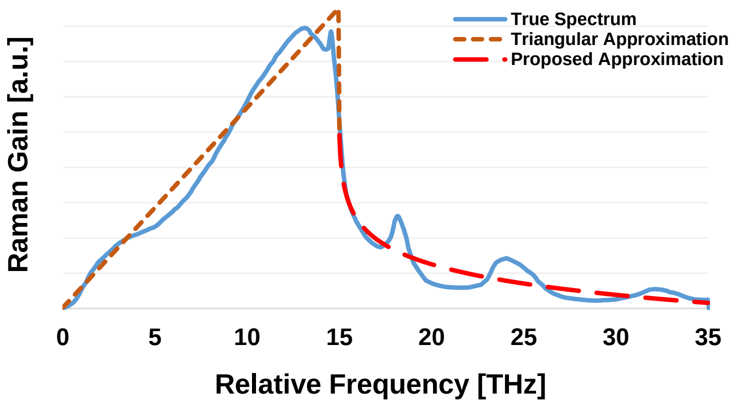

Figure 3-5: True and approximated Raman spectrum for a standard single mode fiber.

To estimate the impact of the SRS between channels of an MB system which is extended beyond 15 THz, we can sum the contributions on the SRS-induced Gain/Loss from two different components as:

$$G_{SRS,i,j} = G_{SRS,\,\leq 15THz,i,j} + G_{SRS,\,>15THz,i,j} \tag{3.2}$$

where the first component represents the interaction of channels with frequency difference up to 15 THz and can be calculated as follows [CHR96]

$$G_{SRS,i,j} = P_{tot,SRS} \frac{e^{\frac{g' \cdot B \cdot L_{eff,i,j}}{2A_{eff,i,j}}(j-1)P_{tot,SRS}}}{\sum_m \left[P_{m,0} e^{\frac{g' \cdot B \cdot L_{eff,i,j}}{2A_{eff,i,j}}(m-1)P_{tot,SRS}} \right]} \tag{3.3}$$

In (3.3), g' is the Raman gain slope equal to $4.9 \cdot 10^{-27}$ m/(W·Hz), $A_{eff,i,j}$ is the effective cross-sectional area of the i^{th} fiber span for the j^{th} channel frequency, m is the index of an interfering channel with a spectral distance up to a 15 THz from j and $P_{m,0}$ is its power at the input of the fiber segment. The term $P_{tot,SRS}$ is the sum of the power from all channels that interact within the 15 THz spectrum and B is the spectral distance of the interfering channels.

The second term in (3.2) is an approximation of the long tail in the true Raman spectrum (Figure 3-5, red curve) for channels with a spectral distance more than 15 THz and it is estimated by

$$G_{SRS,>15THz,i,j} = \sum_k \left[\frac{P_k G_{SRS,peak}}{0.85 P_j} \left(0.49 - 0.08 Log \left[\frac{\left(|k-j| B' - 15 \right)}{0.05} + 1 \right] \right) \right] \tag{3.4}$$

In this expression k is the index of a channel with a spectral distance > 15 THz ($k > m$) from channel j and P_j and P_k are their launch powers at fiber input, respectively. The SRS gain in this spectral region is calculated with the aid of the quantity $G_{SRS,peak}$ which is the maximum Gain/Loss contribution in (3.3) of channel with index m in channel j (in essence the Gain/Loss calculated by (3.3) between these channels minus 1). Further, B' is introduced in (3.4) in THz. With the aid of (3.2)-(3.4), the SRS-induced power exchange for a spectrum up to 35 THz can be estimated.

The formalism of (3.2)-(3.4) is applied in systems with a spectral extent beyond 15 THz by making the *sliding window assumption*. According to this assumption, two sliding windows of triangular shape are employed, the first to calculate the power transfer towards the channel under study from lower wavelengths while the second estimates the power transfer from the channel under study towards the higher wavelengths.

Benchmarking of the proposed formalism against a numerical method

The effectiveness of the proposed formalism is benchmarked against the results from a commercially available simulation tool. The simulation tool is employing the Split Step Fourier Method to numerically solve the corresponding nonlinear equations for the propagation in optical fiber based on the true Raman spectrum of Figure 3-5 (blue curve). A wide sample-mode bandwidth is selected, so the SRS interactions between any pair of channels within the E to the L band are taken into account. The value of the number of simulated bits is set to 8,192 per polarization. Moreover, an in-built Digital Signal Processing (DSP) module is used to mitigate the impact of effects like chromatic dispersion and polarization mode dispersion. In addition, G_{SRS} is calculated after each span by comparing the power of the observed channel at fiber input with its power after the corresponding per band Doped Fiber Amplifier that compensates exactly the fiber loss. To achieve this, the amplification scheme of Table 3-7 is also adopted here while the power per channel is set to -4 dBm in all bands. Figure 3-6 demonstrates the evolution of the G_{SRS} after a single span of 50 km for the central channel in each band as a function of the number of the concurrently active channels. Two closed-form expressions are compared: a) the proposed formalism of (3.2)-(3.4) (the dots) and (b) the use of (3.3) that neglects the impact of SRS beyond 15 THz (the triangles).

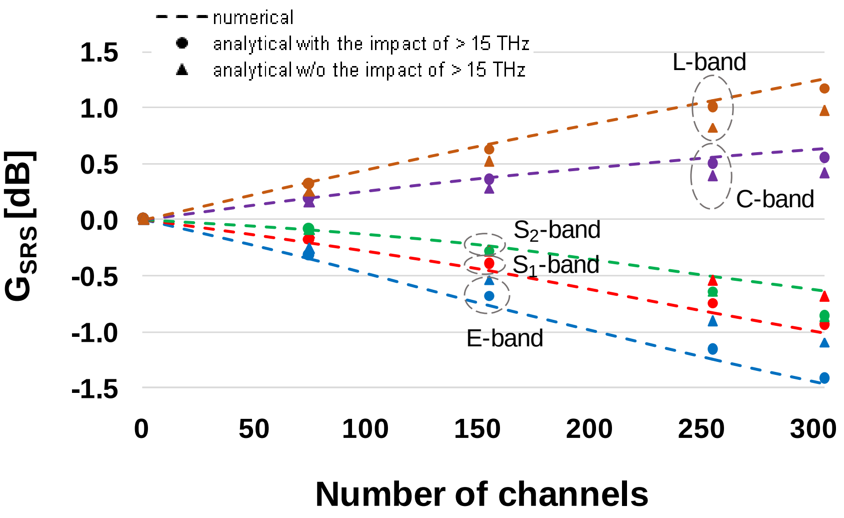

Figure 3-6: Evolution of SRS vs number of channels after a single span of 50 km.

It can be deduced from Figure 3-6 that the maximum deviation between the results from (3.2) -(3.4) and the corresponding from the numerical method is 0.13 dB. In this case, the maximum error is 0.34 dB. While this error accumulates with the number of spans, the impact of SRS is erroneously estimated, as the 0.2 dB per span difference accumulates in longer path links. This error is fully evident when a large number of channels is present but it is less critical when a smaller number of channels is considered (or when lower power per channel is injected in the fiber).

Figure 3-6 demonstrates the G_{SRS} for the central channel of each band only while Figure 3-7. illustrates the G_{SRS} evolution for 255 channels across the MB spectrum after a single span of 50 km. From this figure we can observe that the proposed formalism is in a very good agreement with the numerical results, as the maximum deviation is 0.18 dB. In comparison, when the power coupling of channels spaced more than 15 THz is ignored, the mismatch is up to 0.42 dB.

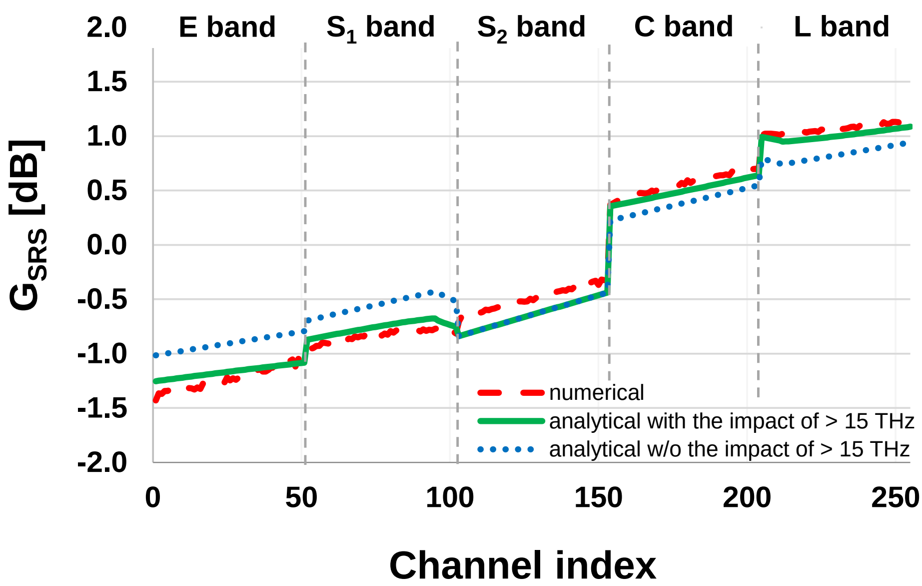

Figure 3-7: SRS Gain/Loss after a single span of 50 km for the different channels of an MB system.

3.2.3.2 Use Case B – Tailoring the OSNIR performance per band across the entire spectrum of interest

Due to SRS, there is a power exchange between the channels in different bands. For this reason, the physical layer performance of all bands needs to be optimized collectively. This optimization is carried out by means of a merit-function F’ that is minimized using the launch-power of the channels in the bands as an optimization parameter. In particular, the merit-function F’ and the optimization goals are the following:

$$\begin{aligned}
&F'\left(P_1, P_2, \ldots, P_{N_{ch,\mathrm{tot}}}\right) = \sum_{b=1}^{N_{ch,\mathrm{tot}}} \alpha_b \left(\frac{1}{OSNIR_b\left(\ldots,\ P_{b-1},\ P_b,\ P_{b+1},\ldots\right)} \right)^2 \\
&\mathit{minimize}\ \ F'\left(P_1, P_2, \ldots, P_{N_{ch,\mathrm{tot}}}\right) \\
&\mathit{subject\ to}\ \ P_{\min} \le P_1, P_2, \ldots, P_{N_{ch,\mathrm{tot}}} \le P_{\max},\quad P_{tot,SRS} \le +21\,dBm
\end{aligned} \tag{3.5}$$

In eq.(3.5), α_b are suitably chosen parameters that weight the impact the OSNIR of the channels in a specific band have on merit-function F’; $N_{ch,total}$ denotes the total number of channels across all bands that contribute to the OSNIR degradation due to SRS. As an indicative example, the following procedure is followed to deduce the optimal launch power that balances the OSNIR performance of the wavelength channels across the entire spectrum of interest:

- The Operator sets high-level performance objectives regarding how the wavelength channels in the available bands are used to transport flows. If the wavelengths are requested to have the same optical reach, F’ is minimized in a way that the OSNIR variation is < 1 dB across all bands for the particular link leading to ‘flat’ performance response. Other high-level goals are also possible e.g. to increase the optical-reach a band has (or a number of bands) at the expense of others. In these cases, the weights for each band are selected accordingly.
- The minimization of F’ is carried out using a number of system-level constraints as follows:
  a) The P_{min} is ‘low-value bounded’ to avoid having OSNR values below a certain (BER defined) threshold. As an example, this value could be P_{min} = - 10 dBm.
  b) The P_{max} is ‘high-value bounded’ to avoid operating the xDFA at the deeply saturated regime. As an example, this value could be P_{max} = + 1 dBm.
  c) The maximum allowable total power in the system due to SRS $P_{tot,max}$ is restricted to an upper value e.g. +21 dBm. By means of this constraint the impact of SRS on NLI becomes a second order effect [SEM18] and thus it can be ignored without a significant penalty. This assumption is well aligned with experimental works [GAL20], [PUT21-1], [PUT21-2] where the overall power in the three bands is always lower than +20 dBm to limit the SRS-induced loss.
- In the case where all bands are present in a link (i.e. b={E, S1, S2, C, L}), the mostly affect band due to SRS is the E band and then, to a lesser extent, is the S_1 and S_2. As a result, the weights {α_b} in eq.(3.5) for a balanced OSNIR performance are set to beef up the OSNIR primarily for the E band and to a lesser extent the S_1 and S_2 bands, at the expense of the OSNIR in C and L bands. That is, the α_e , α_{s1} , α_{S2} are assigned a higher value compared to α_C , α_L. Trial-and-error estimations return the approximate values for the weights {α_b} and with the aid of a mathematical s/w package we obtained the values of launch power per band and the exact values of α_b that minimizes F’. In this particular

case where the OSNIR across all bands vary < 1 dBm, α_b gets the values {12, 1, 1, 0.4, 0.5} for the {E, S1, S2, C, L}, respectively.

- The optimization returns the power for the central channel in the spectrum for each band. Similar procedure is adopted to deduce the per channel or group of channels optimal launch power within a given band.

This optimization method is applied for two paths with 450 km and 900 km in length, respectively. In this example, we assumed inter-node distances of 150 km and span length equal to 50 km. The impact of NLI and ASE noise is estimated using (3.1) and the expressions of the appendix, while the G_{SRS} is calculated via (3.2)-(3.4). To limit the impact of SRS in longer paths, WSS-based nodes are assumed to perform power equalization. This ensures that the power at the egress of all nodes remains constant for the channels of all bands. As the compensation of the SRS induced Loss/Gain is performed in a per node basis, we exploit the formalism of Section 4.2 of [UZU22] to calculate the OSNIR of an entire path. Regarding the corresponding performance estimation via the simulation tool, the computational capabilities of our workstation (AMD Ryzen 5 3600, NVidia GeForce GTX 1660, 80 GB RAM) allow the transmission of up to 155 channels (31 channels per band).

Following the aforementioned procedure with α_b {12, 1, 1, 0.4, 0.5} (~ < 1 dB variation in the OSNIR performance across the entire spectrum of interest), the minimization of F’ in eq. (3.5) leads to a launch power via for the central channels in the {E, S_1, S_2, C, L} bands of {-1.85, -6.3, -7.68, -8.8, -8.6} dBm and {-1.72, -6.6, -8.0, -8.9, -8.8} dBm for two systems with 75 and 155 channels, respectively.

Next, G_{SRS} was calculated for each channel based on Eqs. (3.2)-(3.4) and we used this value to set the attenuation that mitigates the impact of the SRS via the corresponding WSS-based node. Finally, to obtain the corresponding OSNIR via the numerical method, the BER is measured after the DSP based receiver and then the Eq. (5) of [UZU16] is used to deduce the OSNIR value. It is important to mention that, the power allocation strategy stresses the larger wavelength channels, e.g., those in S_2, C- and L-bands to operate in the ASE-limited regime, as their power increases via SRS during transmission. At the same time, the optimum power of E-band is significantly higher compared with the S_2, C- and L-bands, as the power of E is significantly depleted during transmission, via SRS. These are important conclusions, as in order to attain a flat OSNIR performance across all bands, the power of the higher wavelengths needs to be maintained as low as possible, in order to reduce the impact of SRS in the lower ones.

Figure 3-8 illustrates the OSNIR performance using a) the closed-form expression (red, circles) and b) the simulation tool (blue, triangle), for the first, the middle and the last channel of each band (1^{st}, 8^{th}, 15^{th}). The difference between those two methods is < 0.73 dB in all four paths. This error is mainly attributed to a) the non-ideal mitigation of SRS after each node, as even a small error in the calculations becomes considerable after 450 km, and b) the approximations used to generate the closed-form formalism for the NLI in [UZU19]. However, this error is considered acceptable as not only it is less than 1 dB, but also all channels still maintain an almost flat ripple (less than 1 dB) across the entire spectrum of interest spanning over 200 nm.

Another important observation is that the resulting OSNIR value between the two systems (75 and 155 channels) is similar. This is expected, as the power allocation method aims to compute the power in each channel in way that the impact of SRS is minimized, maintaining the power of the higher bands to the deeply linear regime where ASE noise dominates. To further clarify this, the calculated values of G_{SRS} in dB for the channels of {E, S_1, S_2, C, L} bands, using the formalism of (3.1)-(3.5), were {-0.146, 0.068, 0.198, 0.173, 0.169} and {-0.292, 0.142, 0.385, 0.335, 0.329} for 75 and 155 channels, respectively. These values are significantly smaller compared with the G_{SRS} of Figure 3-7 and enhance the argument that the SRS’s impact has to be minimized if the target is to attain a flat OSNIR performance across all bands.

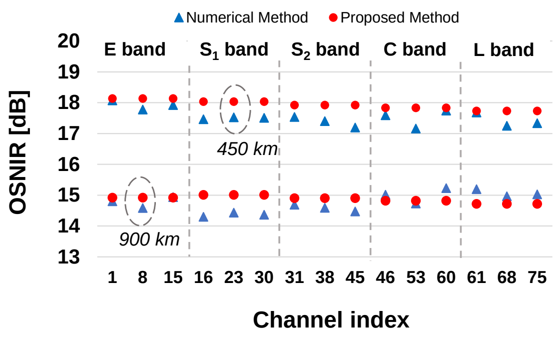

(a)

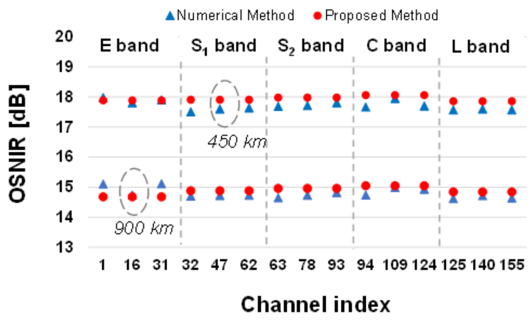

(b)

Figure 3-8: OSNIR performance for a system with a) 75 channels (15 in each band), b) 155 channels (31 in each band) and path distances of 450 and 900 km.

3.2.3.3 Use Case C – modelling of a core network with non-equidistant amplifiers

The proposed closed-form formalism of (3.1) for OSNIR calculation cannot be directly applied to a national network, as the expressions for NLI strictly apply only for transmission paths with equidistant optical amplifiers, which is not the case in a national network. To estimate the OSNIR for a path with non-equidistant amplifiers, we need to make the following assumptions.

a) First, we assume that every optically transparent node across an end-to-end path employs a WSS in its transit path. In this way, all channels in a given band are entering the fiber of the next link at the same nominal power level.
b) Second, we consider that all channels of one band are attenuated in order their power to be aligned with the power of the most depleted channel of the band. To satisfy this, we consider the existence of the corresponding attenuation per channel, including in this way in the modelling the combined effect of fiber attenuation, band filter loss and SRS. As a consequence, the gain of each amplifier is now a function of the SRS gain/loss.
c) Third, although we consider the real inter-node distances for the estimation of SRS and ASE noise impact, for the calculation of NLI in Eq.(3.1) we theoretically assume equidistant amplifier spacing in all links as follows. The distance, $L_{amp,av|link}$, equals to the length of a given link divided by the real number of amplifiers in it and $L_{amp,av|path}$, equals to the length of a given path divided by the real number of amplifiers in it. This approximation allows to calculate $P_{NLI,SCI}$ using the average length of the path and the equations of the appendix in a straightforward way. Next, to calculate $P_{NLI,XCI}$, first we calculate the $P_{NLI,XCI|link}$ for a given link considering the average link length and then the NLI of an end-to-end path by adding the Cross Channel Interference (XCI) contributions from all links. This methodology is illustrated in Figure 3-9 for a path consisting of N_l links and each link comprises $N_{s,l}$ spans.

In this case, the ASE noise for the entire path can be computed using the following formula

$$P_{ASE,j} = \sum_{l=1}^{N_l}\left[\sum_{i=1}^{N_{s,l}}\left[hf_j\left(NF_{i,j}\cdot G_{i,j}-1\right)B_0\prod_{r=i+1}^{N_{s,l}}G_{SRS,r,j}\right]/\left(\prod_{m=1}^{N_{s,l}}G_{SRS,m,j}\right)\right] \quad (3.6)$$

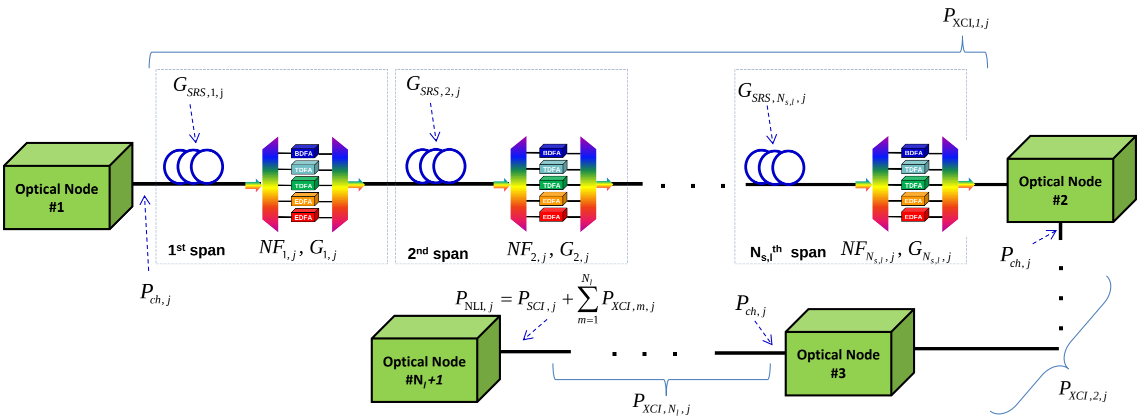

Figure 3-9: Schematical illustration of the proposed methodology used to calculate the impact of NLI within a network path with non-equidistant amplifiers when E, S, C and L bands are considered.

To conclude on design methodologies, many physical layer impairments have been proposed in the recent years, extended from C-band to MB systems. A popular GNPy library can be used beyond C-band by adding extensions or alternatively B5G-OPEN may also rely on OLC-E tool.

Beyond QoT, techno-economics analysis for MB transmission systems can also use the GNpy library. Some recent examples include a comparison of the capacity and energy consumption in translucent and transparent multi-band (from S- to U-band) optical network designs (see ref. [Sad22]) and the investigation of the best band upgrade order on an S+C+L system in a pay-as-you-grow approach, aiming to maximize the end-of-life system capacity under the constraint of not disrupting already running services (see ref. [Sou22]).

3.3 B5G-OPEN DESIGN PARAMETERS

Impairment-aware path computation is a key functionality in optical networks. Traditionally, it has been implemented using proprietary tools and algorithms which leverage on proprietary data models. B5G-OPEN targets the definition of vendor-neutral YANG data models for SDN-based impairment-aware path computations. Besides C-band, full support to multi-band operations is envisioned. Currently, two main initiatives are ongoing for the definition of common models and solutions for impairment-aware path computations. The first one, led by IETF, consists in the definition of a YANG Data Model for Optical Impairment-aware Topology [IETF]. The related Internet Draft is a relatively mature document (version 10) which however considers C-band only. The second initiative, led by the Open Optical & Packet Transport (OOPT) - Physical Simulation Environment (PSE) group of Telecom Infra Project (TIP), refers to development of GNPy [GNPY]. GNPy is a well-known open-source library for building route planning and optimization tools based on the Gaussian Noise Model. Although GNPy does not define a YANG data model, its specific input/output parameters are widely adopted and preliminary extensions to multi-band scenarios have been proposed.

In B5G-OPEN, we aim at defining a comprehensive YANG data model that can be compatible with both the IETF model and GNPy-based solutions in the context of C-band. Furthermore, the model will define the relevant parameters to be considered for multi-band impairment-aware path computation.

3.3.1 Transmission parameters

B5G-OPEN defines and identifies a set of transmission parameters based on different initiatives, previously described and led by IETF and OOPT-PSE group [IETF, GNPY], in order to be used by the impairment validation tool(s) part of the overall control infrastructure of the project.

On the one hand, the IETF characterizes the transceivers by properly describing three different approaches (called "modes") to describe their capabilities from a path computation perspective. In particular, the model includes the standard mode (related to the optical specification to ITU-T G.698.2), the organizational mode (organizations like operator groups, industry fora, or equipment vendors can define their own optical interface specifications and make use of transceiver capabilities going beyond existing standards) and the explicit mode (which allows to encode, explicitly, any subset of parameters). Hence, the identified parameters of the explicit mode are: supported modes, line-coding-bitrate, Bit/symbol rate, max-polarization-mode-dispersion, max-chromatic-dispersion, chromatic-and-polarization-dispersion-penalty, max-diff-group-delay, max-polarization-dependent-loss-penalty, available-modulation-type, min-OSNR, min-Q-factor, available-baud-rate, roll-off, min-carrier-spacing, available-fec-type, fec-code-rate, FEC-threshold, min-central-frequency, max-central-frequency, central-frequency-step, tx-channel-power-min, tx-channel-power-max, ro rx-channel-power-min, ro rx-channel-power-max, ro rx-total-power-max.

As an extension of the IETF model, OpenConfig considers additional parameters to augment the IETF operational mode. It is part of the OOPT-PSE group. These additional parameters are grid type, Otsi media channel, effective media channel, state-of-polarization (SOP), filter shape, and filter order.

On the other hand, the GNPY open-source library is based on the state-of-the-art Gaussian Noise (GN) model. The aim is to provide a vendor-neutral software tool for simulating physical impairments in dispersion unmanaged systems. Ongoing development of GNPY focuses on flexible rate and multiband optical systems. In the current version, GNPY relies on a list of supported transponders which shall include type variety (i.e., a unique ID name), min and max frequency, and mode. The mode or list of modes is defined as follows: format (i.e., a unique ID name), symbol-rate, minimum required OSNR in 0.1nm, bitrate, roll off factor, transmitter OSNR and cost. For each mode, the set of parameters can also be further expanded with vendor-specific data, which consists of symbol-rate, minimum required OSNR in 0.1nm, bitrate, roll off factor, transmitter OSNR, grid spacing, min and max value of received power, max allowed Chromatic Dispersion (CD), max allowed polarization mode dispersion (PMD). Three more parameters may be included soon as they are currently under test, these are CD penalty, Differential Group Delay (DGD) penalty and PMD penalty. Note that GNPY does not track the Forward Error Correction (FEC) performance, so it is recommended to indicate it in the name of the transponder mode.

In Table 3-8, we compare the two main initiatives as well as OpenConfig. Within B5-OPEN, OLC-E is developing a planning tool that is based on a physical layer model described in the previous section and a routing modulation and spectrum assignment (RMSA) detailed in D4.1. To be able to simulate physical impairments it relies on transmitter parameters which are also included in Table 3-8.

As expected, there are many transmission parameters in common which are relevant to predict performance of new lightpaths. Else, we notice that IETF parameters are more numerous and advertise better the supported capabilities of optical front ends. It should then be easier to give an alignment with line system parameters and with interface model. Therefore, the B5G-

OPEN proposed extensions will be based on the IETF explicit mode parameters with the addition of the transmitter OSNR which may be important in some scenarios for performance prediction.

Table 3-8: Comparison of IETF and GNPY transmitter parameters.

IETF explicit mode	GNPY	OpenConfig	OLC-E tool
supported modes	mode		operational mode
bit rate	bit rate		data rate
baud rate	baud rate	baud rate	symbol rate
min OSNR	required OSNR in 0.1nm		can be extracted by 'Additional parameters'
roll off	Tx roll-off	filter roll off	can be extracted by 'Additional parameters'
central frequency step	grid spacing	adjustment granularity	slot spacing
min central frequency	min frequency		min frequency
max central frequency	max frequency		max frequency
rx-channel-power-min	min Rx power		min Rx power
rx-channel-power-max	max Rx power		max Rx power
max CD	CD max		-
max PMD	PMD max		-
chromatic and dispersion penalty	CD penalty		-
	PMD penalty		-
max diff group delay	DGD penalty		-
Additional parameters: min Q-factor, min carrier spacing, rx-total-power-max, tx-channel-power-min, tx-channel-power-max, max PDL penalty, FEC type, FEC code rate, FEC threshold, modulation type	Additional parameters: Tx OSNR	Additional parameters: grid type, otsi media channel, effective media channel, SOP, filter shape, filter order, modulation format	Additional parameters: transmitted power range, emission frequency range, received power range, receiver frequency range, FEC type, FEC code rate, FEC threshold, DSP type, bandwidth, modulation format

3.3.2 Line system parameters

Similar to the transmission parameters, the two main initiatives (i.e. IETF and GNPy) are also defining line system parameters. They can be divided into 4 categories: span, fiber, amplifier and ROADM. The line system parameters are summarized in Table 3-9.

Regarding the optical fiber channel, note that there are various optical fiber types defined by ITU-T, including several fiber-level parameters, such as, fiber-type, length, loss coefficient, PMD, and additional parameters depending on the initiatives.

Table 3-9: Comparison of IETF and GNPy line system parameters.

IETF	GNPY	OLC-E tool
	Span	
Grid Delta Power	Grid Delta Power Range	-
Additional parameters: Generalized SNR, Equalization Mode, Nominal Carrier Power, Nominal Power Spectral Density, Media Channel Group	**Additional parameters:** Maximum Span Length, Fiber Loss Ageing (EOL), Maximum linear fiber loss for Raman.	**Additional parameters**: topology and number of nodes, Inter-node distances, Inter-span distances
	Fiber	
Length	Length	Length
Loss coefficient	Loss coefficient	Loss coefficient
PMD	PMD coefficient	PMD coefficient
Additional parameters: Total loss, Input connector loss, Output connector loss	**Additional parameters:** Dispersion, Dispersion slope, Effective area, Nonlinear coefficient	**Additional parameters:** Dispersion, Dispersion slope, Effective area, Nonlinear coefficient, Raman gain slope
	Amplifier	
Gain	Minimum Gain and Maximum Gain	Gain
Output VOA	Automatic Output VOA Setting	Flat amplification range
Raman Direction	Propagation Direction	-
Raman Pump Frequency	Raman Pump Central Frequency	-
Raman Pump Power	Total Raman Pump Power	-
Additional parameters: Total Output Power, Lower frequency, Upper frequency, tilt target, Input VOA, Nominal Carrier Power, Nominal Power Spectral Density,	**Additional parameters:** Minimum Noise Figure, Maximum Noise Figure	**Additional parameters**: Amplifier type, Amplifier operational mode, Flat amplification range, Noise Figure, Small signal Gain, Maximum output power, Band filter attenuation

ROADM		
PMD	PDM	-
PDL	PDL	-
OSNR	Add/Drop OSNR	-
Additional parameters: Minimum Power, Maximum Power, Typical Power, Lower Frequency, Upper Frequency, Chromatic Dispersion (CD), In-band crosstalk, Minimum Losses, Maximum Losses, Typical Losses, Noise Figure (NF)	**Additional parameters:** ROADM egress channel power setting.	**Additional parameters:** total loss

3.4 DESIGN SOLUTIONS FOR HIGH-CAPACITY METRO-AGGREGATION NETWORKS

Metro-aggregation networks represent one of the most important and fast-growing segments in modern telecommunication networks. It is the bridge between access and core; thus, it is the domain where different technologies meet, namely direct and coherent detection. Nowadays, the former is the main technology employed in access, while the second has recently made its appearance in the metro for what concerns the data centre interconnect market.

In [Bac22], we compared two scenarios, both using coherent detection to aggregate traffic: the PtoP and PtoMP one, to address metro-aggregation. The first assumed the so far existing coherent pluggable working in PtoP; while in the second we employed smart transceivers, which are based on digital subcarrier multiplexing. The latter can generate virtual channel at the transmitter, which can be aggregated with passive optical components, thus enabling filterless network by broadcasting signals. After aggregation, the WDM channel acts as any other ITU-T grid compatible channel, without need of changing anything in the OLS.

The two network topologies studied in [Bac22] were provided by TIM, and they have been used to compare the network design when we consider a PtoP versus a PtoMP coherent pluggable. These topologies, reported in Fig. 2 of [Bac22] depict a typical horseshoes metro scenario, where several leaf nodes are connected to a pair of hubs to allow protection. The considered networks are named “urban-industrial” and “suburban-rural”, where the first resembles the network of a mid-size European city with the presence of industrial sites, the second is typical of a less densely populated area and almost without industrial settlements. In the case of the second network, optical amplifiers were placed every 18 dB of span losses. The assumptions on traffic are also reported in the same article, and they differentiate among three different scenarios about the time horizon: short, medium and long term.

a) *Urban / industrial*

Urban	Short	Mid	Long
P2P	123	123	123
P2MP	84	84	96
Savings	-32%	-32%	-22%

b) *Suburban / rural*

Regional	Short	Mid	Long
P2P	106	106	106
P2MP	70	70	82
Savings	-34%	-34%	-23%

The results presented in the table above show a significant advantage in using PtoMP coherent technology versus an equivalent PtoP, because of the level aggregation, i.e., less transceivers, and the better match with a dynamical-fast-growing traffic: a) report the case for urban/industrial, while b) the one for suburban/rural. Clearly, such an advantage would also translate into additional benefits for what concerns power consumption, reduced number of devices, and footprint.

Further studies on designing optical networks for urban scenarios have been carried out also in [Hos22-1, Hos22-2]. Here, we optimized the deployment of PtoMP transceivers with respect to the case with PtoP ones, reporting saving of ~35% by utilizing a suitable set of data rates for a wide range of traffic loads. Besides horseshoe-based metro networks, we also considered the design of high-capacity ring network in [Pav22-1] for a fault tolerant analysis with more general traffic profiles. Here, we proposed a Mixed ILP formulations for multilayer capacity planning to minimize the total transceiver costs, considering both PtoP and PtoMP transceivers, as well as a heuristic approach for the more complex PtoMP case. Our results indicate that PtoMP optics can bring several advantages for all tested traffic profiles, ranging from pure uniform flows to mostly hub-and-spoke (H&S). Transceiver cost savings are achieved in various cases, greater at higher network loads and for traffic patterns that are mostly H&S. Results also show that PtoMP optics prompt a multilayer redesign of the network with significantly reduced spectrum usage, and a reduced number of IP hops, resulting in Lower Optical-Electronic-Optical and IP processing latency, and lower IP layer equipment costs, for all traffic profiles. This work has been later expanded into [Pav22-2] where we proposed a first generalized dimensioning algorithm for optical networks with DSCM and PtoMP coherent transceivers, which covers hub-spoke determination, transceiver allocation, along with light-tree routing and spectrum assignment, in arbitrary topologies.

Network design is not only about the deployment of elements and devices. In [Sha22-1, Sha22-2], stemming from [Vel21], we show how the particular feature of DSCM can be used for a more efficient usage of the optical spectrum.

At the moment, we are optimizing further aspects concerning the design of optical networks: we submitted an OFC contribution on the optimization of the ratio of the splitter / combiner [Hos23] and we investigate how to exploit the benefits of digital subcarrier to better design a network which can support different type of traffic, varying over time [Her23].

4 OPTICAL SUBSYSTEMS, SWITCHING AND AMPLIFICATION

4.1 TRANSMISSION SUBSYSTEMS

4.1.1 Multiband prototypes

In the framework of T3.2 of B5G-OPEN new transmission solutions based on the adoption of cost-effective, modular MB sliceable bandwidth/bitrate variable transceivers (S-BVTs) have been investigated to enable possible operation across multiple bands such as C-, L-, and S- band, as a way to provide suitable and flexible capacity-scaling towards meeting the beyond 5G stringent requirements in terms of bandwidth, capacity and efficiency. The proposed transceiver architecture, depicted in Figure 4-1, enables network scalability and flexibility as includes multiple bandwidth/bit rate variable transceivers (BVTs)/building blocks that can work in multiple transmission bands and can be enabled and disabled according to the traffic demand and network needs, providing an efficient use of the available resources. Additionally, this approach facilitates and supports the coexistence of both PtP and PtoMP high-capacity optical connections/modes within the metro-aggregation and regional networks.

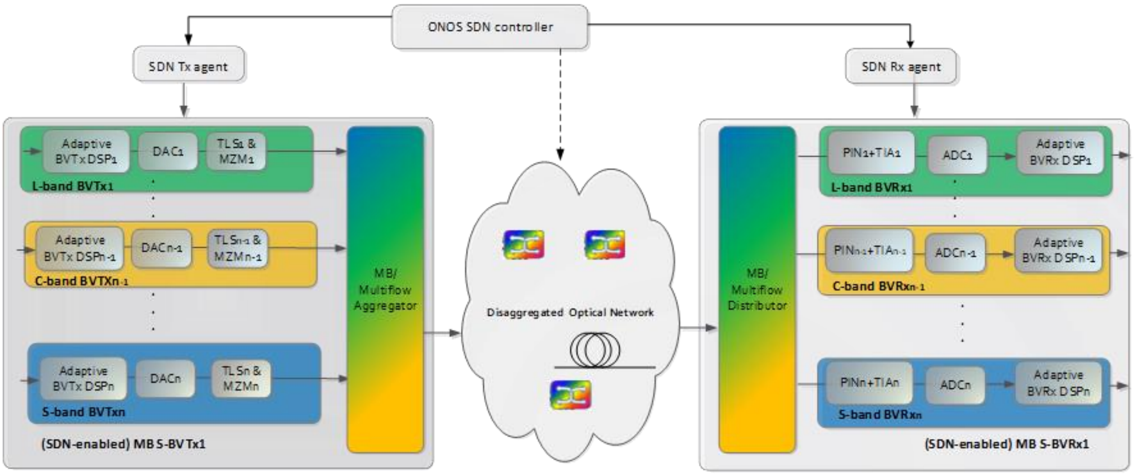

Figure 4-1: (SDN-enabled) MB S-BVT architecture.

In particular, at the transmitter side, the proposed scalable and modular MB S-BVT comprises an adaptive digital-signal processing block which is based on multicarrier modulation (orthogonal frequency division multiplexing, OFDM) in order to enable sub- and super-wavelength granularities, while enhancing the overall system’s flexibility by implementing bit and power loading algorithms, which assign different number of bits and power values at each subcarrier according to the channel profile [Nad22-1, Nad21]. A simple optoelectronic front-end based on a high-speed digital-to-analog converter (DAC), a Mach-Zehnder modulator (MZM) and a tunable laser source (TLS) is investigated to enhance transceiver cost-effectiveness. The TLS can be set up to the suitable wavelength to enable MB transmission. On the other hand, at the receiver side, a simple photo-detector (PIN) followed by a transimpedance amplifier (TIA) and an analog-to-digital converter (ADC) are envisioned to perform direct detection (DD). A key component/device of the transceiver is the MB multiflow aggregator/distributor which should operate at different lambdas beyond C-band to support MB transmission. Hence, different options are investigated within the project to implement such a device. Specifically, it can be implemented by using commercial multiple optical amplifiers and wavelength selective switches (WSSes) working at C- and L-bands or other programmable filters that are limited to a tuning range around a specific wavelength beyond C-band combined with band splitters and/or combiners or optical band pass filters [Nad22-1].

Key programmable transceiver parameters have been identified towards future implementation of software-defined networking (SDN) agents capable to configure the transmission system dynamically and efficiently, while managing the enormous bandwidth available due to MB. It is particularly relevant to consider and investigate open data models, such as OpenConfig, to implement a unique SDN agent for the S-BVT while fostering vertical disaggregation of the transceivers by separating the data plane from the control plane. Some identified programmable transceiver parameters, also aligned with IETF YANG data model for optical impairment-aware topology draft [IETF], GNpy open-source library [GNPY] and OpenConfig data model [OpenConfig], can include the bit/symbol rate, baud rate, modulation format, min-/max- central frequency, min-carrier-spacing or tx-channel-power-min/-max, between others.

Initial simulations and experimental activities have been performed including the assessment of a proof of concept of the proposed (SDN-enabled) MB S-BVT. In particular, as a first step, MB transmission is analyzed over different fiber lengths without considering any amplification and filtering stages, in order to evaluate the performance of the different investigated bands, which include S-, L- and C- band, in similar conditions [Nad22-1, Nad22-2]. On this regard, the setup, depicted in Figure 4-2, has been considered.

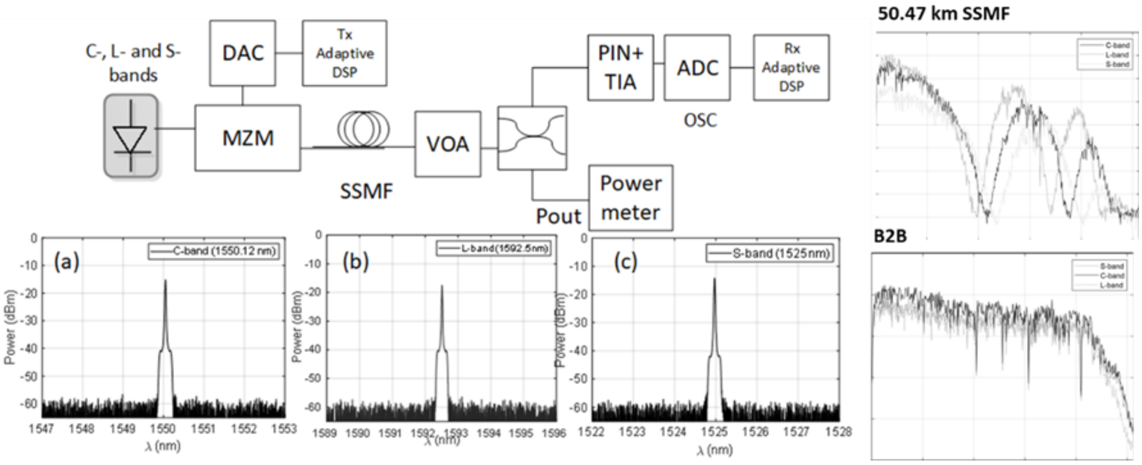

Figure 4-2: Proof of concept of the MB S-BVT. (a) C-band (b) L-band and (c) S-band spectra. In the right insets: SNR (top) after 50.47 km of SSMF (bottom) in B2B of the three analyzed bands.

Double side band 20 GHz OFDM signals with 512 subcarriers are created and digital-to-analog converted with a high-speed DAC working at 64 GSa/s. The analog signal is modulated by means of a MZM, working at the quadrature point, and a TLS with maximum output power of 9 dBm and centered at the different wavelengths, summarized in table Table 4.1, covering different transmission bands (C-, L- and S-bands). At the receiver side, a 100 GSa/s oscilloscope is used as ADC. At the DSP level, different modulation formats per subcarriers are implemented including BPSK and optimized m-QAM constellations ($m = 2^l$; $2 \leq l \leq 8$), according to the bit/power loading algorithm for adaptive mapping. The Levin-Campello rate adaptive bit/power loading algorithm is considered in order to maximize the system capacity at a fixed/target performance according to the estimated SNR per subcarrier. A target BER of $4.62 \cdot 10{-}3$ with standard hard decision FEC, is fixed [Nad22-1]. The considered overheads due to training symbols, cyclic prefix and FEC are 4%, 1.9% and 7%, respectively.

Table 4-1: Simulation parameters.

Parameter	C-band	L-band	S-band
λ (nm)	1550.12	1592.5	1525
D (ps/nm/km)	17.5	19.9	15.27
α (dB/km)	0.23	0.21	0.26

A numerical analysis of the proposed (SDN-enabled) MB S-BVT is performed taking into account the fiber parameters detailed in Table 4-1. In particular, the propagation over SSMF is modeled with the split-step Fourier method, considering different attenuation values (α) and fiber dispersion coefficients (D), according to the selected center wavelength (λ) to transmit at different bands. The transmission of a single slice over different bands (C-, L- and S-bands), without amplification and filtering, and fiber lengths up to 50.47 km has been numerically and experimentally evaluated.

According to the inset of Figure 4-2 (right-bottom), where the back-to-back (B2B) SNR profile of the analyzed slices working beyond C-band is depicted, the three analyzed wavelengths present similar performance. However, after 50.47 km of SSMF, the attenuation peaks due to CD appear at different frequencies, depending on the considered wavelength/band, see Figure 4-2 (right-bottom). Figure 4-3, shows the MB S-BVT proof of concept assessment in terms of capacity vs fiber length, considering a fixed fiber input power of -4.6 dBm, different transmission bands and fiber lengths, up to 50.47 km. The presented numerical and experimental results are in good agreement. From the figure, it can be seen that 64 Gb/s is ensured in B2B for the three analyzed bands. However, the capacity of the C-band slice decreases to 33 Gb/s and 15 Gb/s, after 25.2 km and 50.47 km of SSMF, respectively. The L-band contribution achieves similar results, whereas considering S-band, the capacity is slightly reduced, achieving 28.5 Gb/s and 8.5 Gb/s after 25.2 km and 50.47 km of SSMF.

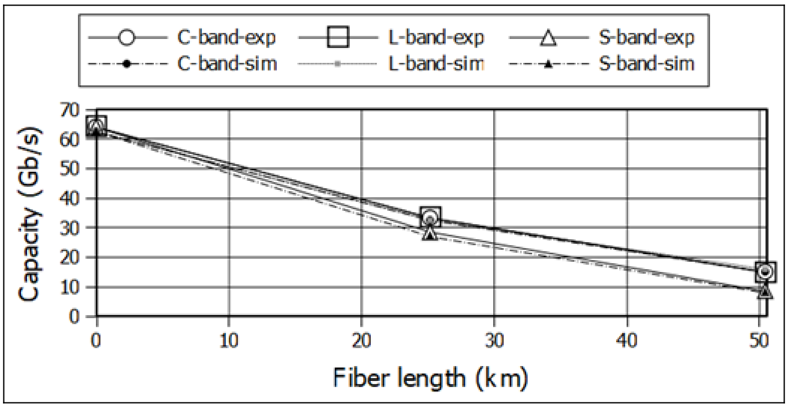

Figure 4-3: Numerical (sim) and experimental (exp) analysis of the achieved capacity vs fiber length for different transmission bands.

Finally, additional experiments are performed by considering different receiver powers, as summarized in Table 4-2. Specifically, a higher capacity per band of 70 Gb/s can be achieved at -2.7 dBm in B2B. After 25.2 km of SSMF, maximum capacities of 45.1 Gb/s and 37.5 Gb/s are achieved working at the selected C-band and L-band wavelengths at −7.2dBm and −9.3 dBm, respectively. 37 Gb/s S-band transmission is ensured at −8.4 dBm. After 50.47 km of SSMF, C-band and L-band transmission allow 26.2 Gb/s and 20.5 Gb/s capacities at −11.4 dBm and −13.6 dBm, respectively. On the other hand, S-band transmission shows a capacity penalty of about

17% at −11.9 dBm, with respect to the two alternative lowest-loss analyzed wavelengths. This is mainly due to the impact of fiber impairments at this wavelength as shown in the SNR profile figure of Figure 4-2.

Table 4-2: Preliminary MB S-BVT performance without considering filtering and amplification stages.

Optical path	C-band max. capacity (Gb/s)	L-band max. capacity (Gb/s)	S-band max. capacity (Gb/s)
B2B	70	70	70
25.2 km	45.1	37.5	37
50.47 km	26.2	20.5	21

These preliminary results show the viability of the MB S-BVT as a key enabler of future 6G networks to target the stringent capacity/bandwidth requirements by means of the exploitation of multiple transmission bands beyond C-band. In fact, taking into account these preliminary numbers, maximum total capacities of 202.3 Gb/s, 120.1 Gb/s and 67.7 Gb/s can be enabled in B2B and after 25.2 km and 50.47 km of SSMF, considering a potential MB S-BVT architecture that aggregates the contribution of the three different slices/bands. Moreover, further scaling the S-BVT capacity, up to 160, 300 and 350 channels of 25 GHz bandwidth can be potentially transmitted occupying the whole available C-, L- and S-band, respectively. Hence, the total aggregated capacity per band can be also scaled with the number of available channels per band. Accordingly, potential aggregated capacities of 54.2 Tb/s, 31 Tb/s and 17 Tb/s can be enabled in B2B and after 25.2 km and 50.47 km of SSMF, by exploiting the full spectra of the available/analyzed bands. In fact, due to its narrow bandwidth (160 channels), C-band provides the lowest aggregated capacity followed by L- and S-band, respectively, so exploiting alternative bands becomes an interesting and suitable solution to face future 6G network needs.

Table 4-3 summarizes the main control parameters to reconfigure the MB-SBVT prototype by means of SDN agents.

Table 4-3: MB-SBVT control parameters.

Prototype	Control Parameters	Mode
MB S-BVT	Explicit/operational mode: bit rate, TX channel power, TX channel frequency (C-, L- and S-bands)	config
	RX channel power, BER, SNR	state

4.1.2 Leveraging commercial pluggables

The recent evolution of transmission technology has driven the introduction of pluggable transceivers provided with coherent detection. B5G-OPEN has investigated the state-of-the-art and performance of two types of coherent pluggable transceivers, preliminary highlighting the potential benefits.

The first type, suitable for point-to-point communications only, can be implemented in different form factors and rates. For example, the Digital Coherent Optics (DCO) transceivers are commercially available at rates of 100, 200 and 400 Gb/s in form factors such as CFP2 (i.e., C form-factor pluggable type 2) or QSFP-DD (i.e., Quad Small Form-factor Pluggable Double Density). The CFP2 transceiver (41.5 mm width, 107.5 mm length, 12.4 mm thickness) is suitable for metro and long-haul interconnections. It typically relies on 7nm technology, providing signal launch power of 0 dBm, being able to traverse multiple ROADMs. Experiments have shown the capability to cover up to 1500 km at 400 Gb/s in a 75 GHz-spaced DWDM System, using 16 Quadrature Amplitude Modulation (16-QAM) at 69 GBaud, probabilistic constellation shaping, and soft-decision forward error correction [Neop]. In addition, excellent interoperability performance has been already achieved by DCO-CFP2 based on OpenROADM multi source agreement (MSA) [Pin19, New20]. The newer 400ZR coherent pluggable module has been standardized to enable interoperable, cost-effective, 400 Gb/s implementations based on single-carrier coherent DP-16QAM modulation, low power DSP supporting absolute phase encoding/decoding, and a Concatenated FEC (C-FEC) with a post-FEC error floor < 1.0E-15. 400ZR operates as a 400GBASE-R PHY. 400ZR has been commercialized in two different form factors: the Octal Small Form Factor (OSFP) and the slightly smaller QSFP-DD (18.35mm width, 89.4 length x 8.5 thickness, see Figure 4-4). The latter currently provides signal launch power of up to -10dBm and it is mainly designed for data center interconnections, covering single span distances of up to 120 km. Slightly better performance in terms of transmission power and optical reach can nowadays be obtained using 400ZR+ proprietary versions as defined within the openZRplus MSA. Additional evolutions and optimization of power consumption and density (and/or new technologies such as co-packaged optics) are however needed to make the smaller QSFP-DD form factor really suitable for metro/regional optical networking.

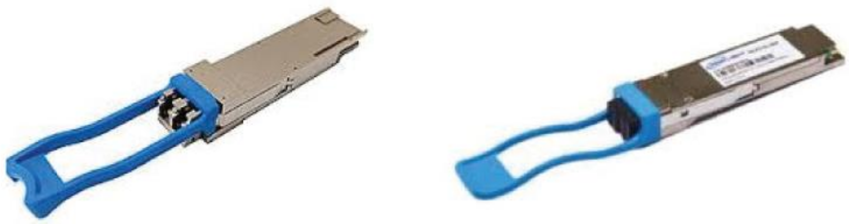

Figure 4-4: 400G coherent pluggables in QSPF-DD and OSFP form factors - Image Source: https://blog.fluxlight.com/2018/11/05/400g-form-factors-qsfp-dd-v-osfp/.

The second type of coherent transceivers is capable of PtoP and PtoMP transmission. Till now, PtoMP has been realised in burst mode, namely in PON, and it could be realised also with S-BVT as proposed. The solution here presented is the one being defined within the openXR MSA and is referred to hereafter as XR [Wel21, Wel22].

On the contrary of pure PtoP transceivers, open XR enables both PtoP and PtoMP applications. This transceiver is a smart pluggable and employs digital subcarrier multiplexing as communication technique to realize high-capacity transmission and at same time to create virtual channels. These channels (subcarriers) can be used to realize optical aggregation and thus filterless networks, so that the overall architecture is significantly simplified.

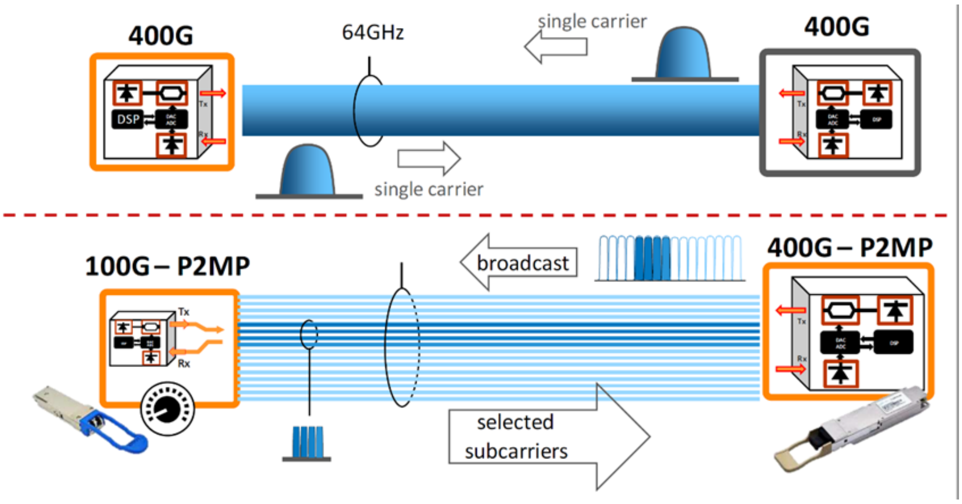

Figure 4-5: Comparison single carrier vs. digital subcarrier-based transceivers, [Wel22].

Figure 4-5 shows a comparison between a single carrier-based system and a digital subcarrier-based one. In the top figure, the single-carrier transmitter realizes a PtoP connection, and it requires that the two transceivers – at both sides of the link – transmit at the same speed, for example, at 400G. This is true also in the case that only 100G is needed. Clearly, this requires more bandwidth occupation of what is actually necessary, thus leading also to higher power consumption. While the bottom figure uses digital subcarrier for the same PtoP connection. In this case the connection can be established also with transceivers transmitting at different speeds as in the example where a 100G is connected to a 400G one. The 100G transceiver could also transmit at lower speed, in step of 25G, down to 25G.

PtoMP transceivers have the intrinsic characteristic that bandwidth can be dynamically assigned thus providing a large list of benefits: (i) power consumption can be optimized, (Ii) bandwidth and active devices match better the instantaneous traffic pattern, (iii) pay as you grow cost models can be developed; etc.

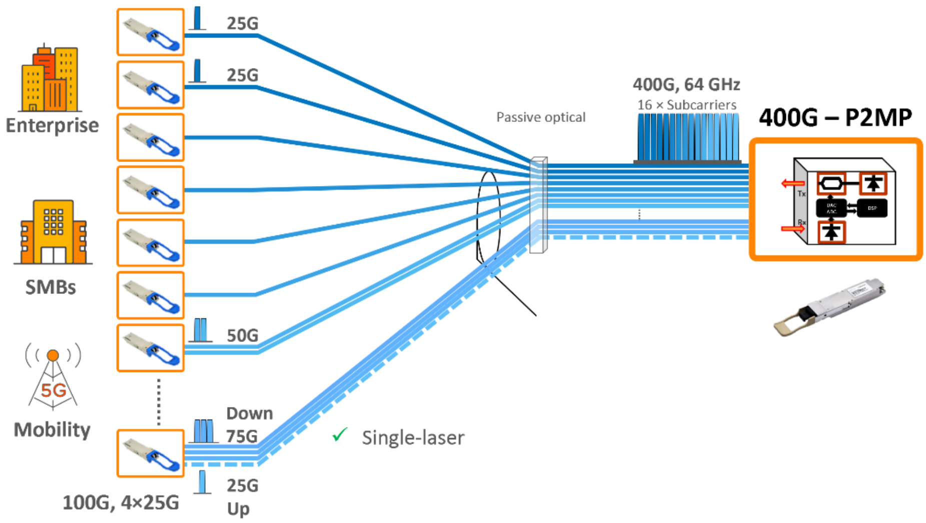

Figure 4-6: PtoMP connection with a myriad of end users.

Figure 4-6 shows PtoMP connection, where a myriad of end users are linked to a hub. The end users can transmit in step of 25G, while the hub is here assumed at 400G, and the traffic is aggregated by utilizing a simple passive optical device. After the optical combiner, the signal is transmitted and treated as any other WDM channel.

The last example was also considered in a joint U3CM, TID, INF-D publication that has been submitted to OFC [Her23]. In this work, we showed the benefit - in terms of device counting - enabled by PtoMP, as with this device a better bandwidth allocation and utilization is enabled.

Similar analyses, although with different use cases, have been carried out in ring networks between E-LIG and INF-D in [Pav22]. Here, we showed that thanks to PtoMP, benefits in terms of planning, allocation and spectral efficiency can be obtained. In [Bac22], as reported in sec. 3.4, TIM and INF-P, INF-D showed the significant gain obtained by using PtoMP in a Metro-Aggregation based on horseshoes based.

The availability of coherent pluggable modules represents an extremely attractive compact solution to be equipped directly within packet switching devices. This would drive the reduction/removal of transponders and muxponders as standalone network elements particularly in metro networks, leading to a number of remarkable benefits: 1) reduced capital expenditure; 2) reduced occupied space in central offices; 3) reduced latency avoiding passing through an intermediate element; 4) reduced power consumption by avoiding the opto/electro/optical interconnection between gray router interfaces and colored transponder line interfaces (overall savings in the range between 50 and 150W every 100Gb/s of nominal traffic, depending on the line rate). Furthermore, coherent pluggables enable tight integration between packet and optical networks, which is of special interest as transport is dominated by Ethernet and IP traffic. For example, a single packet switch can serve as spine in a leaf and spine architecture for intra-data center (DC) traffic aggregation and, thanks to coherent pluggables, also provides effective DC-to-DC interconnection. Despite not all transmission scenarios are suitable for pluggable modules (e.g., ultra long-haul), the interest around packet-optical nodes encompassing coherent pluggables is remarkably growing. This will further increase when the power/performance issues currently affecting the small QSFP-DD form factor will be overcome. Indeed, this factor is the one adopted by most of the switches designed for data center operations, which represents a wider market and with high pace of innovation compared to the traditional telecom market, thus leading to additional CAPEX and OPEX benefits.

In addition to coherent pluggable modules, B5G-OPEN will also investigate the adoption of pluggable modules for PtoMP access connections. Those are implemented over Passive Optical Networks (PONs) that connect a port from an Optical Line Terminal to multiple Optical Networking Units (ONUs). Until very recently, OLTs were exclusively dedicated proprietary devices but lately pluggable versions have appeared [Tibit]. Such pluggable OLTs incorporate the PON MAC and offer a standard Ethernet interface that can be plugged into any white box or switch SFP+ slot and offer a fully functional PON OLT solution using great flexibility: By removing the need for dedicated OLT devices many different PON deployment scenarios can be supported. The OLT management is done In-band, which is a perfect fit with software-defined networking, enabling virtualization and allowing local and/or remote administration.

Specifically, the Tibit MicroPlug OLT supports both the ITU XGS-PON and IEEE 10G-EPON standards and can be configured to work in either mode. An integrated Bridge chip allows the pluggable module to connect the OLT to a standard Ethernet SFP+ and provides the scheduling for the PON upstream traffic from the ONUs. The module handles the PON low level physical layer operation administration and maintenance messages as directed by the SDN controller, while the ONU management is delegated to a virtual function for simplicity and increased flexibility.

Table 4.3 summarizes the main parameters to be controlled in a Software Defined optical Network.

Table 4-4: Preliminary MB S-BVT performance without considering filtering and amplification stages.

Pluggable module	Control Parameters	Mode
100/200G DCO	Operational mode (e.g., 16QAM@200G, 8QAM@200G, QPSK@100G, etc), TX power, TX wavelength (C-band only)	config
	RX power, BER	state
400ZR	TX power, TX wavelength (C-band only)	config
	RX power, BER	state
400XR	TX power (in PtoP mode is the total power, in PtoMP is the subcarrier power), TX wavelength (C-band only)	config
	RX power (in PtoP is the total power, in PtoMP is the subcarrier power), BER (total or individual BER per SC)	state
TIBIT	Operational mode (XGS-PON, 10G-EPON)	config
	TBD	state

4.2 Multiband Optical Switch

In Task 3.2 of B5G-OPEN new multiband optical switching solutions have been investigated. The multiband optical switches should operate across multiple bands such as O-, S-, C-, and L- band in order to provide flexibility and higher capacity of the B5G-OPEN networks for fulfilling the beyond 5G stringent requirements in terms of bandwidth, capacity, flexibility, and efficiency due to the transparent operation. The schematic of the multiband optical node architecture with the main functional optical building blocks is reported in figure 4.5. The node architecture consists of two multiband optical cross-connect switches (MB-OXC) for adding/dropping and bypass the traffic from/to the Metro Aggregation and the traffic to/from Metro-Core, respectively. The separation of the MB-OXC in two distinct building blocks allows for a modular architecture with efficient design based on the traffic, number of channels, channel granularity, number of bands, and number of ports (or degree of the switch). In particular, the network element facing the Aggregation network should comply with the systems used in the aggregation segment. Therefore, the MB-OXC Aggregation, located at the edge of the horse-shoe network that interconnect the metro Aggregation nodes, is characterized by lower data rates and channel granularity with respect to the Core as well as a maximum degree equal to 3. Instead, as the network element facing the Core network should comply with systems used in Metro Core segment, the degree of the MB-OXC can be larger as well as the channel granularity to accommodate higher data rate links. As shown in the Figure 4-7, the core components to realize the node architecture is a programmable photonic circuit capable to add/drop channels from/to the network as well as bypass the S-, C-, and L- band traffic on-demand and according to the network requirements. Moreover, drop and continue operation is also a desirable feature. We have then focussed on the design and implementation of a programmable multiband optical add/drop multiplexer (MB-OADM) capable to operate in the O-, S-, C-, and L- band with drop and continue operation.

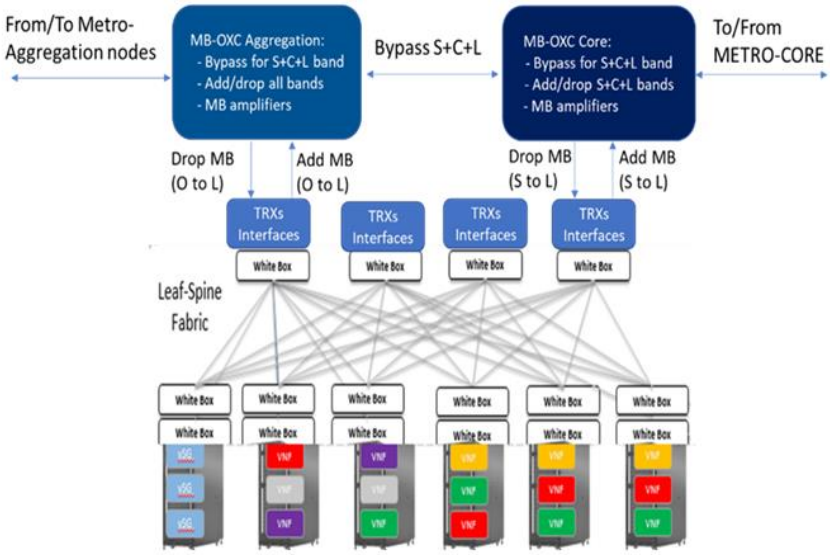

Figure 4-7: Multiband optical node architecture with functional building block.

The schematic of the MB-OADM is depicted in Figure 4-8. It consists of a band demultiplexer and multiplexer used to separate and combine the input MB signals. The band demultiplexer/ multiplexer can be implemented by commercial fused fiber WDM splitters. After the bands separation, each band signals are fed into the respective OADMs operating at O-, S-, C- and L-bands. Each OADMs consists of a demultiplexer to separate the single band signals into individual channels, an array of SOAs that selectively and dynamically blocks or passes each channel, and a multiplexer for combining the channels. The drop stages are realized by a 3 dB splitter before each SOA and the add stages are realized in the same manner after the SOA and before the multiplexing stages. The SOAs compensate the muxes/demuxes as well as the 3dB splitters losses. Note that each SOA operates with a single channel, avoiding FWM, XGM and XPM nonlinearity that can degrade the signal quality. This implementation allows drop and continue operation of each individual channel. Moreover, the modular architecture allows to be expanded, in a pay as it grows approach, to process multiple bands based on the increase of the traffic demands. Each module is capable to process the data channels of one of the multiband, starting from C-band and then L-band to S-band or O-band if needed. This enables a future-proof architecture supporting the growth of the traffic even in the long-term scenario.

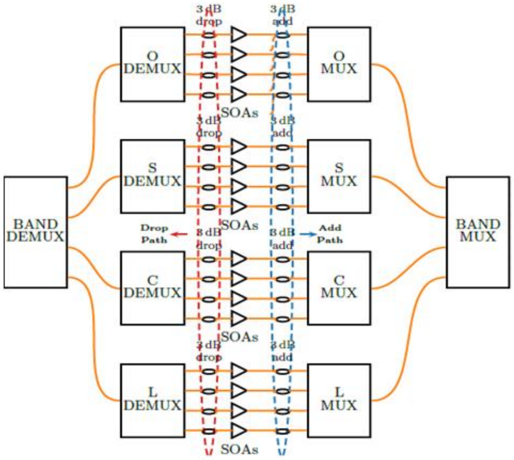

Figure 4-8: MB-OADM node architecture.

To validate the operation of the MB-OADM, we have assessed the first MB-OADM prototype operating in the O- and C-bands in a network scenario. Moreover, the cascadability of the MB-OADM was experimentally assessed over the typical distances for three cascaded nodes and 8 WDM channels at 25 Gb/s.

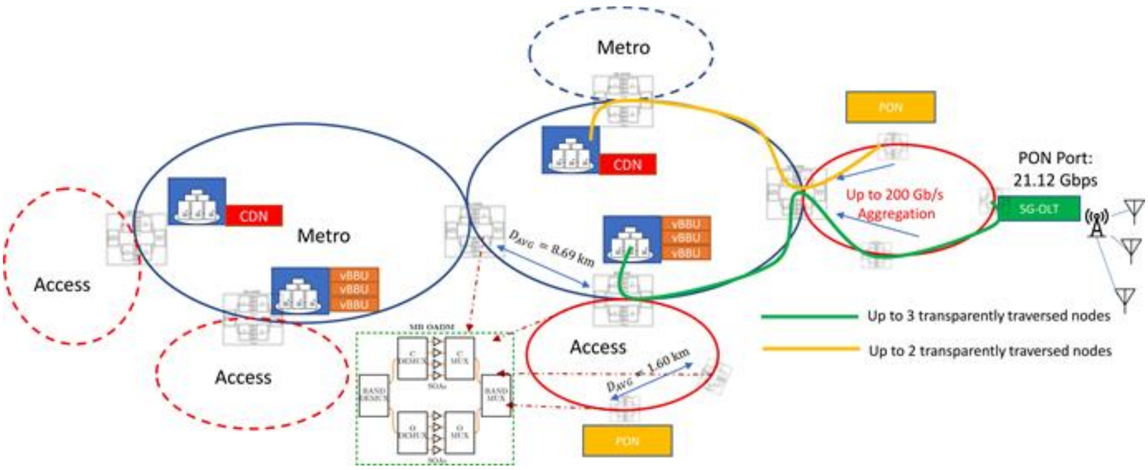

Figure 4-9: Network scenario employed to assess the MB-OADM.

Figure 4-9 depicts several typical connectivity scenarios in a metro-network, such as data-center to data-center communications, CDN caching for end-used in a PON and data transmission between remote virtual baseband units (BBU) and 5G OLTs. One of the scenarios considered is traffic between a 5G OLT and its remote BBU units located in the edge data-center. In this case, the traffic will transparently traverse up to 3 MB-OADMs over different fiber spans until the edge node. Transmission distances of 16 km, 6 km and 1 km were evaluated by inserting fiber spans between the MB-OADMs. In the same figure it can be seen that no EDFAs were inserted between the MB-OADMs. The MB transmitter was comprised of 8 WDM channels, 4 in the O-band and 4 in the C-band. All channels were modulated at 25 Gb/s non-return-to-zero on-off keying with pseudorandom bit sequences 2^15-1. To verify eventual penalties caused by each SOA, such as OSNR and non-linear effect accumulation, we investigated the effects of the cascade of several OADM blocks as shown in Figure 4-9. The performance assessment of the switched WDM channels at different nodes in terms of BER are reported in Figure 4-10.

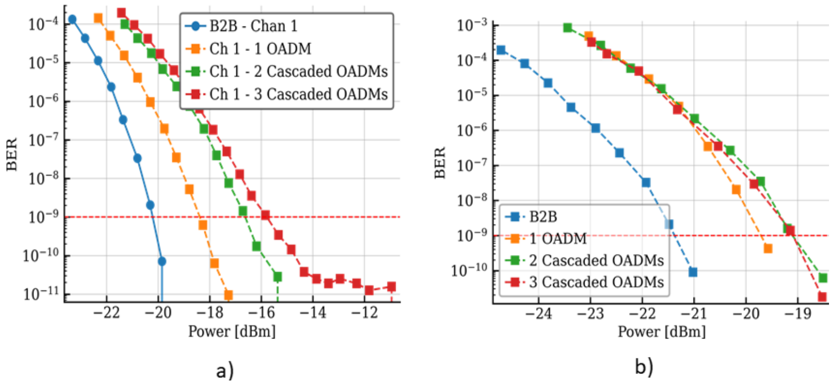

Figure 4-10: BER penalty after cascading MB-OADM nodes for a) O-band, and b) C-band.

For the O-band channels at 25 Gb/s, the power penalty at a BER = 10−9 increased from close to 2 dB for 1 OADM to 4 dB after 3 cascaded OADMs, as can be seen in Figure 4-10(a). In the C-band case (Figure 4-10(b)), the penalty by cascading 3 OADMs increased by less than 1 dB from the 1 OADM case. More detailed results are reported in [Kra22].

The results confirm that expanding the OADM for other bands in the low-loss window is feasible, given the wideband operation of the O- and C-band SOAs and the availability of SOAs with peak gain in other bands. Our future work is to expand the MB-OADM operation to the S-band and L-band as well as assess it at higher data rates.

Table 4.5 summarizes the main control parameters to reconfigure the MB-OADM prototype by means of SDN agents.

Table 4-5: MB-OADM control parameters.

Prototype	Control Parameters	Mode
MB OADM	Explicit/operational mode: drop channels (O-, C-, L- and S-bands), add channels (O-, C-, L- and S-bands), drop and continue channels (O-, C-, L- and S-bands), channel power (O-, C-, L- and S-bands)	config
	RX channel power (O-, C-, L- and S-bands)	state

4.3 MULTIBAND AMPLIFIER

Multiband amplification is typically associated with steps of large bandwidth increase achieved by enabling the use of additional wavelength bands that are at least as large as the C-band. However, these steps typically require the development of new amplification technologies. An overview over the different technologies has been elaborated and published in a previous project.

This split-band approach comes with challenges making handling, maintenance and management of the systems more difficult. During the first year of this project different aspects of multiband amplifier has been addressed:

1. An amplifier design avoiding above mentioned challenges with providing a noticeable bandwidth increase has been developed and analyzed.
2. Nonlinear fiber effects limit the maximum increase of the bandwidth. Margin required for achieving a given increase of bandwidth has been determined.

3. Hardware requirements for upgrading existing C-band systems by adding additional bands has been identified.

4.3.1 Moderate capacity increase with amplifier design using a common optical path

Signal amplification in optical networks is mainly achieved by means of erbium–doped fiber amplifiers (EDFAs) that have reached a very mature level of development with low failure rates. Although this technology is able to cover wavelength ranges of 80 nm width and more, the bandwidth of commercial amplifiers is typically limited to around 35 nm for performance reasons.

To achieve sufficient efficiency, typically separate amplifiers designed for the conventional wavelength band (C–band) and the long wavelength band (L–band), respectively, are used in parallel for increasing capacity. However, such a solution entails additional challenges with regard to the design of optical transmission systems and their control. Furthermore, the overall performance of the amplification node suffers from noise figure degradation caused by the passive losses of the band splitter.

Not all links in an optical network need to be upgraded to the full capacity offered by the two wavelength bands in the next time such that extending the gain range of C-band EDFAs to longer wavelengths is sufficient for a longer time period while avoiding many of the drawbacks of a split–band solution (setup B in Figure 4-11). However, such amplifiers are known for increased noise figures.

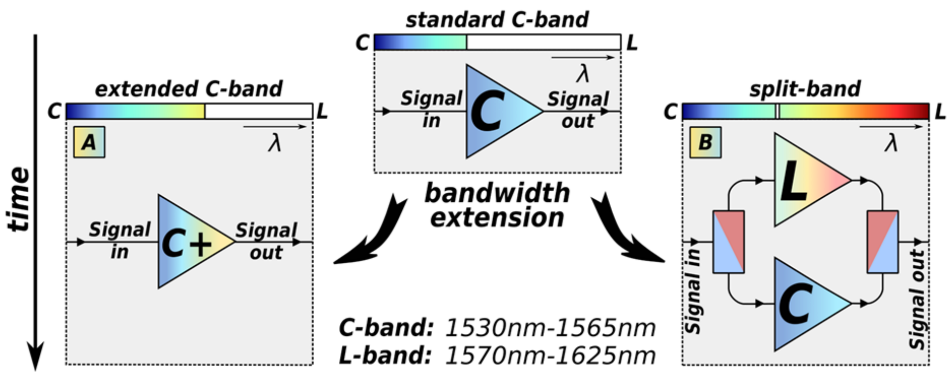

Figure 4-11: Capacity extension of existing C-band links by using an extended C-band amplifier (left side) of by parallel amplification of signals in two wavelength bands (right side).

In this work, the single device solution (left side in Figure 4-11) has been compared with the split–band approach (right side in Figure 4-11) using two amplifier devices in parallel in various scenarios and in view of different parameters for a typical two-stage setup. In particular, an amplifier design avoiding the reported noise figure degradation of extended C-band amplifier has been proposed. In addition, a split-band amplifier design for improved noise figure has been investigated and it could be shown that this setup provides a significant noise figure improvement in the C-band, whereas it is not efficient in the long wavelength part of the L-band.

In the following, the noise performance of these amplifier designs has been compared. In particular, the dependence of noise figure (NF) on gain bandwidth and measures for improvement have been determined. Noise figure versus bandwidth is illustrated in Figure 4-12 for different scenarios and output powers using the extended C-band amplifier design. The results indicate that increasing the bandwidth by 20 nm as compared with the standard C–band is possible with a quite small increase of the maximum noise figure by 0.5 dB. Furthermore, it has been shown that an extended C-band amplifier performs better than the optimized split-band amplifier for bandwidths up to around 55 nm. Worth mentioning is the fact that the main source of noise figure degradation, namely the power profile, could be identified. Thus, design guidelines for extended C-band amplifier could be provided.

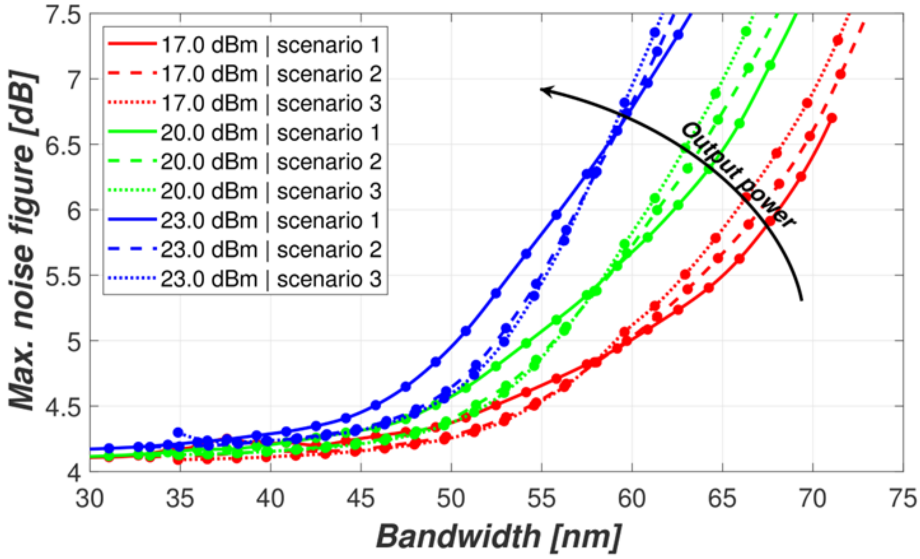

Figure 4-12: Noise figure versus bandwidth for various output powers and scenarios.

In summary, it has been shown that the reported increase of the noise figure can be avoided by appropriate amplifier designs. Furthermore, it has been analyzed up to which capacity the use of single EDFA is advantageous over a split-band design.

4.3.2 Upgrade limitations of existing C-band systems

A major nonlinear fiber effect limiting capacity of multi–band systems is stimulated Raman scattering (SRS), which introduces a power transfer from shorter wavelengths to longer wavelengths. For bandwidths smaller than the so-called Raman shift, this power transfer quantified in logarithmic units scales linearly with the total power launched into the fiber. When spreading the channels over a larger wavelength range, the power differences among the channels also increase even if the total power is kept constant. For compensation, usually a tilt is introduced in the optical spectrum at the input of each fiber span producing an almost flat optical spectrum at its output and thus constant optical signal-to-noise ratio (OSNR) at the receivers. In order to keep the impact of nonlinear fiber effects such as self–phase modulation (SPM) and cross–phase modulation (XPM) at an acceptable level, the power of each channel must not exceed a characteristic power limit. An upper limit for the bandwidth to which existing links can be upgraded has been determined. Results indicating the maximum achievable relative bandwidth increase of an existing C-band system are given in Figure 4-13 as a function of the span length and the OSNR margin for C-band operation.

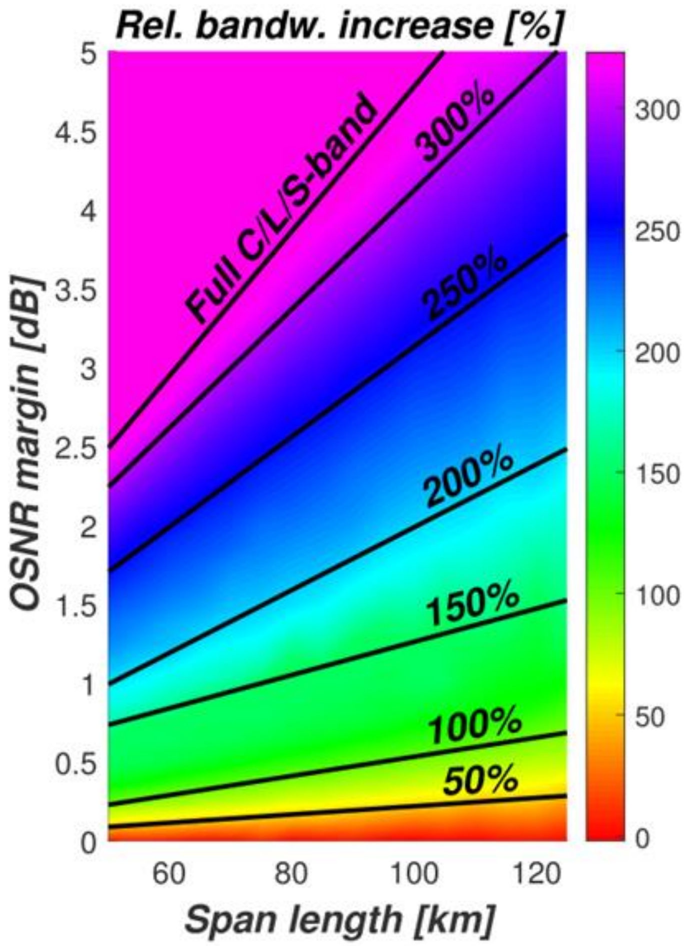

Figure 4-13: Achievable relative bandwidth increase versus span length and OSNR margin.

In conclusion, increasing capacity of installed fiber links by enlarging the used optical bandwidth leads to reduced OSNR at the receivers due to stimulated Raman scattering (SRS). For a link composed of spans of equal length of standard single mode fibers and wavelength channels transmitting data at 400 Gbit/s (dual polarization 16QAM) with a channel spacing of 100 GHz, the extent of this reduction has been determined for various fiber lengths per span. It has been shown that an OSNR margin of 2.5dB is required for upgrading a link composed out of 50 km spans to full C/L/S–band operation, whereas a margin of even more than 5.0dB is needed for span lengths of 125 km. For a typical span length of 80 km, the necessary margin amounts to approximately 3.9dB.

4.3.3 Challenges for introducing multi-band amplification in existing C-band networks

Increasing the capacity of existing C-band systems is faced to many challenges. First, such an upgrade is only possible in systems and networks with direct access to the amplification sides and is therefore not suitable for submarine links and unrepeatered submarine links with embedded remote optically pumped amplifier. Furthermore, such an upgrade involves performance degradation due to increased fiber attenuation at some added wavelengths, degradation of the noise figure, and nonlinear fiber effects. Thus, the available margin might not be sufficient for achieving the target increase of the capacity.

Many installed systems have not been prepared for the planned increase of the bandwidth. For example, many C-band amplifiers are not equipped with the required upgrade ports which will involve traffic interruption. Furthermore, further usage of the installed C-band amplifiers will lead to a decrease of the maximum C-band power such that the C-band channels cannot be operated at the optimum power level. Furthermore, installed racks have not been designed to provide the fast communication channels required between the amplifier cards for guaranteeing transient performance and therefore need to be replaced.

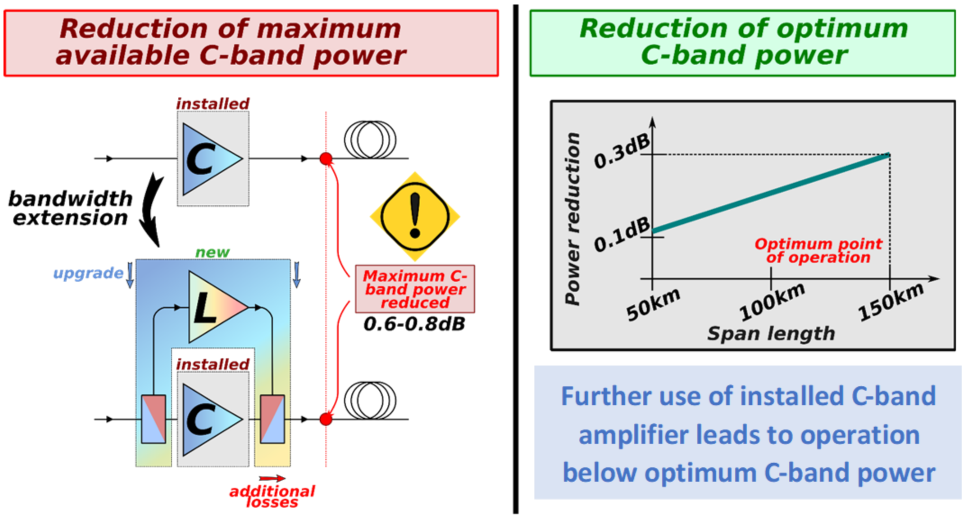

Figure 4-14: Illustration of power reduction for installed C-band systems.

In summary, the planned bandwidth upgrade will require the installation of new equipment in addition to the new amplifiers. Furthermore, the network needs to be reconfigured in many cases since the OSNR available after upgrade will not be sufficient for many paths. In some cases, it might be possible to solve this issue by rerouting, but in some cases even new regenerators might be required.

5 INTEGRATED ACCESS AND X-HAUL OPTIONS

5.1 B5G-OPEN ACCESS NETWORK ARCHITECTURE

During the last twenty years or so, the deployment of TDM PONs was aiming to render Access COs (also known as Local Exchanges –LEXs) redundant. This deployment would allow to amass all (expensive) electronic processing terminals deeper in the network i.e., in Metro or Metro-Core nodes so the operators would benefit from the corresponding economy of scale. As such, operators would be able to reduce the CapEx/OpEx needed to build and maintain LEXs and in many cases LEXs are completely scraped off.

Nowadays, the advances related to high performance computing and the quest for end-user applications with superior QoS performance (primarily latency) put this assumption under question. Contemporary architectural approaches [Mat15], [Vel15], [Orp15] are moving in the opposite direction as they favor the deployment of Cloud Access COs at the immediate vicinity of the final end-user. The proliferation of Cloud Access COs reverses the centralization tide as processing & storage resources spread to network periphery, raising the prospect of Cloud Access CO virtualization in the context of NFV. Nevertheless, it is key to acknowledge here that the resources to be allocated to these Cloud Access CO are limited due to cost considerations, as a Cloud Access CO at the footprint of a LEX is still a CapEx/OpEx intensive operation. Moreover, practical considerations related to the housing of Cloud Access COs set further limit to the resources a Cloud Access CO may host.

Therefore, the emerging Access & Aggregation network architecture is as depicted in Figure 5-1. There are two major Cloud nodes in this segment which are the Access CO at point B and the Regional CO at point C. The different end-user groups i.e., residential users, business users, mobile X-haul terminals, IoT application terminals etc, connect to these two types of nodes with diverse connectivity requirements in term of traffic’s peak-rate and burstiness, resulting to traffic patterns featuring a substantial traffic spatial asymmetry and a great variation to the requested lines rates. Because of this heterogeneity, the emerging Access & Aggregation network segments need to support all existing connectivity modes, them being PtoP, PtoMP and TDM-PON.

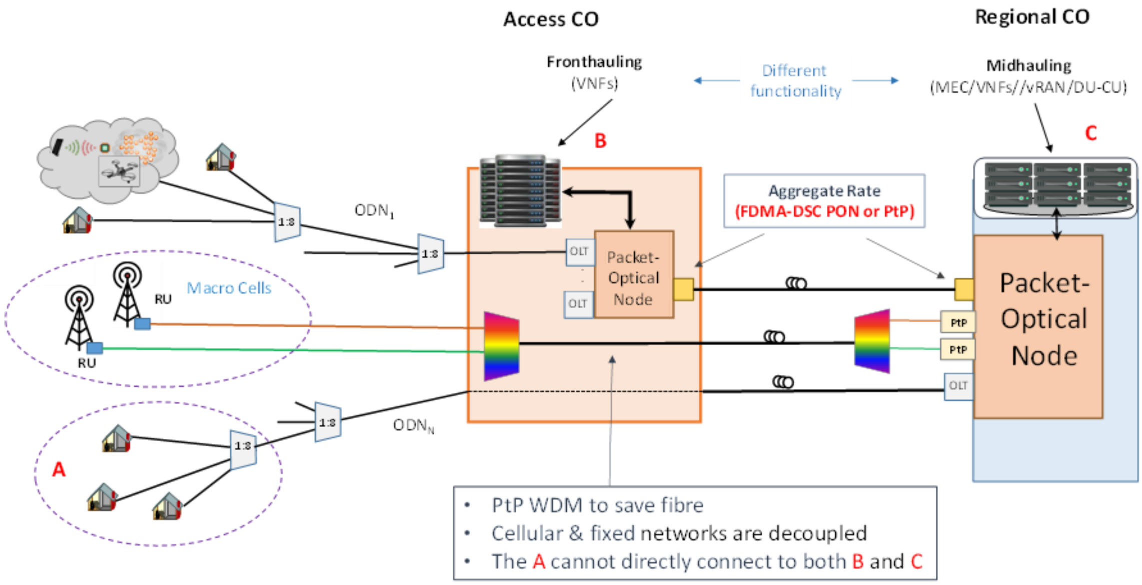

Figure 5-1: Schematic representation of the contemporary Access-Aggregation architecture.

In the B5G era, a number of advances create a new landscape in transportation of Access & Aggregation segments. A summary of these changes is made evident with the aid in Figure 5-2:

- An important development is the introduction of WDM technology in the Access network. This decision was made to facilitate the transportation of the capacity-hungry mobile network functional splits, like splits 8, 7.3 and 7.2, while saving fiber in the Aggregation segment [ITU-T G.Sup66-201907].
- Cellular and Wireline networks still remain relatively decoupled from each other as the joint use and optimization of the transportation resources attracted relatively little attention as of this moment.
- The existing connectivity modes allow the optical termination to take place either to the Access CO or to the Regional CO but not in both nodes. Therefore, the connectivity between the end-user terminals and the two different CO families is ensured only by means of electronic switching and aggregation. This operation is designated with the two packet-optical switches in tandem in Figure 5-1and Figure 5-2.

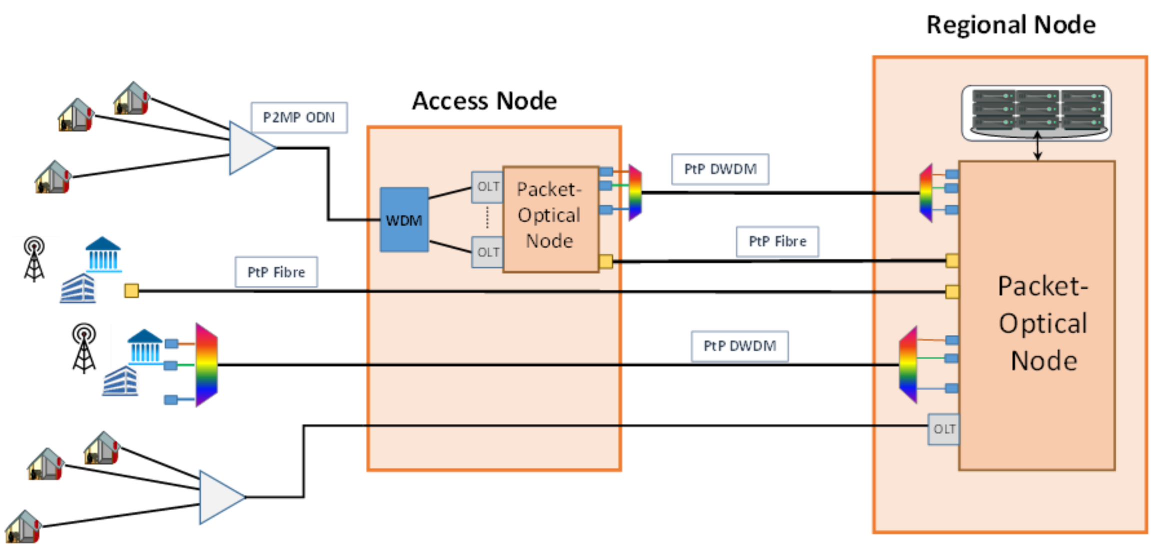

Figure 5-2: The emerging Access-Aggregation landscape in the B5G era.

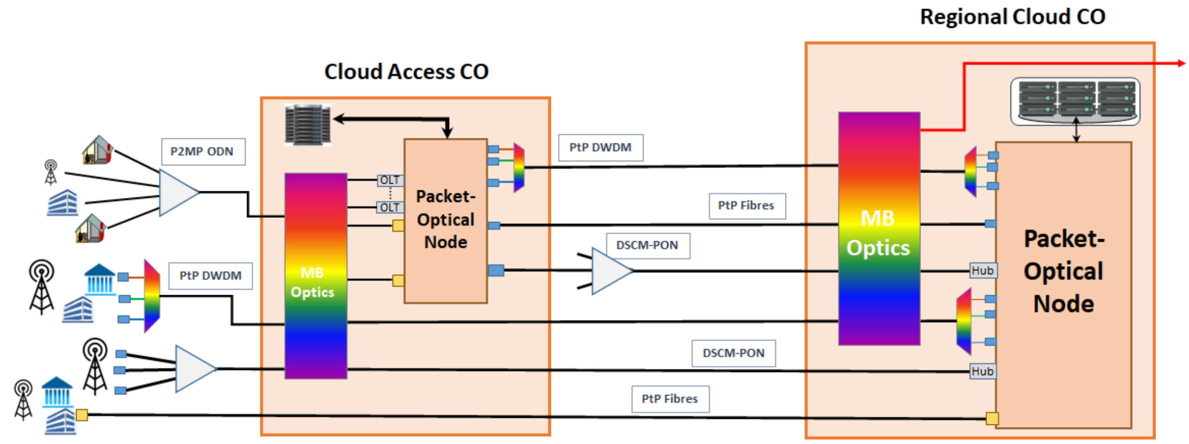

Figure 5-3: Overview of the proposed B5G OPEN architecture in Access & Aggregation.

B5G-OPEN capitalizes on these advances and it further extends this framework. B5G-OPEN proposes a converged wireline and wireless next-generation architecture in the Access& Aggregation segments which is schematically presented in Figure 5-3. The architecture rests on three key enablers:

1. Following the WDM principles applied in Core and Metro segments during the last 20 years, WDM in Access & Aggregation becomes an attractive transportation technology not only due to WDM's transparency to line-rate, modulation format and protocol type but also due to the wavelength-routed network mode WDM is offering where the flows who are in transit from certain node to transparently cut-through these nodes. The wavelength-routed network mode allows channels to 'bypass' certain nodes and as such to alleviate those nodes from the corresponding h/w as well as to alleviate the latency budget from additional delays at the switches' buffers. This creates the conditions of *'optical continuum'* and Metro-Access and Access-Core integration leading to flatter-hierarchy layouts.
2. The WDM transportation in Access & Aggregation is, by default, multi-band (MB). The wireline connectivity modes under consideration i.e. burst-mode TDM-PON, and the constant-bit-rate (CBR) PtoP and PtoMP technologies were standardized to operate in different optical bands within the second and third low attenuation window of the SMF. In particular, TDM-PONs explore O and L bands (but also standardization is extended for a WDM operation in E and S bands) while CBR PtoP and PtoMP operate in C and L bands. Since WDM is not used only as means to increase the transported capacity between two end-point but also as means for the transit traffic to bypass certain nodes, the deployment of low-cost MB optical technologies for the handling of these WDM channels is a necessity.
   Such technologies are designated as *'MB Optics'* in Figure 5-3 which may range from simple passive elements to advanced optical circuitry that offer similar functionality as in Core and Metro networks i.e. 'add/drop', 'steer', 'separate/combine', 'route' etc. Section 5.1.3 elaborates a number of use-cases where progressively more advanced technologies provide higher-level functionality.
3. Unlike the current trend where wireline and cellular Access & Aggregation transportation technologies are decoupled, in B5G OPEN there is an integrated transportation over the same fiber plant for the following reasons:

- o Although Operators are aggressively deploying fiber in the two segments, a rationalization of the deployed fiber plant is necessary to safeguard against future connectivity requirements and to address possible fiber shortages due to cell densification challenges.
- o Transportation based on CMR PtoP, PtoMP and TDM-PON technologies is carried in parallel over the same Optical Distribution Network (ODN) which offers the alternative to tailor the terminals of a specific technology to requirements the end-user sets.

5.1.1 Use-cases of possible functions different optical technologies provide

i. <u>MB Optics is a WDM filter:</u> With reference to Figure 5-4, each ODN hosts dissimilar transportation technologies like TDM-PON (burst-mode technology) and the DSCM-PtoMP (CBR technology). A passive WDM device (e.g. a band-filter) is attached to each ODN in the Access CO which allows the TDM-PON and the PtoMP systems to terminate at different COs (Access and Regional, respectively in Figure 5-4). This makes it possible to bypass, in a static way, the Access CO whenever this is requested using an arrangement of passive optical devices. For example, assuming a future 800G DSCM-PtoMP technology (like XR optics), in Figure 5-4 one particular Macro-cell is able to transport traffic up to 50G while another Macro-cell may transport traffic up to 25G. Both flows terminate to the Regional CO. At the same time, a TDM-PON (10G, 25G or 50G) is used to support traffic from residential users through the same ODN and the corresponding flows terminate at the Access CO.

Moreover, the remaining capacity of the DSCM-PtoMP is used to transport the aggregate flows from all TDM-PONs towards Metro-Core (the Access CO forwards the 'local' traffic either towards the µDC to implement the corresponding VNFs/IT processing and/or back to the local end-users)

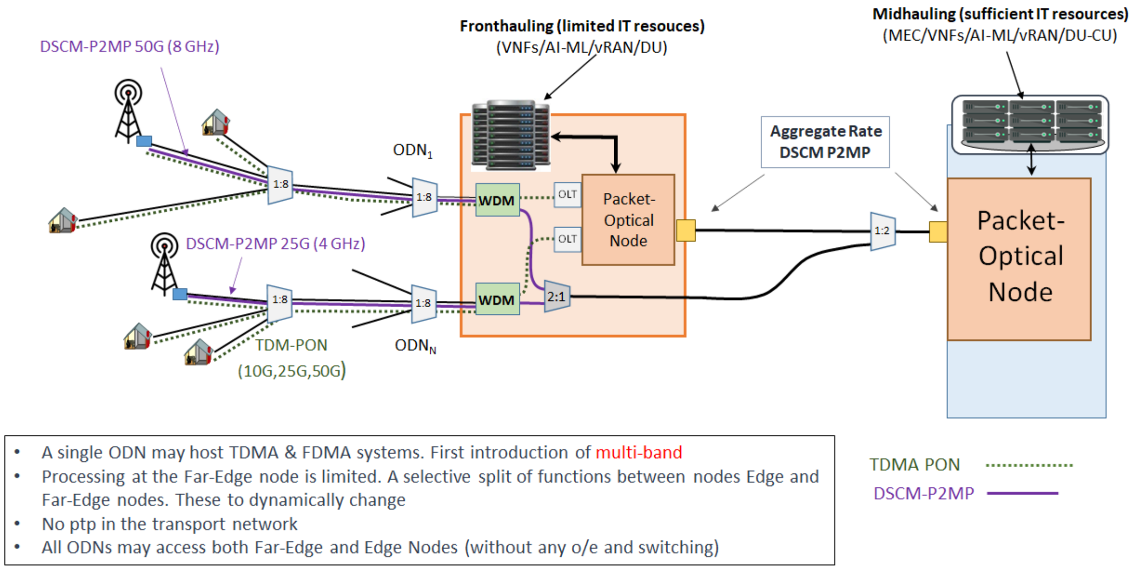

Figure 5-4: First-day introduction of optical multi-band in the Access network segment.

ii. MB Optics is AWG technology: Although the aforementioned scheme saves fiber in the Aggregation segment, it is still limited in terms of the offered flexibility. The configuration in Figure 5-5. is a far more versatile system. Now the 'MB optics' block consists of a *N x N* AWG (or an array of band-optimized AWGs) where *N* being the number of ODN branches. In this case the number of WDM channels per ODN is allocated independently between different ODNs. The ONTs (ONUs and the corresponding PtoMP terminals) tune to the specific WDM channel and the number of ONTs per channel define the attainable maximum line-rate per end-user terminal. Compared to Figure 5-4, this scheme allows far greater flexibility to address spatial traffic asymmetry while it offers a far greater upgradeability albeit the introduction of tunable transceivers.

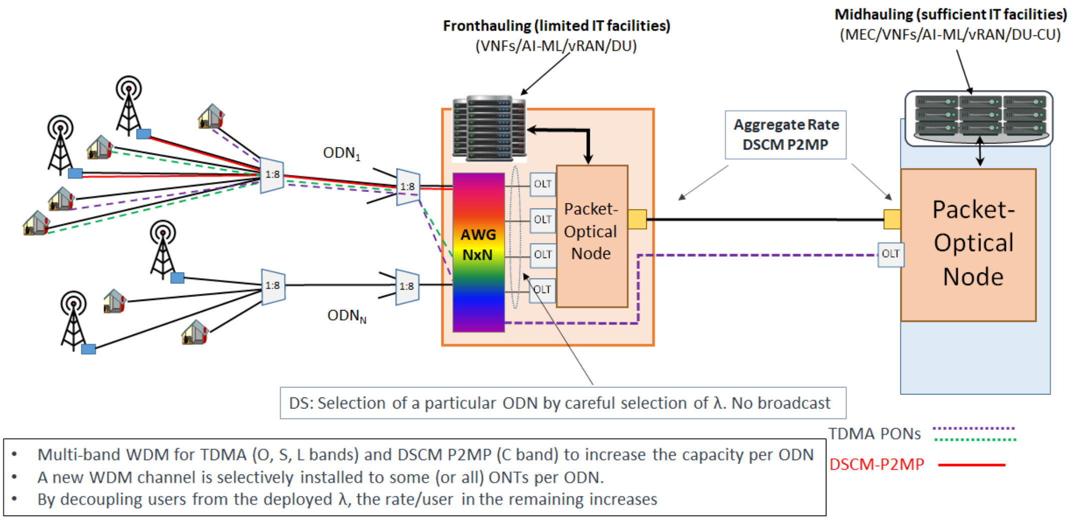

Figure 5-5: Evolution of optical multi-band technologies in the Access network segment.

iii. MB Optics is a WSS technology: Finally, Figure 5-6 shows the long-term evolution of the B5G OPEN architecture with the use of a multi-band WSS. This is a 2xN device where the second port on the side towards the Aggregation segment allows to seamlessly terminate any number of channels in the multi-band comb either to the Access CO of the Regional CO.

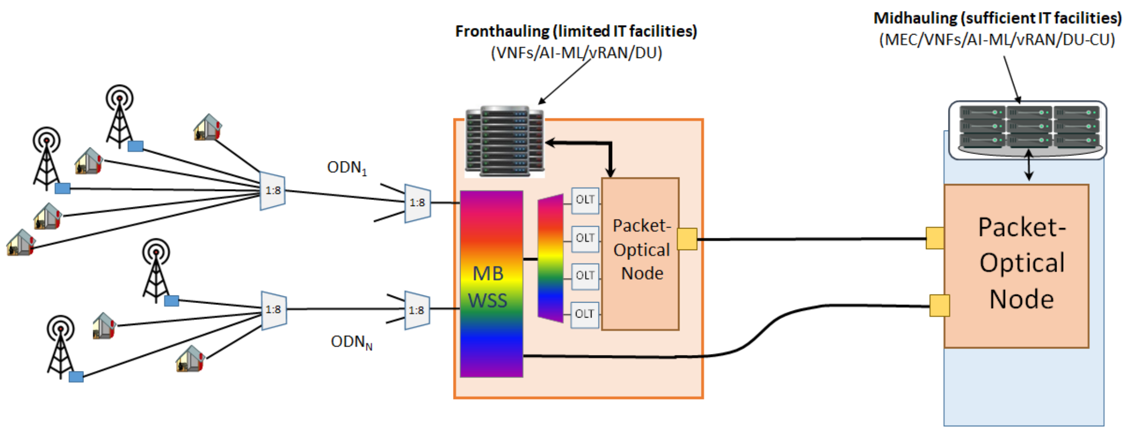

Figure 5-6: Long-term evolution of optical multi-band in Access.

5.1.2 The cases of Optical Continuum in the converged Access- Aggregation-Metro segments

Fig.5.3 depicts three bypassing cases in the converged Access, Aggregation and Metro segments. Assuming that a sufficient number of WDM channels are deployed in this multi-band scheme then the three bypassing cases are the following:

- A wavelength channel from the final end-user may bypass the Access CO to directly terminate at the Regional CO
- A wavelength channel from the Access CO (that aggregated traffic from a number of last-drop technologies) may bypass the particular Regional CO and terminate at the Core-Metro node or at another Regional CO. The advantages of this approach in terms of power consumption have been validated [Mat15], [Orp15].
- A wavelength channel from the final end-user may bypass the Access CO and the Regional CO and terminates at the Core-Metro node or at another Regional CO.

Via node bypassing the B5G OPEN architecture integrates the three segments creating a flatter network hierarchy. Although a flat-hierarchy network is not a new concept, the means used to implement it, based on MB WDM, is something that becomes practical for the first time.

5.2 AN ACCESS PLANNING TOOL

5.2.1 Motivation

The multitude of technologies and architectural choices detailed in the previous section requires a careful evaluation of the pros and cons of the offered alternatives. The adoption of an access planning strategy is a challenging task under the aforementioned framework. Moreover, different access planning strategies should be tailored to a diverse set of deployed environments: dense-urban, urban, suburban or rural scenarios need to be thought of for a diverse mixture of users: residential, business, mobile. In addition, the coexistence of both residential and mobile users over the same ODN, imposes new challenges as the integrated transportation scheme should be able to support concurrently the traffic from residential users and the traffic generated at the mobile sites. The latter is a considerable add-on to the complexity as there are different types of mobile stations (e.g. macro, small and pico cells) featuring dissimilar densities and traffic volumes (that depend on the adopted mobile function split). Therefore, a tool that takes into account all these parameters is necessary to provide solid arguments for the viability of different evolution plans.

5.2.2 Overview of the Access planning tool

The access planning tool takes into consideration the parameters (inputs) illustrated in Table 5-1 and it returns a deployment configuration that accommodates the traffic demands while it minimises the number of PON systems engaged and the total fiber length of the deployment.

The tool is using two clustering algorithms to cluster the total number of nodes (residential users or/and mobile sites) into a set of PON networks: a) a K-Means clustering algorithm and; b) Constrained K-Means clustering algorithm [Bra00]. Both algorithms return minimum distance clusters which is an essential step to minimize the fiber length a PON network employs. However, the [Brad00] is more appropriate in the case in which we would like also to generate PON networks that can support the total requested traffic of their nodes. The tool supports both Euclidean and Manhattan but the latter is more practical in Access deployment scenarios as fiber ducts are laid out along streets.

The tool can support both one-stage splitting or two-stage splitting between a designated CO and the ONUs (end-users) therefore can support all the practical PON deployment scenarios. In the first alternative we assume that all splitters are located in a street cabinet (e.g. 1:4 and 1:16 splitters), while in the second alternative the first splitting can be located in the cabinet and the second one closer to the user (e.g. in the entrance of a block of apartments).

The geospatial location of the users (either residential or mobile sites) is imported as topological csv files or by means of a generator which generates known distributions based on the specific details of the area and the numbers of users.

What is also important to point out is that the tool supports both greenfield and brownfield deployments. In the former case, the tool freely selects the (optimal) location of splitters (and of any other elements in general) anywhere in the area of interest, while in the latter case the position of splitters is set at the already deployed locations (e.g. street cabinets in specific positions in the area of interest).

The tool is developed using python, while the following python libraries are used: *pandas, numpy, sklearn, seaborn, scipy and k_means_constrained.*

Table 5-1: Access planning tool parameters.

Parameter	Description
Area of interest	Dimensions of area
Residential users	csv file with their coordinates or total number and selected distribution
Mobile sites	csv file with their coordinates or total number and selected distribution
Residential traffic	Traffic demand per household (Mb/s)
Mobile traffic	Traffic demand per mobile site (Mb/s)
Mobile split option	Mobile split option (e.g. F1)
Mobile ISD	Mobile sites intersite distance (m) (e.g. 560m down to 50m to capture all cell types: macro, small, pico)
5G (mobile) deployment / configuration	Options: a) Sub-6HZ band: 3.5/3.7 GHz, 100 MHz, 256-QAM, 16T16R; b) Sub-6HZ band:3.5/3.7 GHz, 100 MHz, 256-QAM, 64T64R; c) mmWave band: 26/28 GHz, 2*400 MHz, 256-QAM, 4T4R; d) mmWave band: 26.5-27.5 GHz, 200 MHz, 16x16 MIMO; e) custom mobile configuration
PON technology	GPON with data rate: 10, 25 or 50 Gb/s
Access nodes	csv file with their coordinates
Cabinets	csv file with their coordinates
Max split ratio	Max split ration (e.g. 64)
Number of splitter locations per path	Integer (1,2)

5.2.2.1 Illustrative examples

Two examples are considered: in the first case the PON deployment serves exclusively residential users while in the second case, the PON serves exclusively mobile base stations. In these illustrative examples, a uniform and equidistance distribution of terminals is assumed with respect to the CO (Access Co or Regional CO) that is located in the centre of the area of interest. In particular, Figure 5-7 illustrates the output the tool returns in the particular scenario where only residential users are served while in Figure 5-8 the corresponding configuration is shown when mobile stations are served.

- The figures allow to visualize the location of splitters and the ONUs with respect of the CO in the two cases
- The results include a set of critical system parameters like the total number of PON trees and the number of users per PON (assuming a 1:64 split) as well parameters like:
  - Total fiber length (Manhattan) (Km)
  - Total fiber length from access node to splitters (Manhattan) (Km)
  - Total fiber length from splitters to ONUs (Manhattan) (Km)
  - Average fiber length in each PON (Manhattan) (Km)
  - Average PON Utilisation (%)
- The geospatial position (coordinates) of the corresponding elements (access nodes, splitters, ONUs) in topological csv files.

Results	Values
# PONs	242
# ONUs per PON	50
Total fiber length (Manhattan) (Km)	2,320
Total fiber length from access node to splitters (Manhattan) (Km)	974
Total fiber length from splitters to ONUs (Manhattan) (Km)	1,346
Average fiber length in each PON (Manhattan) (Km)	9.58

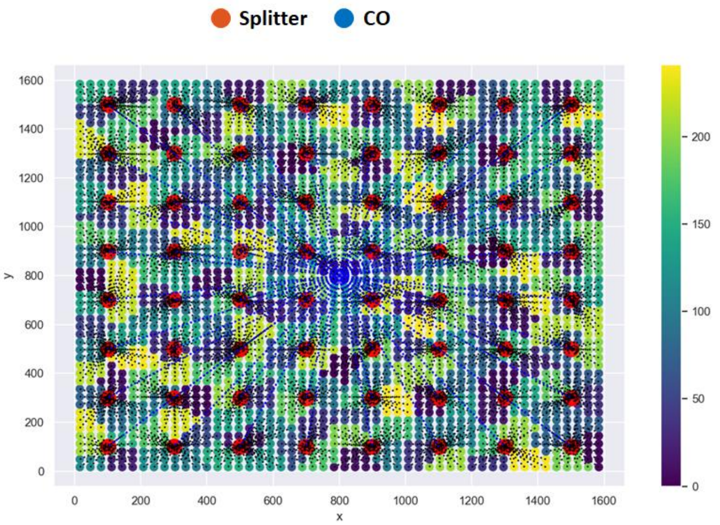

Figure 5-7: Access planning tool GUI – Serving residential users.

Results	Values
# PONs	22
# Mobile sites per PON	3
Total fiber length (Manhattan) (Km)	26.6
Total fiber length from access node to splitters (Manhattan) (Km)	18.2
Total fiber length from splitters to Mobile sites (Manhattan) (Km)	8.4
Average fiber length in each PON (Manhattan) (Km)	1.21

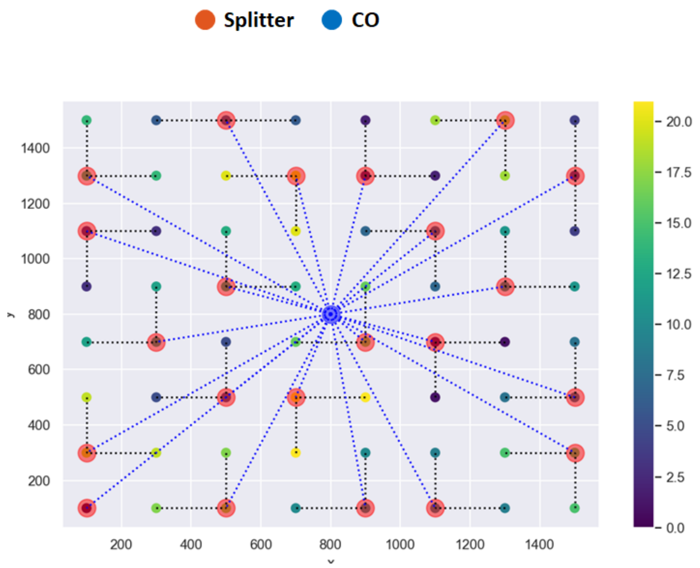

Figure 5-8: Access planning tool GUI – Serving mobile Stations.

5.3 LIFI ACCESS

LiFi is enabled by an ecosystem of multiuser techniques, resource allocation algorithms and security strategies. A LiFi network illustration is shown in Figure 5-9. A complete LiFi network includes downlink, uplink, and backhaul connections. In addition, the system should provide a handover function, mobility support, and multiple access capability [Haa20].

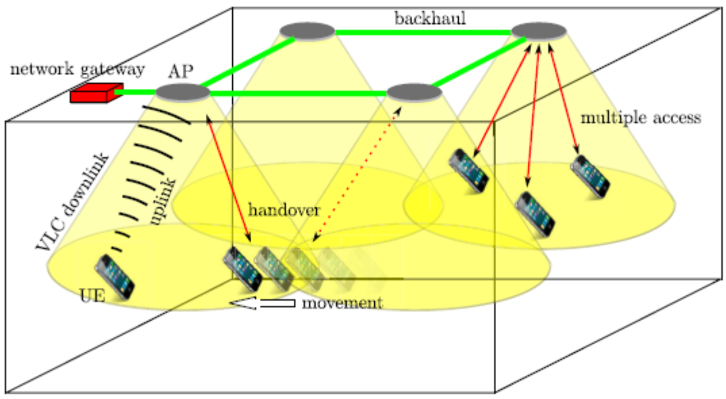

Figure 5-9: LiFi network illustration [Haa20].

LiFi-XC (a commercial product of pureLiFi), supports fully networked cellular communications. Each access point offers full-duplex links with 43 Mbps throughput on downlink and uplink. Multi-user access and roaming between access points (AP) are supported.

The LiFi AP node includes a set of devices that could convert and deliver data packets in the form of light. These devices are:

- LiFi AP. The system architecture of LiFi-XC AP is shown in Figure 5-10(a).
  - A Physical layer implementation based on 802.11 OFDM PHY.
  - Digital-to-analogue and analogue-to-digital convertors which convert the digital signal to analogue signal for downlink transmission, and covert the received analogue signal to digital signal for uplink decoding.
  - A MAC layer interface between the PHY and the upper layers, with functions defined in IEEE 802.11. The implemented MAC could be modified to provide full-duplex operation, high protocol efficiency and multiuser support.
- Transmitter driver, for driving the light luminaire.
- LiFi transmitter, which acts as both luminaire for illumination and antenna for optical wireless signals. It is usually an LED lamp for general use cases, and it can be within either visible light spectrum or infrared spectrum.

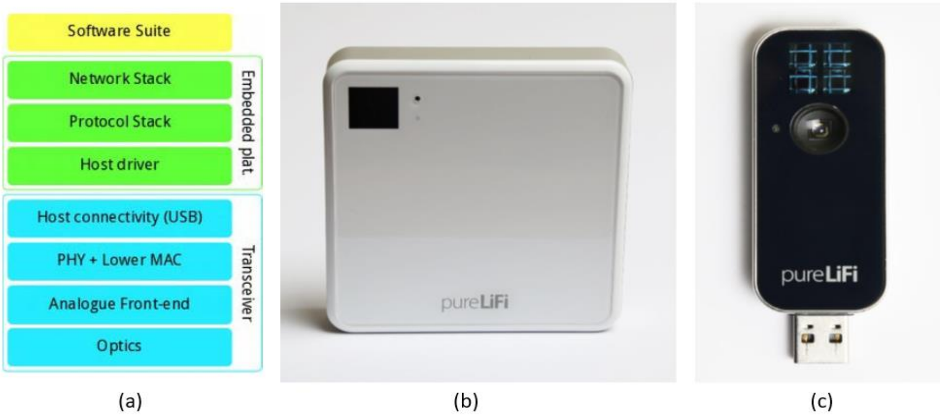

Figure 5-10: (a) LiFi-XC AP architecture; (b) LiFi-XC AP; (c) LiFi-XC User dongle.

Figure 5-11 below shows a typical LiFi network architecture based on LiFi-XC system. Two LiFi access points (APs) are illustrated connecting via ethernet cables to a switch where the internet connection is provided. The APs could be either powered by the PoE+/UPoE ports or by DC power supply. A commercially available lamp is connected to an AP via a transmitter driver. This lamp will provide illumination functionality as well as being a transmitter for light signals. Such downlink optical signal is captured by the receivers integrated in the USB dongle which works as the user station unit. Since full-duplex bi-directional communication is implemented, the station unit also sends uplink infrared signal from the equipped transmitters. On the AP, an array of infrared detector is utilised for the uplink reception. Each AP is cable of providing up to 43 Mbps data rate and supports up to 8 users at the same time.

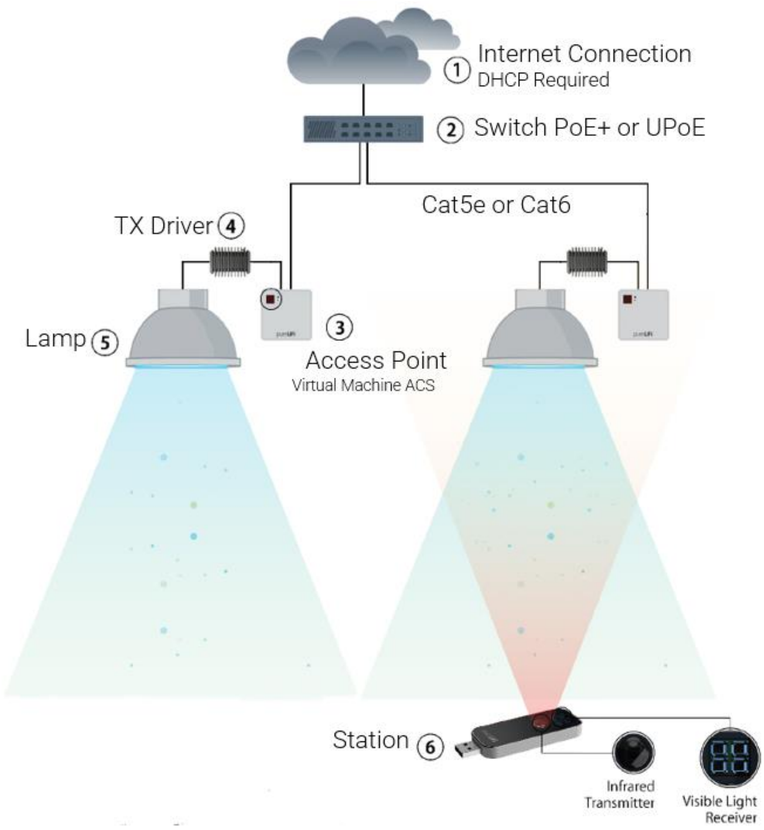

Figure 5-11: Typical LiFi network architecture based on LiFi-XC system.

6 Packet and Optical Monitoring

6.1 Monitoring in Packet-Optical Networks

The recent evolution of coherent transmission technology has driven the miniaturization of transmitter and receiver components, enabling the reduction from traditional 8RU-size modules to small pluggable form factors such as CFP2-DCO (41mm width) and QSFP-DD (18mm width). Although the smallest form factor still suffers from some limitations (e.g., low optical TX power), in the next few years coherent pluggable modules are expected to become the most adopted solution, particularly in the context of metro-edge scenarios. The miniaturization process towards QSFP-DD (e.g., 400ZR module), in addition to space and power savings, will also enable installing coherent modules on off-the-shelf packet switches that are designed for data center operations. This way, the telecom industry has the opportunity to exploit new powerful and cost-effective hardware platforms as well as to open the traditionally closed optical network market to new manufacturers and system integrators. Such switching platforms already make available impressive throughput performance as well as new programmable functionalities, leveraging on the P4 technology. P4 enables the development of new in-network functions designed to operate at wire speed. Several P4 applications have been presented in the literature. They include innovative monitoring and telemetry solutions (e.g., in-band telemetry - INT), hardware acceleration of 5G network functions, dynamic scheduling for low-latency applications, and cyber-security operations (see [CUG22] and ref therein). So far, these works have not considered the specific use of the P4 technology in hardware platforms supporting coherent pluggable modules and thus tightly integrated with the optical transport.

In B5G-OPEN we consider packet-optical nodes equipped with coherent pluggable modules and supporting P4 packet switching programmability. The combination of such technologies is particularly attractive since it may lead to both CAPEX and OPEX savings while guaranteeing more effective traffic engineering solutions as well as new features directly implemented in the data plane. For example, packet-optical nodes may enable the removal of standalone transponders (reducing latency while avoiding O/E/O conversions), may provide a tight and effective integration between the packet and the optical layers, and may enable the implementation of faster and secure networking solutions at wire speed.

In this section we present an innovative monitoring solution enabled by programmable packet-optical white boxes. The solution takes advantage of P4 in-network processing to accelerate the exchange and processing of optical telemetry parameters.

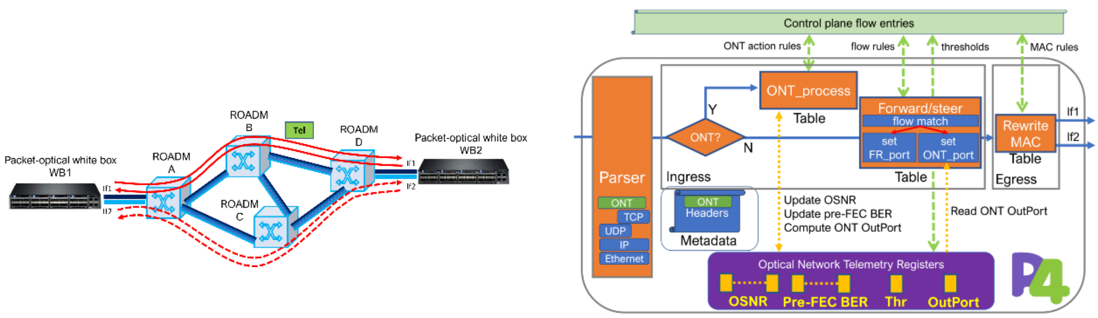

Figure 6-1: Reference network scenario (left). P4 architecture for P4 processing of optical telemetry (right).

Figure 6-1(left) shows a simplified reference scenario including an optical transport network composed of four ROADMs and two packet-optical white boxes (WB1 and WB2 in the figure). Two bidirectional lightpaths are configured at the coherent pluggable interfaces If1 and If2 respectively, at both WB1 and WB2. WB1 monitors the performance of the active lightpaths by collecting relevant optical parameters at the receiver side, e.g., RX of If1. Parameters can include, among others, received optical power, Signal to Noise Ratio (SNR), and pre-FEC Bit Error Rate (BER). These parameters are collected by the driver of the pluggable module. The increasing adoption of the Coherent Common Management Interface Specification (C-CMIS) is expected to guarantee standardized access to pluggables provided by different manufacturers. For example, C-CMIS is largely used to control the 400ZR coherent parameters, called data path coherent monitors, which encompass more than twenty parameters including TX and RX power levels, optical and electrical signal to noise ratio (OSNR and eSNR), and modulator bias values. To access the driver data, two methods can be adopted. The first method exploits a lightweight script directly interfacing the C-CMIS driver. The second method reads the internal database of the operating system of the packet-optical box (e.g., Redis DB in case of SONiC OS), which already has access to the driver data. The latter method has the benefit of abstracting the complexity of directly accessing the driver. Moreover, it represents a unified solution to collect all node parameters. However, it may suffer from scalability issues given the involvement of the database in charge of controlling the whole node. Once the parameters are extracted, they are stored in local P4 registers. To this purpose, a Thrift connection could be adopted between a client reading the driver (or the Redis database) and a server running within the P4 docker including the P4 software development kit (SDK).

P4 registers, exploiting the P4 stateful capabilities, implement a floating window mechanism considering for example the last N values. Basic operations including average and identification of minimum and maximum values can be automatically performed in P4 on the stored values. These values are then compared with pre-defined thresholds/ranges which identify critical deviations. This enables the detection of performance degradations at RX due not only to hard failures (e.g., fiber cut) but also to soft-failures (e.g., malfunctioning of an intermediate amplifier, or narrow filtering induced by laser shift). Extracted data, particularly if above thresholds, are then included in P4-generated telemetry reports sent to WB2, i.e., to the node including the lightpath TX interface. These reports are newly generated packets specifically designed for telemetry purposes, derived from the telemetry reports sent to telemetry collectors in traditional InBand Telemetry (INT) systems. When the telemetry report reaches the WB2 node managing the TX interface, in-network P4 data processing takes place also at WB2. Collected data, possibly handled through P4 registers for further elaborations, are eventually evaluated using flow rule matching operations which can enforce specific traffic steering rules (e.g., rerouting) on either all or selected traffic towards WB1. For example, in case a soft failure related to a moderate increase of pre-FEC BER is experienced at the RX interface of WB1, a telemetry report is sent to WB2. The report triggers a predefined flow rule which steers the high-priority traffic towards an alternative available route (e.g., through If2), securing such traffic against subsequent possible hard failures.

The scheme of Figure 6-1(right) details the internal data plane design of the proposed P4 switch in charge of steering optical traffic based on the indications provided by in-network optical telemetry (i.e., switch WB2 of Figure 6-1(left)). The parser stage classifies the packet protocol stack, including the in-network optical telemetry extra-header and content, referred to as optical in-network telemetry (ONT), thus the switch is able to process both traffic and telemetry packets. Implementation details can be found in [CUG22].

The implemented architecture and related P4 code have been validated in a network testbed reproducing the scenario of Figure 6-1(left), i.e. including the interconnection of two programmable packet switches through an optical fiber link. Two types of switches have been considered: the Behavioral Model version 2 (software switch) and a commercially available programmable switch implementing P4 operations in hardware (e.g., in ASIC).

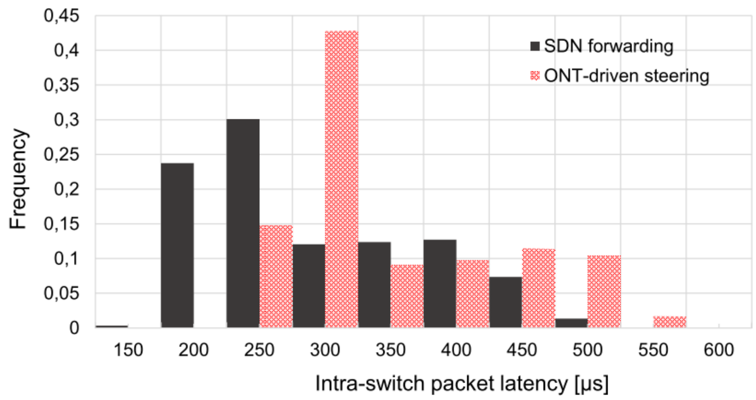

Figure 6-2: Latency distribution for packets subject to forwarding and steering (bmv2 software switch).

The plot of Figure 6-2 reports the intra-switch latency distributions experienced by tributary traffic packets subject to different matching conditions inside the same switch instance. The intra-switch latency distribution is computed by considering the time elapsing between the reception of the packet at the input interface and the transmission of the same packet at the output interface, using the Linux tcpdump application. The plot reports the distribution of a population of 1000 packets (UDP traffic, 256-byte length). The graph shows that the ONT-driven steering distribution (average 320µs) is shifted with respect to standard forwarding (average 270µs) of around 50µs. This value represents the additional complexity burden of the steering action in the ingress pipeline and the additional MAC rewrite action in the egress pipeline if compared to standard forwarding procedures.

However, this introduced extra latency becomes negligible when the P4 operations at WB2 are performed in ASIC. In this case, the results, evaluated by means of a 10GbE SFP+ optical connectivity exploiting the Spirent N4U traffic generator and analyzer, show that less than 1.8µs are always experienced up to 95% wirespeed rate for the overall forwarding across the switch without additional measurable latency when the aforementioned P4 operations are implemented.

This result is particularly relevant since it shows that optical parameters such as OSNR and pre-FEC-BER can be successfully elaborated in the P4 pipeline and, besides delivered to remote monitoring collectors (e.g., through post-card telemetry), they can also be processed locally by the P4 ASIC without extra burden. This way, telemetry packets related to optical performance can trigger automated forwarding decisions towards pre-established alternative routes. In particular, such rerouting can be effectively enforced in less than 2µs upon P4 register update, also in case of soft failures.

This work has been published in the Journal of Optical Communication and Networking [CUG22], where additional details are reported.

6.1.1 List of prototypes

B5G-OPEN focuses on packet-optical nodes supporting (i) P4 programmability, (ii) coherent pluggables, and (iii) Open operating system (e.g., SONiC). Currently, such box is not commercially available yet. For this reason, the prototype currently considered in the project consists of a combination of two boxes, the first one providing P4 programmability, the second one supporting coherent modules. This way, most of the innovative data and control plane solutions for packet-optical boxes can be experimented with adequate level of accuracy.

Two sets of parameters are suitable to control and monitoring within SONiC-based packet-optical boxes. The first set refers to pluggable modules, whose main prototypes and control parameters are described in Section 4. Figure 6-3 left shows an example of transceiver information retrieved in a SONiC box. The second set refers to packet forwarding resources (e.g., queues, packet loss, etc). Figure 6-3 shows two examples of parameters that can be retrieved within a packet-optical box operated with SONiC operating system.

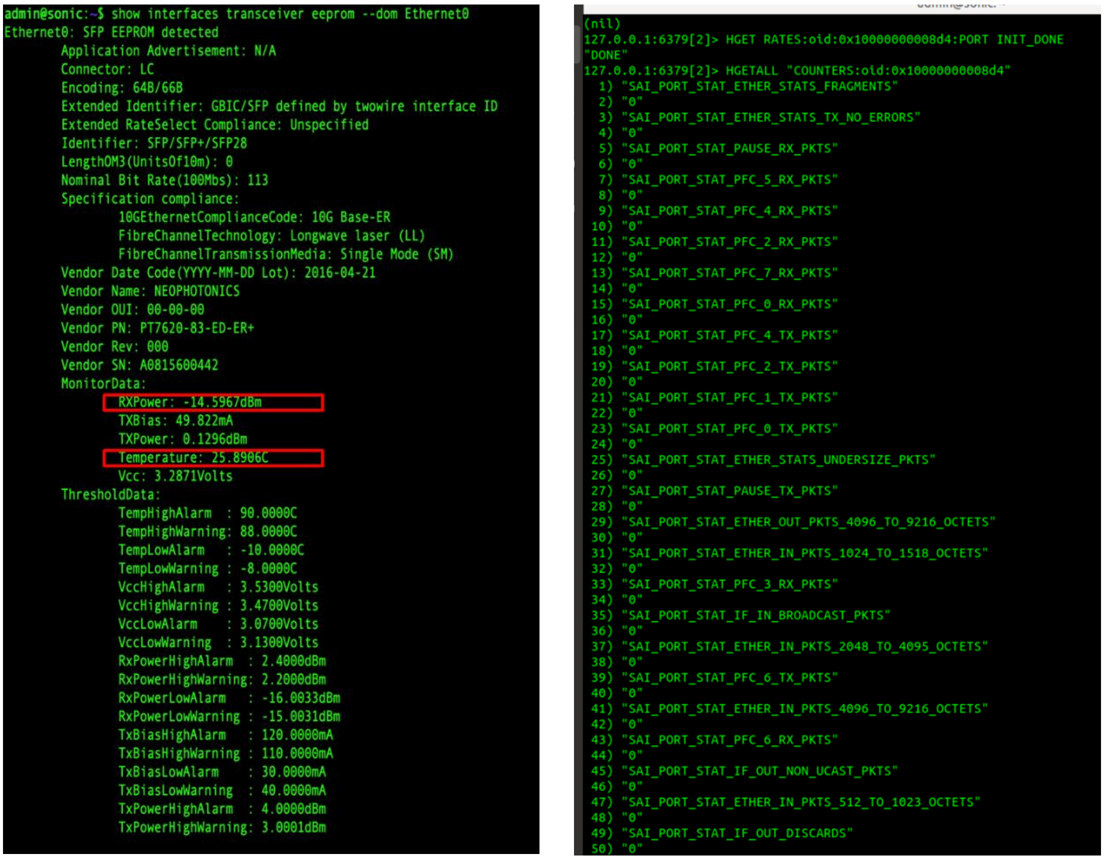

Figure 6-3: Transceiver parameters (left) and counters collected from Redis database.

6.2 Optical Monitoring

Optical communications apply advanced DSP techniques such as modulation format, probabilistic shaping, forward error correction and various equalizers to increase capacity close to the Shannon’s fundamental limit.

To further optimize capacity, the network dimension has to be considered. In particular, close to zero-margin optical network will allow additional capacity to accommodate the unstoppable traffic growth. To get one step closer to marginless operation, massive monitoring needs to be deployed to gather as much information as possible about optical transmission and components impairments. It would allow the detection of soft failures as well as their localization, to make better and faster decisions in terms of operational maintenance and outage avoidance. Recent works on monitoring focused on soft failures detection and identification while localization during operation is often limited to span granularity [Vel18].

Additional hardware may be needed, notably for filter faults identification with the use of optical spectrum analyser (OSA) or for power losses characterization with the use of optical time-domain reflectometers (OTDR). The rise of coherent transmission with powerful DSP at the receiver side opens advanced monitoring capabilities with no extra hardware. This is an appealing area of research. A challenge with receiver-based technique is to have access physical parameters at a given distance of the link beyond cumulative quantities of the entire link, e.g. cumulative chromatic dispersion, PDL.

6.2.1 Longitudinal power profile monitoring

Recently, successful estimations of longitudinal power profiles were demonstrated from a single coherent receiver based on nonlinear back-propagation techniques [Tan20, Sas20, Tan21]. This allows a distance-wise monitoring of physical parameters. Such techniques can localize at a fine granularity (~1km) but cannot estimate the value of the loss. In [May21], it has been experimentally demonstrated that it is also possible to retrieve the amplitude of the loss. The accuracy is dependent on the position of the loss, i.e. it is more accurate at the beginning of the span. Additional phenomena can also be monitored based on [Tan20] such as fiber attenuation [Gle21], or PDL values [Eto22, May22-2].

In this deliverable, we propose other applications and extensions to the initial power profile technique introduced in [Tan19]. A first contribution focuses on the applicability of estimating the value of the power loss in a networking environment, where scalability of our previous work [May21] is investigated. A second contribution is the estimation of power versus wavelength versus distance applied to multiband optical systems. A novel DSP-based monitoring technique was presented (hereafter named link tomography) in order to accurately estimate gain and power profile of C+L-band optical amplifiers without direct measurement [Sen22-1][Sen22-2].

6.2.1.1 Power profile monitoring in a networking scenario

We propose to investigate for the first time how to leverage the diversity of lightpaths in a networking scenario where each of them brings additional monitoring information to enhance the localization and the estimation of a power loss [May22-1].

We proposed in [May21] a model which gives the evolution of the peak amplitude $A_{\text{peak}}(z_0, T_0)$ of the anomaly indicator (AI) - the difference between a reference power profile and a monitored one - for a loss of value $(1 - T0)$ located at the distance $z0 - z(k)$ from the position $z(k)$ of the beginning of the kth span:

$$A_{\text{peak}}(z_0, T_0) = C \cdot P_{\text{ref}}\left(z^{(k)}\right) \cdot (1 - T_0) \cdot 10^{-\alpha_{\text{fiber,dB}} \cdot \frac{z_0 - z^{(k)}}{10}} \quad (6.1),$$

with $\alpha_{\text{fiber,dB}}$ the fiber attenuation coefficient and $P\text{ref}$ the channel launch power of the kth span in the reference profile. The loss distance $z0 - z(k)$ is given by the distance between AI peaks during calibration and monitoring phase. We introduced in [May21] the calibration factor $C \cdot P\text{ref}(z(k))$ which corresponds to the slope of the AI peak amplitude as a function of the loss value $(1 - T0)$ for $z0 = z(k)$. It allowed us to determine this factor by emulating a known loss $(1 - T0)$ at the beginning position $z0 = z(k)$, e.g. by varying the node output power. In [May21], losses were inserted in a single span in a transmission with a single transmitter, a single receiver and a single launch power. Therefore, only one calibration factor was needed to estimate loss values. However, many parameters, such as the channel launch power or the total accumulated noise, could impact the height of the AI peak since it depends on the amount of generated nonlinear effects and on the quality of the received signal. In a network, where each lightpath will go through several spans and have different propagation distances, if no indication on the evolution of the calibration factor is given, the number of needed calibrations will be very high. Therefore, we first propose to extend and generalize the calibration method to multiple lightpaths and powers and then, to take advantage of the diversity of lightpaths – called “line” in the rest of the study - in a network to improve the quality of the results.

To extend the calibration validity, we performed experiments on the meshed optical network testbed depicted in Figure 6-4(a). It is composed of seven nodes built from 3 vendors (Nokia, Lumentum and a prototype). The outer ring ranges 475 km of SSMF optical fiber. We load the network with 20 ASE channels aligned on the 50GHz ITU grid. Three 32 GBaud PDM-QPSK channels are generated by a Nokia 1830 PSI-2T, named Line 1, 2 and 3 (in blue, red, and green), injected from distinct source nodes, A, B and D and received at the same destination node G after propagating through 421 km, 341 km and 202 km of optical fiber, respectively. These optical channels are both decoded by a Nokia 1830 PSI-2T and sent to an offline coherent receiver with 70 GHz bandwidth and 200 GSamples/s real-time oscilloscope. The network testbed is operated in a constant power mode, i.e., the output power of nodes is maintained constant regardless of the input power. Finally, a programmable variable optical attenuator (VOA) is placed after 24.02 km (OTDR estimation) of propagation in the penultimate fiber span, i.e., between node E and F, and enables the insertion of extra power loss (red lightning in Fig. 1a). When not specified, the channel launch power is 5 dBm.

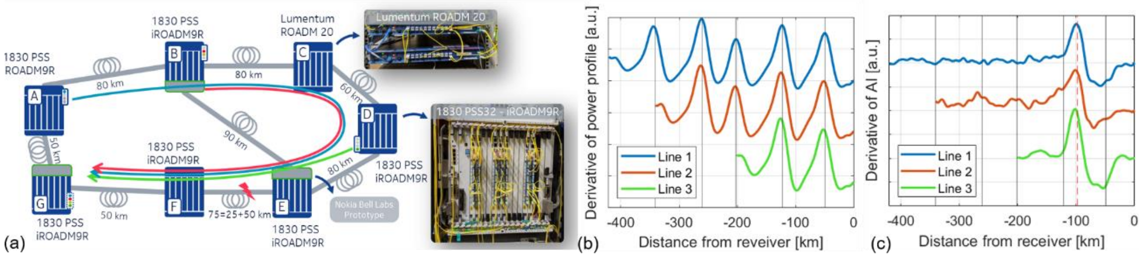

Figure 6-4: (a) Experimental optical network testbed; (b) Derivative of power profile monitoring of 3 lightpaths; (c) derivative of the anomaly indicator when a los of 4.5dB occurs at 25km after node E.

For each loss and line, 65000 raw power profiles were computed. Each profile is computed using 2048 received samples. In Figure 6-4(b), we plot the derivative of the average reference power profiles for the 3 lines such that the position of the peaks corresponds to the position of the nodes (vertical solid black line). For each line, the calibration factor $C \cdot P_{\mathrm{ref}}\left(z^{(k=E)}\right)$ is obtained by varying the output power of the node E. Then we perform loss estimations by using the amplitude and position of the AI peaks. For example, inFigure 6-4(c), we plot the derivative of the AIs for each line for a 4.5 dB loss, all showing a peak around the position of the inserted loss (vertical dashed red line).

To reduce the number of required calibrations, we propose to use the same calibration factor for several lines. We perform loss estimation using 12000 raw profiles for line 1 and 3 with different calibration factors: one with the corresponding factor (inner calibration) and one with the factor of another line (outer calibration). We plot in Figure 6-5(a), (resp. Figure 6-5(b)), the mean estimated loss (over 5 realizations) for line 1 versus inserted loss when the calibration factor of line 1 and 2 are used, (resp. for line 3 with factor of line 3 and 1). The errors bars correspond to the maximum and minimum estimated values. We notice that though the estimation is better when the inner calibration factor is used in Figure 6-5(b) (red squares), in Figure 6-5(a), it is not the case. We attribute such discrepancy to the intrinsic error of the estimation which is of the same order of magnitude as the outer calibration error. Either way, we see that, confirming our proposition, the estimation remains accurate when using the calibration of a line with a different propagation distance, from 202 km (line 3) to 421 km (line 1), and different performance.

We also propose to extend the calibration factor validity to different launch powers. We determine $C \cdot P_{\text{ref}}\left(z^{(k=E)}\right)$ for various span launch powers per channel, from 5 dBm (3.16 mW) to -2.5 dBm (0.56 mW). The results are reported for each line in Figure 6-5(c). We see that the calibration factor is proportional to the launch power, which validates the proposed formulation of the calibration factor as the product $C \cdot P_{\text{ref}}\left(z^{(k=E)}\right)$ in [May21] and allows us to rely only on the value of its first term C.

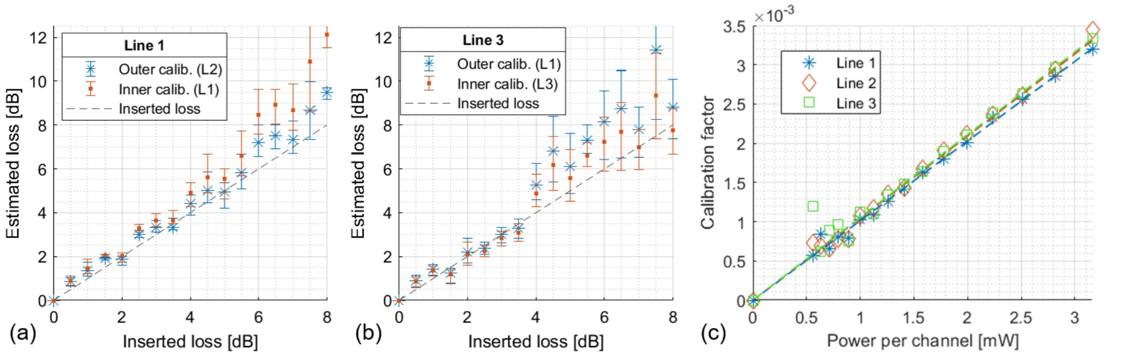

Figure 6-5: (a) Loss estimations from line 1 with calibration factors from line 2 and line 1. (b) Loss estimations from line 3 with calibration factors.

In an optical network, when an extra loss occurs in a span, several receivers would have estimated both its distance to node and its value. In monitored networks, we can combine these estimations to refine them and increase reliability by avoiding having to trust a single line. We perform another series of experiments, varying the VOA attenuation from 0.5 to 8 dB. In the following, the AIs are computed using 28000 raw profiles with a 1-km resolution and we use only one calibration factor (from Line 2). For each line and each loss, we estimate the distance from node E and loss value.

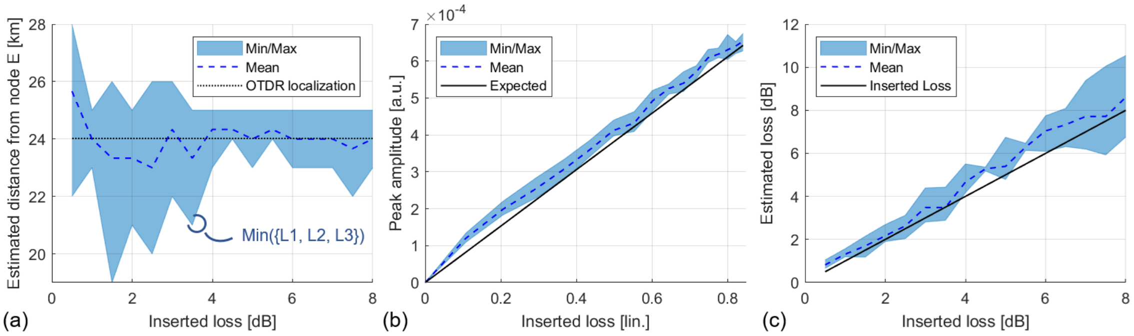

Figure 6-6: Estimation statistics over Line 1, 2 and 3: (a) Estimated distance of the losses from node as a function of inserted loss. (b) Peak amplitude as a function of inserted loss. (c) Estimated loss as a function of inserted loss.

In Figure 6-6(a), we report the mean, maximum and minimum estimated loss distances from the node E over the three lines as a function of inserted losses. We circled a point which corresponds to an attenuation of 3.5 dB and is the minimum estimated distance of the three lines, equal to 21 km. We see that the mean estimated distance over lines is very close its measured value (by

OTDR) 24.02 km. We observe that for small losses, the single line estimations (maximum or minimum) can be quite far away from the OTDR value. For instance, for a loss of 2.5 dB, the single line error in localization can be up to 4 km, while it is reduced to 1 km when the three estimations are averaged. Thus, estimation diversity helps reducing the localization error. This increase in localization accuracy will also reduce the error on the fiber propagation loss term in Eq.(6.1) and thus reduce the loss estimation error. In Figure 6-6(b), we report, in the same way, the peak amplitudes statistics over the three lines. We also plot the expected peak values obtained from Eq.(6.1) with the known position and values of the losses. We see that the difference between maximum and minimum values over the three lines is small, confirming the possibility to use a single calibration factor for the three lines for the estimation at z_0=24.02km. Finally, we plot in Figure 6-6(c), the maximum and minimum single line estimations as well as the estimations using the mean values of distance and peak amplitudes over the three lines. We observe that taking these mean values to perform the estimation allows an improvement of the accuracy. For example, for an attenuation of 3 dB, the combined estimation error is 0.50 dB whereas one of the three lines alone gives an error of 1.40 dB. Overall, for all losses, the maximum error of the mean value is <1.0 dB, and <0.7 dB for losses <4 dB. This highlights the benefits of combining the results of several lines.

6.2.1.2 Receiver DSP-based Line System Monitoring

A secure migration from today’s C-band based optical networks to a MB scenario heavily relies on monitoring mechanisms that can accurately measure not only wavelength-resolved characteristics of MB optical components (e.g., amplifiers, switches, and transceivers) but also distance-wise properties of optical links across nationwide networks. That is relevant because these monitoring capabilities will support MB network provisioning strategies in multiple of the nowadays’ challenges, for instance, reducing uncertainties about physical layer parameters, discovering types of fiber deployed in the link and/or assertively identifying origin of transmission faults. However, despite the variety of optical performance monitoring (OPM) techniques and devices traditionally employed in current commercial optical systems, a central and open question in the optical communication community is: how to efficiently distribute monitors across complex networks in a cost-effective way in order to capture wavelength-resolved spatially-distributed information. Recently, several monitoring features have been obtained by solely exploiting receiver (Rx) digital signal processing (DSP) modules, thus minimizing the requirements of distributed node-level measurement devices. The popularity of these Rx-based OPM approaches is due in part to their capability of unveiling multi-span link properties, such as longitudinal power profile [Sas21], [Eto22], frequency response of bandpass filters, span-wise chromatic dispersion mapping [Sen22-1] and Raman gain [Tur18]. One successful example of such application was introduced in [Sas21], where the authors proposed an in-situ power profile estimator (PPE) that reconstructs the channel power evolution along the link with sub-km resolutions [Eto22]. An insightful application that we foresee from this technique is that by overlaying the in-situ PPE from multiple WDM channels it is possible to create a distance-wise, wavelength-dependent link tomography [Sas20]. This link tomography embodies the relation power versus wavelength versus distance and discloses multi-degree characteristics of the optical link.

By applying the in-situ PPE to multiband optical systems, a novel DSP-based monitoring technique was presented (hereafter named link tomography) in order to accurately estimate gain and power profile of C+L-band optical amplifiers without direct measurement [Sen22-1][Sen22-2]. The relevance of the technique was validated by utilizing the proposed link tomography for two different use-cases: longitudinal power profile monitoring and anomaly detection. The first use-case utilizes the power profile to infer amplifier characteristics, such as gain and tilt within the system. The second use-case studies anomaly detection, in which optical amplifier anomalies, such as, gain, tilt and narrowband gain compression are observed. Additionally, it was shown how advanced DSP tools based on denoising algorithms can improve the visualization and accuracy of the anomaly location by reducing positioning uncertainty.

The experimental testbed used during the validation of the technique is shown in Figure 6-7(a). The transmitter is composed by a 4-ch 92 GSa/s DAC, and a commercially available C-band optical multi-format transmitter comprising a quad-set of driver amplifiers and a dual-polarization (DP) IQ-modulator. Two tunable external cavity laser (ECL) sources were utilized to cover the tested wavelengths in the C-band (1527.5 – 1565 nm), and L-band (1570 – 1600 nm). Then, a 64-GBd DP 16-QAM signal generated with a 2^15 random bit sequence and shaped with a root-raised cosine pulse filter with roll-off factor 0.1 was transmitted over a 280-km SMF link consisting of two 80-km spans (1st and 3rd spans) and two 60-km spans (2nd and 4th spans). All three in-line EDFAs deployed in the link were operated in the wavelength intervals of 1540-1565 nm (C-band) and 1570-1605 nm (L-band). After the signal is received, it is digitized by a 200 GS/s RTO and forwarded to the receiver-DSP chain. The emulation of the multiple WDM carriers was performed by tuning the ECL in steps of 2.5 nm (single-channel experiments) in [Sen22-1] and by shaping ASE noise through wavelength selective switches (multi-channel experiments) in [Sen22-2].

The goal of the first use-case is to solely rely on the transceiver monitoring capability to estimate spectral features of the 1st, 2nd and 3rd in-line EDFAs, highlighted in red in Figure 6-7(b). That is possible because the p-th in-line EDFA gain (Gp), for a fixed wavelength, can be estimated from the in-situ PPE, as shown in Figure 6-7(b). To validate the possibility of extracting the spectral gain from the link tomography, Figure 6-7(c) showcases the estimated gain for in-line EDFA 1 in unison with the b2b OSA characterization. As it is possible to see, the spectral gain obtained from the link tomography has a good agreement with the OSA measurement, yielding a mean absolute error over all wavelengths of around 0.6 dB. In addition, by calibrating the in-situ PPE result from Figure 6-7(b) in accordance with the measured spectra, a spectral visualization estimation is also obtainable. This is visible in Figure 6-7(d), where the measured spectra of the in-line EDFA 2 is compared to the power spectral density estimated by the calibrated link tomography.

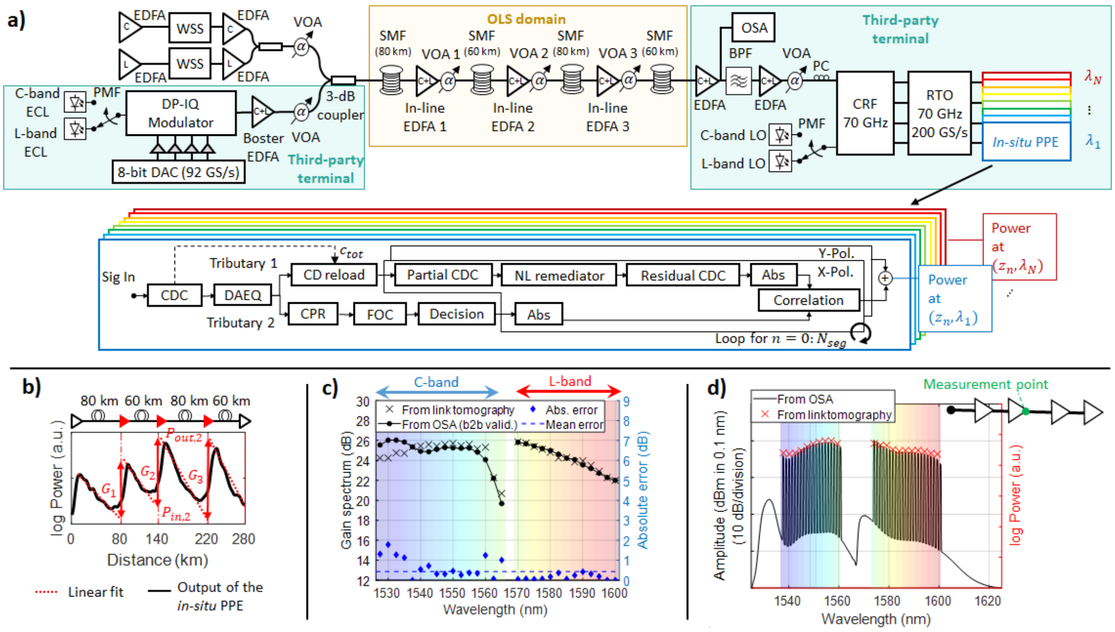

Figure 6-7: (a) Experimental testbed and DSP scheme used in the link tomography. (b) Output of the in-situ PPE, where G1, G2 and G3 indicate the estimated gain of the 1st, 2nd and 3rd in-line EDFA (at fixed wavelength), respectively. (c) Link tomography used to estimate the spectral gain profile. (d) Link tomography used to obtain spectral features in a multi-channel multiband optical system.

The second use-case aims to validate the capacity of the technique to detect failures, or anomalies within the system. In order to confirm whether the link tomography can successfully capture an anomaly, an excessive attenuation is emulated at the input of in-line EDFA 2 by inserting a VOA with a spectrally flat 6-dB attenuation profile. By doing so, it is expected that a gain tilt will be generated at the output of the inline EDFA 2, since the incoming power is now 6 dB lower. Then, a simplified failure detection scheme is applied, which is based on the direct difference between two monitored states of the link tomography, i.e., one without anomaly (reference) and one with anomaly (continuously monitored), as proposed in [Tan19] and depicted in Figure 6-8(a). The result of this subtraction is then projected on a heat map as illustrated in Figure 6-8(b). As can be observed, two important anomaly “signatures” are clearly visible from the heat map. The first one, in the vicinity of 140 km, indicates the emulated tilt on the in-line EDFA 2. Given the wavelength-dependency of this signature and the proximity to the in-line EDFA 2, this anomaly is easily distinguishable from other link faults, such as excessive attenuation points in the fiber, which has a wavelength-independent profile. The second signature, in the proximity of 220 km, shows a cascaded effect at the in-line EDFA 3, which is a direct consequence of the different input spectrum experienced by this amplifier. In other words, the first tilt profile (from in-line EDFA 2) provokes a tilt in the in-line EDFA 3. This demonstrates how effective the link tomography can be in determining wavelength-dependent disruptions in optical links.

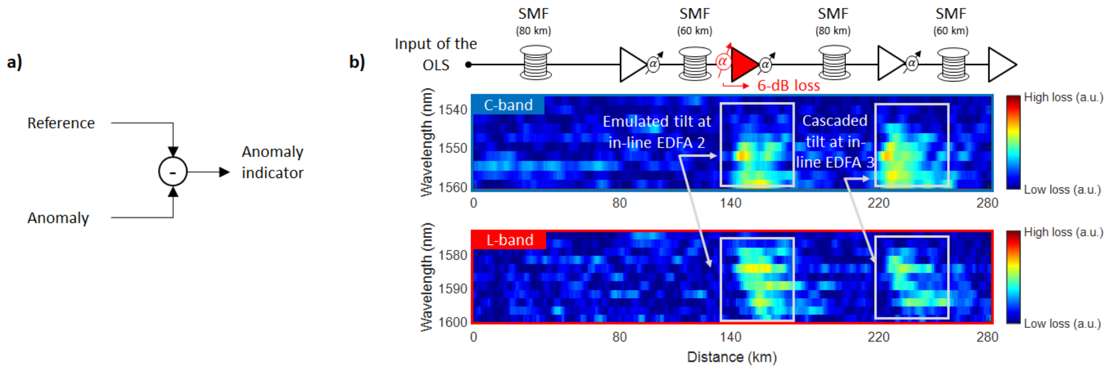

Figure 6-8: (a) Anomaly detection scheme based on the subtraction of the anomalous link tomography from the reference one. b) Anomaly indicator map based on the subtraction scheme.

While Figure 6-8 demonstrates that the subtraction scheme can already provide an approximate indication of the location of the fault, it also reveals that the non-uniformity and sparsity of the signatures can hinder the identification of the problem. One alternative to improve the subtraction scheme is by inserting a numerical differentiation with respect to the spatial domain, as proposed in [Tan20] and likewise illustrated in Figure 6-9(a). Yet, this approach is still very dependent on multiple trace averaging to guarantee an accurate estimation. Therefore, [Sen22-2] proposes a novel detection method based on wavelet denoising of the link tomography as illustrated in Figure 6-9(b).

In order to emulate anomalies that could affect the performance of the in-line EDFAs 2 and 3, an additional VOA was installed at the output of these amplifiers and programmed with a spectrally flat attenuation profile of 3 dB. This emulation of an anomaly, could, for example, correspond to an excessive loss originated from inappropriate amplifier-to-fiber connectors or simply a depletion in the amplifier's pump current. In Figure 6-9(c), it is possible to visualize on the heat map the result of the subtraction + differentiation method from Figure 6-9(a) for the in-line EDFA 3. Qualitatively speaking, the heat map can give a rough indication of the fault location, which in this case occurred in the vicinity of 220 km. However, it is clearly visible that the "signature" caused by these anomalies leave a non-uniform pattern in the heat map, which is further penalized by the noisy profile of heat map. Now, in Figure 6-9(d), the outcome of the proposed approach in Figure 6-9(b) is evaluated. In this new method, it is possible to observe that a significant improvement with respect to the noisy profile experienced in Figure 6-9(c) was achieved. Additionally, an enhancement regarding the uniformity of the signature is likewise noticeable in comparison to Figure 6-9(c).

Quantitatively, it is also possible to measure an improvement with respect to the location of the anomaly. In the plot in Figure 6-9(e), it is illustrated, for a fixed wavelength (1549 nm), the results from subtraction + differentiation and wavelet denoising to locate the positioning of the fault, i.e., position of in-line EDFA 2. As can be seen, the proposed approach, i.e., via wavelet denoising, can improve the location of the fault by 3 km, which in this case is represented by the position of peak in Figure 6-9(e). Furthermore, a smoother anomaly detection curve (red solid line) is acquired, in comparison to the subtraction + differentiation method (blue solid line). This helps to easily distinguish the real anomaly from other irrelevant spikes that may lead to false conclusions.

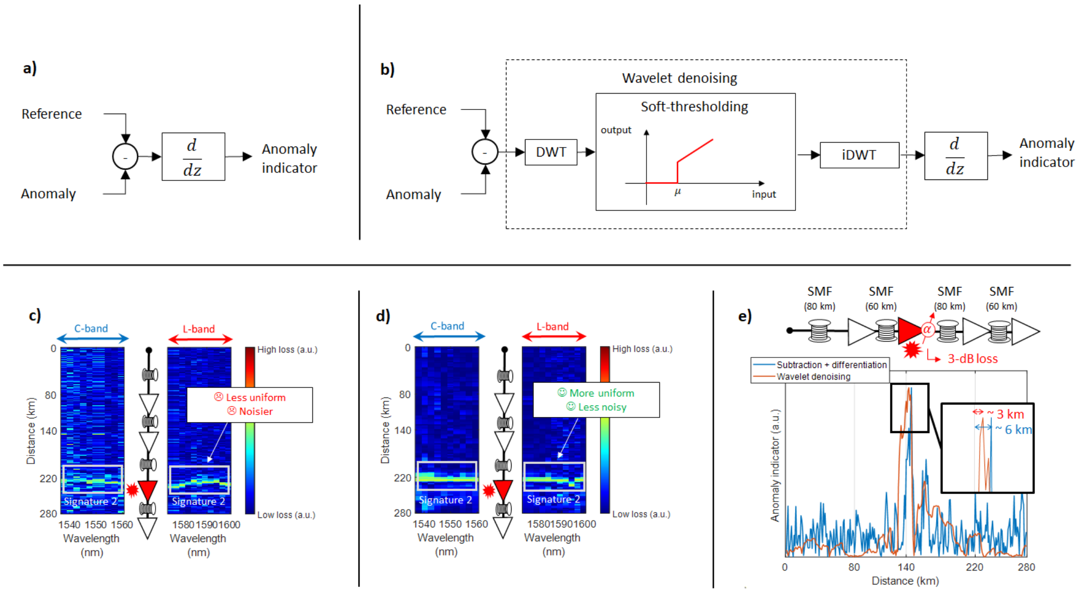

Figure 6-9: Anomaly detection schemes based on a) the subtraction + differentiation and b) wavelet denoising. Anomaly indication maps, when c) subtraction + differentiation and d) wavelet denoising are applied to detect power depletion in in-line EDFA 3. e) Anomaly detection curve for power depletion in in-line EDFA 2, when subtraction + differentiation and wavelet denoising are applied on a single wavelength (1549 nm).

6.2.2 List of monitored values feeding WP4

The optical layer can be monitored by collecting data from transponders and/or from the node themselves. Widespread monitoring metrics available in commercial product like at the transponder side are pre-FEC BER, post-FEC BER, cumulative chromatic dispersion, power. In deployed commercial networks, monitoring periodicity is usually set to 15 minutes, but faster data acquisition is also possible down to the second level. In addition to these metrics, with offline transmission system or additional hardware equipment, it also possible to get access to the received optical spectrum. There are ongoing discussions between Nokia and UPC to feed WP4 with optical spectrum where the challenge is to report the appropriate level of information (resolution, periodicity) to the monitoring plane.

7 CONCLUSIONS

This deliverable reports on the activities of the WP3 during the first year of the project. A relevant architecture for optical continuum multiband data plane was developed in WP2 and taken as an input for WP3. For each different domain, a subset of technologies options was identified to match the different characteristics and hence requirements in terms of cost, capacity, reach, scalability, flexibility, etc. This was first discussed as an overview of the definition of requirements per domain, from the end user to the cloud. Then, for each domain a detailed requirements for the transport platform and nodes were provided.

To design the physical layer, different assumptions can be accounted for and result in different methods to predict performance. This deliverable compared state-of-the art methodologies and with a detailed view of assumptions, pros and cons. Physical layer characterization was then discussed as it influences the accuracy of the prediction. A physical layer modelling tool is then presented across C, L, S, and E bands with detailed explanation of the modelling.

To use such modelling methods in a multi-vendor context, it is important to agree on the definition of vendor-neutral YANG data models beyond C-band. During the first year, B5G-OPEN studied existing initiatives for C-band and compared them as reported in this deliverable. Preliminary design solutions are also presented for metro-aggregation.

For less than 1500km optical reach, B5G-OPEN also targets to use commercial solutions like pluggable modules. This deliverable presented the existing solutions under investigation which include PtoP (e.g. 200G DCO, 400ZR, 400XR) and PtoMP (e.g. 400XR, TIBIT) transmission. The latter PtoMP targets filterless domain like the access domain.

Advanced solutions for multiband optical networks were also presented, detailing B5G-OPEN prototypes ranging from transponders to optical switches. A multiband sliceable transponder is proposed over C-, L- and S-bands and performance evaluation across these bands was reported. Multiband OADM capable of operating in the O-, S-, C- and L-band with drop and continue operation was also investigated. Regarding multiband amplifiers, the first year was devoted to the understanding of how nonlinear effects limit the maximum increase of bandwidth and the hardware requirements for upgrading existing C-band systems.

Integration in the access part of different technologies including wireline and wireless network elements is reported in D3.1. Different architectures are presented for short, medium and long-term introduction of multiband optical systems in the access domain. For the long-term evolution, a multiband WSS will allow to seamlessly terminate any number of channels either at the access CO or the regional CO. Convergence of wireless and wireline optical fiber was also presented with a particular focus on the LiFi architecture.

Finally, advanced monitoring solutions are presented for both packet and optical network elements in order to efficiently use the network resources. By proposing a novel monitoring architecture based on P4 processing, the packet-optical node allows peer to peer telemetry reports of commonly use optical monitoring information. Additionally, D3.1 reported evolution of the optical monitoring capabilities by presenting results on power profile monitoring based on coherent receiver. This requires no additional hardware to be deployed and may expose in the medium term more optical parameters to the control and management plane.

This deliverable feeds WP4 for the definition of control and management of the network elements to enable the required flexibility as well as the continuum of resources throughout different network domains. For such cost-effective management, packet and optical monitoring is key and WP4 details the monitoring and analytics architectures envisaged.

8 REFERENCES

[Bac22] Bäck, Johan, et al. "A Filterless Design with Point-to-multipoint Transceivers for Cost-Effective and Challenging Metro/Regional Aggregation Topologies." *2022 International Conference on Optical Network Design and Modeling (ONDM)*. IEEE, 2022

[Bra00] P. S. Bradley, K. P. Bennett, A. Demiriz “Constrained K-Means Clustering”, May 2000.https://www.microsoft.com/en-us/research/wp-content/uploads/2016/02/tr-2000-65.pdf

[Can18] M. Cantono et al., “On the Interplay of Nonlinear Interference Generation With Stimulated Raman Scattering for QoT Estimation," in J. Lightwave Technol., vol. 36, no.15, pp.3131-3141, 2018.

[CAS21] R.Casellas, E. Kosmatos, A. Lord, C. Matrakidis, R. Martınez, D. Uzunidis, R. Vilalta, A. Stavdas, R. Munoz, “An SDN Control Plane for Multiband Networks Exploiting a PLI-aware Routing Engine”, in Optical Fiber Communication Conference (OFC), 2022.

[CHR96] D. N. Christodoulides and R. B. Jander, "Evolution of stimulated Raman crosstalk in wavelength division multiplexed systems," in IEEE Photonics Technology Letters, vol. 8, no. 12, pp. 1722-1724, Dec. 1996.

[CHR84] A. R. Chraplyvy, "Optical power limits in multi-channel wavelength-division-multiplexed systems due to stimulated Raman scattering," in Elect. Lett., vol. 20, no. 2, pp. 58-59, 19 January 1984.

[CUG22] F. Cugini et al, “Telemetry and AI-based Security P4 Applications for Optical Networks”, JOCN 2022.

[Dam22] A. D'Amico et al., "GNPy Experimental Validation for Nyquist Subcarriers Flexible Transmission up to 800 G," 2022 Optical Fiber Communications Conference and Exhibition (OFC), 2022.

[Eto22] M. Eto et al., “Location-Resolved PDL Monitoring With Rx-Side Digital Signal Processing in Multi-Span Optical Transmission Systems,” in Optical Fiber Communication Conf., 2022

[FER20] A. Ferrari et al.,"Assessment on the Achievable Throughput of Multi-Band ITU-T G.652.D Fiber Transmission Systems," J. Lightwave Technol. vol. 38, no.16, pp.4279-4291, 2020.

[GAL20] L. Galdino et al., "Optical Fiber Capacity Optimisation via Continuous Bandwidth Amplification and Geometric Shaping," in IEEE Photonics Technology Letters, vol. 32, no. 17, pp. 1021-1024, 1 Sept.1, 2020.

[Gle21] S. Gleb et al., “Fiber Link Anomaly Detection and Estimation Based on Signal Nonlinearity,” European Conference on Optical Communication, 2021.

[GNPY] GNPy: Optical Route Planning Library. [Online]. Available: https://gnpy.readthedocs.io/en/master/

[Haa20] Haas, H., Yin, L., Chen, C., Videv, S., Parol, D., Poves, E., Alshaer, H. and Islim, M.S., ‘’Introduction to indoor networking concepts and challenges in LiFi,” Journal of Optical Communications and Networking, 2020, 12(2), pp. A190-A203.

[Her23] J. A. Hernandez, F. Arpanaei, G. Martinez, O. Gonzalez de Dios, J. P. Fernandez-Palacios, A. Napoli, Clustering-based dynamic bandwidth allocation for point-to-multipoint coherent optics, submitted to OFC2023

[Hos22-1] Mohammad M. Hosseini, Joao Pedro, Antonio Napoli, Nelson Costa, Jaroslaw E. Prilepsky, Sergei K. Turitsyn, Long-Term Cost-Effectiveness of Metro Networks Exploiting Point-to-Multipoint Transceivers, ONDM

[Hos22-2] M. Hosseini, J. Pedro, N. Costa, A. Napoli, J. Prilepsky, S. Turitsyn, Multi-Period Planning in Metro-Aggregation Networks using Point-to-Multipoint Transceivers, GLOBECOM 2022

[Hos23] Mohammad M. Hosseini, Joao Pedro, Nelson Costa, Antonio Napoli, Jaroslaw E. Prilepsky, Sergei K. Turitsyn , Optimal Design of Filterless Horseshoe Networks Supporting Point-to-Multipoint Transceivers, submitted to OFC2023

[IETF] IETF YANG Data Model for Optical Impairment-aware Topology draft. [Online]. Available: https://datatracker.ietf.org/doc/html/draft-ietf-ccamp-optical-impairment-topology-yang-09#section-2.5.2.

[ICOP2022] M. Quagliotti, et al., "Applicability of a new generation of photonic devices in backbone network scenarios", in Proceedings of Italian Conference on Optics and Photonics, ICOP 2022, 15-17 June 2022, Trento, Italy

[ITU-T G.Sup66-201907] ITU-T G.Sup66-201907, “5G wireless fronthaul requirements in a passive optical network context”, 07/2019

[Kra22] R. Kraemer, H. Santana, S. Zhang, B. Pan, and N. Calabretta, “Lossless SOA-based Multi-band OADM Nodes in Metro Networks,” OECC2022.

[Mat15] C. Matrakidis, T. Orphanoudakis, A. Stavdas, J. Palacios and A. Manzalini: "HYDRA: a Scalable Ultra Long Reach/High Capacity Access Network Architecture Featuring Lower Cost and Power Consumption", OSA/IEEE Journal of Lightwave Technology Vol.33 (2), pp. 339 - 348, 2015

[May21] A. May et al., “Receiver-Based Experimental Estimation of Power Losses in Optical Networks,” IEEE Photon. Technol. Lett., vol. 33, no. 22, 2021, pp. 1238–1241.

[May22-1] A. May et al., “Demonstration of Enhanced Power Losses Characterization in Optical Networks,” Optical Fiber Communication Conf., 2022.

[May22-2] A. May et al., “Receiver-Based Localization and Estimation of Polarization Dependent Loss,” OptoElectronics and Communications Conference (OECC) and 2022 International Conference on Photonics in Switching and Computing (PSC), 2022.

[Nad22-1] L. Nadal, M. S. Moreolo, J. M. Fàbrega and F. J. Vílchez, "SDN-Enabled Multi-Band S-BVT Within Disaggregated Optical Networks," in Journal of Lightwave Technology, vol. 40, no. 11, pp. 3479-3485, 1 June1, 2022, doi: 10.1109/JLT.2022.3158388.

[Nad22-2] L. Nadal, M. S. Moreolo, J. M. Fàbrega and F. J. Vílchez, "Enabling Programmable Multiband High-Capacity Optical Transceivers," 2022 27th OptoElectronics and Communications Conference (OECC) and 2022 International Conference on Photonics in Switching and Computing (PSC), 2022, pp. 1-4, doi: 10.23919/OECC/PSC53152.2022.9850140.

[Nad21] Laia Nadal, Josep M. Fàbrega, Michela Svaluto Moreolo, F. Javier Vílchez, Ramon Casellas, Raul Muñoz, Ricard Vilalta, and Ricardo Martínez, "Programmable disaggregated multi-dimensional S-BVT as an enabler for high capacity optical metro networks," J. Opt. Commun. Netw. 13, C31-C40 (2021).

[Neop] https://www.neophotonics.com/press-releases/?newsId=12486 (2021). [Online; accessed 15-July-2021].

[New20] M. Newland, R. Schmogrow, M. Cantono, V. Vusirikala, and T. Hofmeister, “Open optical communication systems at a hyperscale operator,” J. Opt. Commun. Netw. 12, C50–C57 (2020).

[OpenConfig] OpenConfig, “OpenConfig web site,”Mar. 2018. [Online]. Available: http://www.openconfig.net

[Orp15] T. Orphanoudakis, C. Matrakidis, A. Stavdas, "Greening Next Generation Optical Networks through a Collapsed Access and Metro Network Architecture ", 20th European Conference on Networks and Optical Communications - (NOC), 2015

[Pav22-1] P. Pavon Marino, N. Skorin-Kapov, M. V. Bueno-Delgado, J. Back, A. Napoli, On the Benefits of Point-to-Multipoint Coherent Optics for Multilayer Capacity Planning in Ring Networks with Varying Traffic Profiles, JOCN

[Pav22-2] Pablo Pavon-Marino, Nina Skorin-Kapov, Antonio Napoli, A Network Dimensioning Algorithm for Exploiting the Capabilities of Subcarrier-based Point-to-Multipoint Coherent Optics, ECOC 2022

[Pin19] E. Pincemin, Y. Loussouarn, Y. Pan, G. Miller, A. Gibbemeyer, B. Mikkelsen, A. Gaibazzi, W. Way, T. Yamazaki, A. Hayashi et al., “Interoperable CFP-DCO and CFP2-DCO pluggable optic interfaces for 100G WDM transmission,” in 2019 Optical Fiber Communications Conference and Exhibition (OFC), (IEEE, 2019)

[PUT21-1] B. J. Puttnam, R. S. Luís, G. Rademacher, Y. Awaji and H. Furukawa, "319 Tb/s Transmission over 3001 km with S, C and L band signals over >120nm bandwidth in 125 µm wide 4-core fiber," 2021 Optical Fiber Communications Conference and Exhibition (OFC), 2021, pp. 1-3.

[PUT21-2] B. J. Puttnam, R. S. Luís, G. Rademacher, M. Mendez-Astudilio, Y. Awaji and H. Furukawa, "S, C and Extended L-Band Transmission with Doped Fiber and Distributed Raman Amplification," 2021 Optical Fiber Communications Conference and Exhibition (OFC), 2021, pp. 1-3.

[POG17] P. Poggiolini, and Y. Jiang, “Recent advances in the modeling of the impact of nonlinear fiber propagation effects on uncompensated coherent transmission systems,” Journal of Lightwave Technology, vol. 35, no. 3, pp. 458–480, 2017.

[RAP22] L. Rapp and M. Eiselt, "Optical Amplifiers for Multi–Band Optical Transmission Systems," in Journal of Lightwave Technology, vol. 40, no. 6, pp. 1579-1589, 15 March15, 2022

[Sad22] R. Sadeghi et al., "Capacity and Energy Consumption Comparison in Translucent versus Transparent Multi-band Designs," 2022 International Conference on Optical Network Design and Modeling (ONDM), 2022, doi: 10.23919/ONDM54585.2022.9782854.

[Sas20] T. Sasai et al., “Simultaneous Detection of Anomaly Points and Fiber types in Multi-span Transmission Links Only by Receiver-side Digital Signal Processing,” in Optical Fiber Communication Conf., 2020.

[Sas21] T. Sasai et al., “Revealing Raman-amplified Power Profile and Raman Gain Spectra with Digital Backpropagation,” presented at the Optical Fiber Communications Conference and Exhibition (OFC), 2021, pp. 1-3.

[SEM17] D. Semrau, R. Killey, and P. Bayvel. "Achievable rate degradation of ultra-wideband coherent fiber communication systems due to stimulated Raman scattering." Opt, Expr. 25.12 (2017): 13024-13034.

[SEM18] Semrau, D., Killey, R. I., & Bayvel, P., “The Gaussian noise model in the presence of inter-channel stimulated Raman scattering.” J. of Lightw. Technol., vol. 36, no.14, pp.3046-3055, 2018.

[Sen22-1] M. Sena et al., "DSP-Based Link Tomography for Amplifier Gain Estimation and Anomaly Detection in C+L-Band Systems," in Journal of Lightwave Technology, vol. 40, no. 11, pp. 3395-3405, 1 June1, 2022, doi: 10.1109/JLT.2022.3160101.

[Sen22-2] M. Sena et al., "Advanced DSP-based Monitoring for Spatially resolved and Wavelength-dependent Amplifier Gain Estimation and Fault Location in C+L-band Systems," in Journal of Lightwave Technology, 2022, doi: 10.1109/JLT.2022.3208209.

[Sha22-1] H. Shakespear-Miles, M. Ruiz, A. Napoli, and L. Velasco, Dynamic Subcarrier Allocation for Multipoint-to-Point Optical Connectivity, OECC/PSC

[Sha22-2 H. Shakespear-Miles, M. Ruiz, A. Napoli, and L. Velasco, Multi-Agent-based Dynamic Optical Subcarrier Allocation for Near Real-Time P2MP Operation, ECOC 2022

[Sou21] A. Souza et al., "Accurate and Scalable Quality of Transmission Estimation for Wideband Optical Systems," 2021 IEEE 26th International Workshop on Computer Aided Modeling and Design of Communication Links and Networks (CAMAD), 2021, doi: 10.1109/CAMAD52502.2021.9617794.

[Sou22] A. Souza et al., "Optimal Pay-As-You-Grow Deployment on S+C+L Multi-band Systems," 2022 Optical Fiber Communications Conference and Exhibition (OFC), 2022.

[Tan19] T. Tanimura et al., "Experimental demonstration of a coherent receiver that visualizes longitudinal signal power profile over multiple spans out of its incoming signal," presented at the European Conference on Optical Communications (ECOC), 2019, pp. 1-4.

[Tan20] T. Tanimura et al., "Fiber-Longitudinal Anomaly Position Identification Over Multi-Span Transmission Link Out of Receiver-end Signals," J. Lightwave Technol., vol. 38, no. 9, 2020, pp. 2726–2733.

[Tan21] T. Tanimura et al., "Concept and implementation study of advanced DSP-based fiber-longitudinal optical power profile monitoring toward optical network tomography," J. Opt. Commun. Netw., vol. 13, no. 10, 2021.

[Tibit] https://tibitcom.com/ [Online; accessed 20-October-2022].

[Tur18] A. Turukhin et al., "Power-Efficient Transmission Using Optimized C+L EDFAs with 6.46 THz Bandwidth and Optimal Spectral Efficiency," presented at the European Conference on Optical Communication (ECOC), 2018, pp. 12–14.

[Uzu22] D. Uzunidis, C. Matrakidis, E. Kosmatos, A. Stavdas and A. Lord, "On the Benefits of Power Optimization in the S, C and L-Band Optical Transmission Systems," Computer Networks, vol. 211, pp. 108958, Jul. 2022.

[Uzu21-1] D. Uzunidis, E. Kosmatos, C. Matrakidis, A. Stavdas and A. Lord, "Strategies for Upgrading an Operator's Backbone Network Beyond the C-Band: Towards Multi-Band Optical Networks," in IEEE Photonics Journal, vol. 13, no. 2, pp. 1-18, April 2021.

[Uzu21-2] D. Uzunidis, C. Matrakidis, E. Kosmatos, A. Stavdas, P. Petropoulos, A. Lord, "Connectivity Challenges in E, S, C and L Optical Multi-Band Systems", in European Conference of Optical Communications, ECOC' 21, 2021.

[Uzu19] D. Uzunidis, C. Matrakidis, and A. Stavdas, "Closed-Form FWM Expressions Accounting for the Impact of Modulation Format," Opt. Commun., vol. 440, pp. 132–138, Jun. 2019.

[Uzu16] D. Uzunidis, C. Matrakidis, and A. Stavdas, "Application of a simplified FWM expression in mixed-fiber links," in 2016 24th Telecommunications Forum (TELFOR), 2016.

[Vel18] A. P. Vela et al., "Soft Failure Localization During Commissioning Testing and Lightpath Operation," J. Opt. Commun. Netw., vol. 10, no. 1, Jan. 2018.

[Vel15] L. Velasco, L. M. Contreras, G. Ferraris, A. Stavdas, F. Cugini, M. Wiegand, J. P Fernández-Palacios, “A Service-Oriented Hybrid Access Network and Cloud Architecture”, IEEE Communications Magazine, Vol.53, Issue: 4, pp.159-165, 2015.

[Vel21] Velasco, Luis, et al. "Autonomous and energy efficient lightpath operation based on digital subcarrier multiplexing." *IEEE Journal on Selected Areas in Communications* 39.9 (2021): 2864-2877.

[Wel22] D. Welch, et al. "Digital Subcarrier Multiplexing: Enabling Software-Configurable Optical Networks." Journal of Lightwave Technology (2022)

[Wel21] D. Welch et al., "Point-to-multipoint optical networks using coherent digital subcarriers." Journal of Lightwave Technology 39.16 (2021): 5232-5247

9 ANNEXES

9.1.1 List of prototypes and commercial hardware to be used.

What	SW/HW	Partner	Segments	Comments
OLC-E design tool	SW	OLC-E	metro / core	impairment validation tool
XR design tool	SW	INF	access / metro	to be checked filterless network; to validate XR performance
wireline planning tool	SW	OLC-E	access / metro	crossing local CO ?
PtoMP trx	HW	CTTC	metro	using OFDM; slice of 12.5GHz; API in OpenConfig
ZR + Sonic switch	HW	CNIT		openconfig
XR	HW	INF		
Tibit	HW	OLC-E	access	to be checked
offline trx	HW	HHI	metro / core	to be checked C+L+S point-to-point
2-degree ROADM	HW	TUE		up to C+L+S+O with SOA; fixed grid; max 40 channels; OpenROADM 4 prototypes in C band, 2 in O-band, 1 in L-band
space switch	HW	TUE		O to L band; 4x16
Filterless		HHI		
amplifier	HW	Adva		which band ? only at ADVA; CNIT agent for monitoring
S-band amplifier	HW	CNIT		only as back up
P4 switch	HW	CNIT		
7-node mesh network	HW	Nokia		C-band only; 12 real channels else noise loading;
power profile monitoring	SW	HHI		DSP block

9.1.2 Closed-form expressions for the physical layer performance estimation of MB systems

To estimate the impact of NLI, we select the expression of P_{NLI} in [UZU19] as it is closed-form allowing for fast optimizations of the physical layer performance, a necessary prerequisite when power optimizations on a network scale are sought. Second, it accounts for different power levels between the channels, again, an important prerequisite in a power optimization mechanism. Third, it can be applied in a network comprising fiber spans smaller than 35 km. The majority of core networks, such as BT’s 21CN, includes some spans smaller than 35 km.

The formalism of [UZU19] can be decoupled into two parts: Self Channel Interference (SCI) and Cross Channel Interference (XCI). In this way, SCI incorporates the NLI products generated due to the interactions between the frequencies of the observed channel only, whilst XCI incorporates the NLI products caused by the interactions between the observed with all other channels. Expanding [UZU19], after performing some simple algebra, the two components are given by

$$P_{SCI}=\frac{32}{27}\frac{\gamma_j{}^2 L_{eff,j}{}^2 P_{ch,j}{}^3 N_s{}^2 c}{\lambda^2 B^2 D_j\sqrt{z_1}}\left(1+\frac{4e^{-a_jL}}{\left(1-e^{-a_jL}\right)^2}\right)asinh\left(\frac{\pi\lambda^2 D_j B^2}{8c}\sqrt{z_2}\right)-\frac{32}{27}\frac{\gamma_j{}^2 L_{eff,j}{}^2 P_{ch,j}{}^3 N_s{}^2 c}{\lambda^2 B^2 D_j\sqrt{z_1+12L^2}}\frac{4e^{-a_jL}}{\left(1-e^{-a_jL}\right)^2}asinh\left(\frac{\pi\lambda^2 D_j B^2}{8c}\sqrt{z_2+12L^2}\right) \tag{3.7}$$

$$P_{XCI}=\frac{32}{27}\frac{\gamma_j{}^2 L_{eff,j}{}^2 P_{ch,j} N_s{}^2 c}{\lambda^2 B^2 D_j}\left(\frac{1}{\sqrt{z_1}}\left(1+\frac{4e^{-a_jL}}{\left(1-e^{-a_jL}\right)^2}\right)-\frac{1}{\sqrt{z_1+12L^2}}\frac{4e^{-a_jL}}{\left(1-e^{-a_jL}\right)^2}\right)\sum_{n=-\frac{N_{ch}-1}{2},n\neq 0}^{\frac{N_{ch}-1}{2}} P_{ch,n}{}^2\left(1-\frac{5}{6}\Phi_n\right)\left|Log\left(\frac{n+1/2}{n-1/2}\right)\right| \tag{3.8}$$

where γ_j is the nonlinear fiber coefficient, D_j and α_j are the dispersion and the fiber attenuation parameter of the jth channel, respectively, L is the span length and B is the channel bandwidth. Next $z_1=\left(\frac{2}{a_j}\right)^2+2L^2\left(N_s{}^2-1\right)/\left(\sum_{k=x_1}^{x_2}\frac{1}{1+\left(2k\pi/\left(a_jL\right)\right)^2}\right)^2$, $x_1=-\frac{\lambda^2 B^2 D_j L N_{ch}{}^2}{16c}$, $x_2=\frac{\lambda^2 B^2 D_j L N_{ch}{}^2}{2c}$, $z_2=\left(\frac{2}{a_j}\right)^2+2L^2\left(N_s{}^2-1\right)$ with x_1 and x_2 rounded to the nearest integer less than or equal to their values. Index n includes all co-propagating channels of the link and takes values within the range $-\left(N_{ch}-1\right)/2\le n\le\left(N_{ch}-1\right)/2$ where N_{ch} is the total number of channels of the band. $P_{ch,n}$ denotes the power of the n^{th} interfering channel, respectively. Φ_n is a modulation format depended parameter taking the value of 1 for BPSK and QPSK, 17/25 for 16-QAM and 13/21 for 64-QAM.

Next, $P_{ASE,j}$ denotes the total ASE power in a link and is given by the following formula

$$P_{ASE,j}=\sum_{i=1}^{N_s}\left[hf_j\left(NF_{i,j}\cdot G_{i,j}-1\right)B_0\prod_{r=i+1}^{N_s}G_{SRS,r,j}\right] \tag{3.9}$$

where $G_{i,j}$ *is* the amplifier gain, $NF_{i,j}$ is the noise figure at the i^{th} amplification stage, f_j the central frequency of the channel under study and B_o the optical bandwidth.